PERFORMANCE ANALYSIS OF A NEW AUGMENTED SOLAR CHIMNEY POWER PLANT DESIGN

BY

FAISAL MOIZ HUSSAIN

A Thesis Presented to the
DEANSHIP OF GRADUATE STUDIES

KING FAHD UNIVERSITY OF PETROLEUM & MINERALS

DHAHRAN, SAUDI ARABIA

In Partial Fulfillment of the
Requirements for the Degree of

MASTER OF SCIENCE

In

MECHANICAL ENGINEERING

MAY 2017

KING FAHD UNIVERSITY OF PETROLEUM & MINERALS

DHAHRAN- 31261, SAUDI ARABIA

DEANSHIP OF GRADUATE STUDIES

This thesis, written by **FAISAL MOIZ HUSSAIN** under the direction of his thesis advisor and approved by the thesis committee, has been presented and accepted by the Dean of Graduate Studies, in partial fulfillment of the requirements for the degree of **MASTER OF SCIENCE IN MECHANICAL ENGINEERING.**

Dr. Fahad A. Al-Sulaiman
(Advisor)

Dr. Zuhair Mattoug Gasem
Department Chairman

Dr. Esmail M. A. Mokheimer
(Member)

Dr. Salam A. Zummo
Dean of Graduate Studies

Dr. Shafiqur Rehman
(Member)

7/11/19

Date

عمادة الدراسات العليا
DEANSHIP OF GRADUATE STUDIES

Dedicated to

My Family

ACKNOWLEDGMENTS

All Praise belongs to Almighty Allah (s.w.t) for bestowing me with courage and perseverance to carry out this work sincerely. Peace and Blessings of Allah be upon his Prophet Mohammed for enlightening us with the path to lead our lives here and to achieve thereafter.

I would like to express my profound gratitude and deep regards for my thesis advisor, Dr. Fahad A. Al-Sulaiman. In spite of his busy schedule for guiding and supporting me at every step of my research work at KFUPM. I deeply appreciate and thank him for his patience, insightful comments, mentorship, and for being a powerhouse of motivation. I am especially thankful and grateful to my thesis committee members Dr. Esmail M. A. Mokheimer and Dr. Shafiqur Rehman for their review of the thesis and the useful comments on the research conducted.

My deepest thanks to undergraduate students Mr. Mohammed Al-Hazzaa, Mr. Abdul Khaliq Al-Shamrani, Mr. Nasser Al-Khalidi, Mr. Ali Al-Blushi, and Mr. Abdullah Al-Mutlaq for their tremendous and tireless effort in setting up the working model.

Acknowledgement is due to King Fahd University of Petroleum and Minerals for providing me the financial support and good academic environment during the course of my M.Sc. I would also like to thank the Indian community for making my stay at KFUPM a memorable experience.

Lastly, I would like to thank my family for their consistent prayers and support throughout my life.

TABLE OF CONTENTS

LIST OF TABLES

LIST OF FIGURES

LIST OF ABBREVIATIONS

CFD	:	Computational Fluid Dynamics
CPVC	:	Chlorinated Polyvinyl Chloride
CSP	:	Concentrated Solar Power
EES	:	Engineering Equation solver
FSC	:	Floating Solar Chimney
FSCPP	:	Floating Solar Chimney Power Plant
HUST	:	Huazhong University of Science and Technology
KFUPM	:	King Fahd University of Petroleum and Minerals
LEC	:	Levelized Electricity Cost
MENA	:	Middle East and North Africa
PCM	:	Phase Change Material
PV	:	Photo-Voltaic
PVC	:	Polyvinyl Chloride
RI	:	Research Institute
SCPP	:	Solar Chimney Power Plant
UAE	:	United Arab Emirate

ABSTRACT

Full Name : [Faisal Moiz Hussain]

Thesis Title : [Performance analysis of a new augmented solar chimney power plant design]

Major Field : [Mechanical Engineering (Thermo-Fluids)]

Date of Degree : [May 2017]

An improved model for a solar chimney power plant (SCPP) is developed and validated. With the quest of higher power output, a new model for a solar chimney power plant aided with reflectors is developed and a comparative study is conducted with an SCPP model without reflectors. Furthermore, a laboratory scale model of SCPP is built to determine the variance of real results with an analytical model developed in the present study. Detailed energy and exergy analyses are used for the thermodynamic assessment of the proposed SCPP models. All the formulated energy and exergy equations are solved simultaneously using engineering equation solver (EES) software. The improved SCPP model is used to determine the effective diameter of the collector and the heat transfer coefficient between the deck, floor, and air. The study reveals that the power output is directly proportional to the mass flow rate, which depends on the geometry of the system, air velocity, and the density of air. Though the power output is high during the summer months, the SCPP is more efficient in the winter months. The exergy destruction is highest for the floor, as it attains the highest temperature due to the incidence of solar radiation, and the air cannot absorb all the heat from the floor due to the low heat absorbing capacity of air. Thus, the floor has the highest exergy improvement potential.

Dhahran, Saudi Arabia was selected as an illustrative example to evaluate the proposed models. For solar irradiation data of 2016, the average power output, energetic and exergetic efficiencies of the SCPP are 99 kW, 0.523%, and 0.581%, respectively. For the new model of SCPP aided with reflectors, the study reveals that the increase in incident solar radiation with the aid of reflectors enhances the energy efficiency and power output by 22.6% and 133%, respectively. However, the improvement in power output is due to the higher mass flow rate generated. The average power output, energetic and exergetic efficiencies of the SCPP model aided with reflectors are 371 kW, 0.636%, and 0.71%, respectively. The models developed predicts the empirical values with a variance of 5%. Moreover, the power output, energy and exergy efficiencies, a variation of temperature for the floor, deck, chimney, and air, and the variation of velocities at location 1, 2, and 3, density variation of air in the collector for each month of the year are reported. Furthermore, a comparative study of SCPP aided with reflectors and a conventional SCPP is presented.

ملخص الرسالة

لاسم الكامل: فيصل معز حسين

عنوان الرسالة: تحليل أداء تصميم جديد لمحطة طاقة مدخنة شمسية مُعزَّزَه

التخصص: الهندسة الميكانيكية

تاريخ الدرجة العلمية: مايو 2017

تم تطوير نموذج مطوّر لمحطة طاقة مدخنة شمسية (SCPP) والتحقق منه. سعياً وراء إنتاجية أعلى من الطاقة؛ تم تطوير نموذج لمحطة طاقة مدخنة شمسية مُزَّود بعواكس وتم عمل دراسة مقارنة مع نموذج مماثل بدون عواكس. بالإضافة الى ذلك، تم بناء نموذج لمحطة طاقة مدخنة شمسية بقياس معملي لتحديد تغير النتائج الفعلية مع النموذج التحليلي الذي تم تطويره في الدراسة الحاليه.

تم استخدام تحليلين مفصلين للطاقة والاكسيرجي في التقييم الديناميكي الحراري لمنظومات (SCPP) المقترحه. تم حل جميع المعادلات المستنبطة للطاقة والاكسيرجي بالتزامن باستخدام برنامج (EES). استخدم نموذج (SCPP) المطور لتحديد القطر الفعال للمُجمِّع ومعامل انتقال الحرارة بين السطح، الأرضية والهواء.

كشفت الدراسة أن إنتاجية الطاقة تتناسب طرديا مع معدل سريان الكتلة الذي يعتمد بدوره على شكل المنظومة، سرعة الهواء وكثافته.على الرغم من أن انتاج الطاقه يكون أعلى خلال أشهر الصيف فإن منظومة (SCPP) تعمل بكفاءة أعلى في فترة الشتاء. كانت قيمة معدل تدمير الاكسيرجي الأعلي في الأرضية لكونها تمتلك أعلى درجة حراره لسقوط الإشعاع الشمسي، عدم قدرة الهواء على امتصاص كل الحراره من الأرضية لانخفاض سعة امتصاص الحراره. لذلك كان للأرضية أعلى إمكانية لتحسين الاكسيرجي.

تم اختيار مدينة الظهران، المملكة العربية السعودية كمثال توضيحي لتقييم النموذجين المقترحين. باستخدام بيانات الأشعاع الشمسي لعام 2016 كانت قيم كل من متوسط انتاج الطاقة، كفاءتي الطاقة والاكسيرجي لمنظومة (SCPP): 99 kW، 0.523% و 0.581% على التوالي. أما للمنظومة الجديده المُعزَّزَه بالعواكس كشفت الدراسه أن الزيادة في الإشعاع الشمسي بمساعدة العواكس تُحسِّن كفاءة الطاقة وإنتاج الطاقة بنسبة 22.6% و 133% على التوالي. لكن مع ذلك فان الزيادة في انتاج الطاقة كانت بسبب الزيادة الناتجة في معدل سريان الكتله. كانت قيم كفاءة الطاقه، كفاءة الاكسيرجي وإنتاج الطاقة لنموذج (SCPP) المُزود بعواكس: 0.636%، 0.71 و 371 kW على التوالي. علاوة على ذلك؛ تم تسجيل كل من انتاج الطاقة، كفاءة الطاقة و، تغير درجة الحرارة لكل من الأرضية، السطح، المدخنة والهواء وتغير السرعات عند النقاط 1، 2 و 3، تغير كثافة الهواء في المُجمّع لكل شهور السنة. بالإضافة لذلك تم عرض دراسة مقارنة بين نظام SCPP تقليدي وآخر مُزوَّد بعواكس.

CHAPTER 1

INTRODUCTION

Energy is vital to human existence and indispensable for the socio-economic development of any nation. It is the bedrock of industrialization and development. Humankind is using fossil fuels to satisfy energy demands, and fossil fuel provides very significant fraction of the world energy needs. Fossil fuels are in abundant supply and are in use by humankind in heating, transportation, and energy generation. Unfortunately, the use of fossil fuels come with some adverse effects. Prominent among which is the emission of greenhouse gases, predominantly carbon dioxide (CO_2), which significantly contribute to the global warming and consequently causing adverse climatic change.

With an ever-increasing concern of depletion of fossil fuels and increment of CO_2 emissions, there is a need to find efficient alternate energy resources. Alternate energy sources like nuclear power and renewable energy are carbon neutral and can present a favourable condition by reducing CO_2 emissions to the atmosphere. Unfortunately, they are not yet in abundant supply to meet demand. Much research and work are still needed to make these available in ample quantity to cater our energy demands.

Alternate energy sources such as solar, biomass, geothermal, wind, and hydro, can be good alternatives to the conventional fuel sources. These sustainable energy sources are available in sufficient quantities and have minimal adverse impact on the environment. Solar energy is one such alternative and there are two ways in which this energy can be

harnessed to generate electrical power, through photovoltaic and solar thermal or concentrated solar power (CSP). Photovoltaic technology provides a direct method to convert solar radiation into electricity. This implies that the photovoltaics can only be employed during the daylight hours and storing electrical energy is not an efficient process. On the other hand, in a solar thermal system, a device which collects the solar energy is used to run the turbine to produce electricity or use the radiation to heat the fluids and store the energy. Alternatively, storing heat is far easier and efficient as compared to storing electricity. The heat which is stored during the daylight hours can be utilized in the night by converting it into electricity. Because of this capability, solar thermal technologies are emerging as a potential technology among other sustainable technologies.

Though Saudi Arabia is a leading oil producer and possesses proven reserves of gas and crude oil. Keeping in view the competition for energy production by alternate energy resources, by the major economies. Here is a need to assess the performance of these resources for Saudi Arabia.

1.1 Solar Energy

Solar energy is the flow of heat and light from the sun. Sunlight and heat are transformed and absorbed by the environment in a multitude of ways. Some of these transformation leads to biomass, wind, and waves as well. From Musunuri et al. [1], the Earth receives 174 petawatts (PW) of solar radiation at the upper atmosphere. While traveling through the atmosphere 7% of the incoming solar radiation is reflected and 16% is absorbed. Clouds, dust, and pollutants further reduce the radiation by 25% through reflection and 1% through absorption. 26% of solar radiation reaches the earth surface directly, 14% is diffused by clouds, dust, and pollutants, and 11% is diffused by the atmosphere. Finally, 51% of the

solar radiation reaches the earth surface. Of it, 5% (Albedo) is reflected back from the earth surface. Figure 1.1 is the line representation for the losses and incident radiation that is reaching the earth surface.

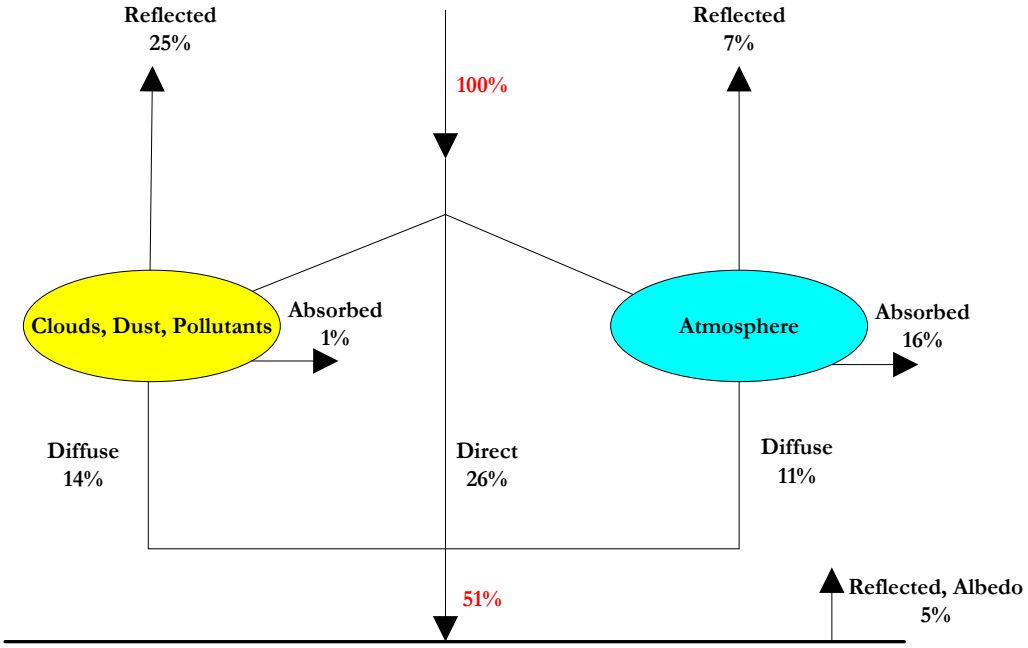

Figure 1.1. Line representation of solar energy reaching earth surface [1]

In addition to its availability, solar energy has two other factors in its favor [2,3]. Firstly, unlike fossil fuels and nuclear power, it is an environmentally safe source of energy. Secondly, it is free and available in adequate quantities in almost all parts of the world. The energy obtained from the sun can be utilized by direct or indirect methods. Direct means include thermal and photovoltaic conversion, while indirect means include the use of water power, winds, biomass, wave energy and the temperature differences in the ocean. Figure 1.2 depicts the broad classification of methods of utilization of solar energy.

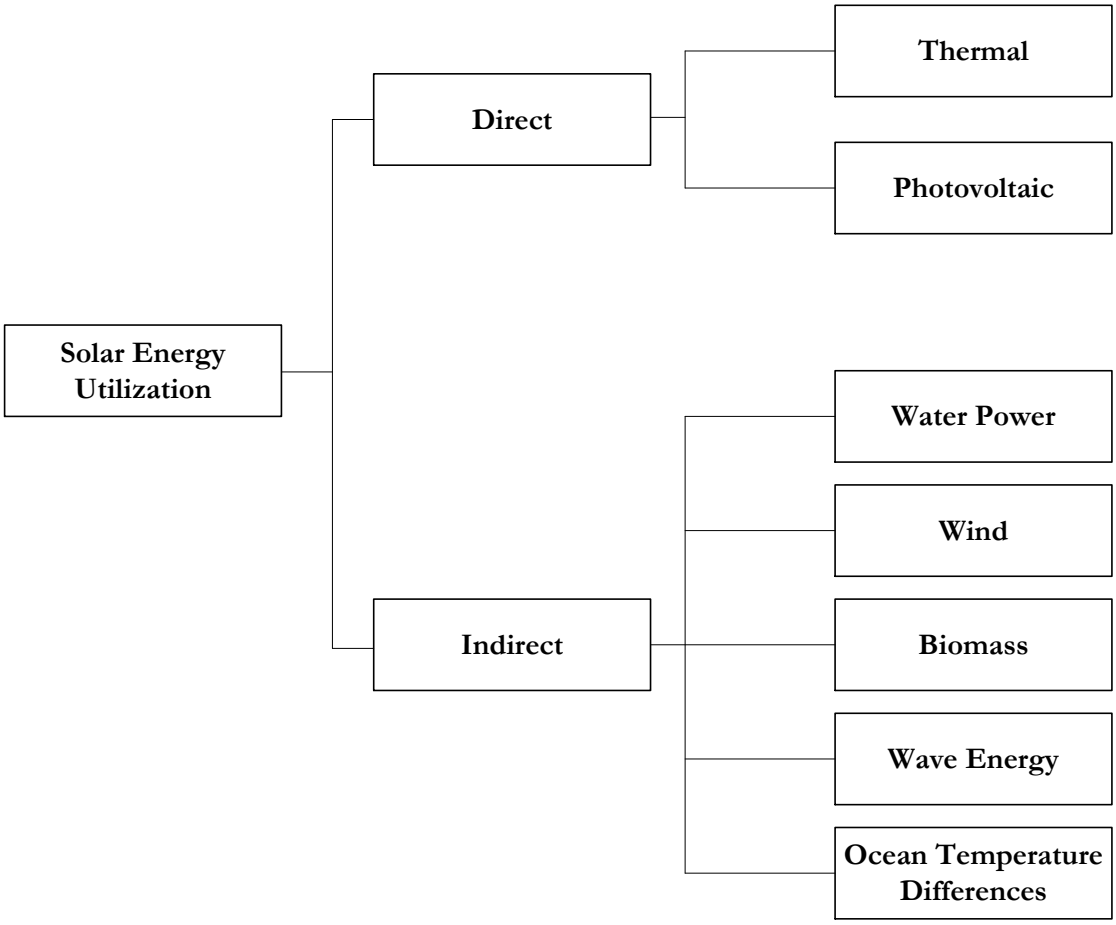

Figure 1.2. Broad classification of solar energy utilization

1.2 Solar Thermal Energy

Solar thermal energy is produced by concentration of light from the sun to create heat, and that heat is used to store energy or run a heat engine, which turns a generator to produce electricity. Solar thermal energy has enormous potential like all other available energy resources. Much research is emphasized to increase the efficiency. Different techniques of solar thermal power generation are technically feasible and cost-effective. But, this technology is highly dependent on the local climate, daily, and yearly availability of solar radiant energy. Figure 1.3 depicts the long-term average of global horizontal irradiation received on the earth surface [4]. The Higher amount of radiant energy is received by MENA (Middle East and North Africa) region. Hence for solar thermal applications,

MENA region is one of the best options to focus and invest. As far as, Saudi Arabia is concerned, with an area of 2.3 million km^2 [5], on average, it receives up to 2200 KWh/m^2 yearly and 6.0 KWh/m^2 daily. With the sparse population and much free space, Saudi Arabia becomes the coveted place for solar thermal power generation.

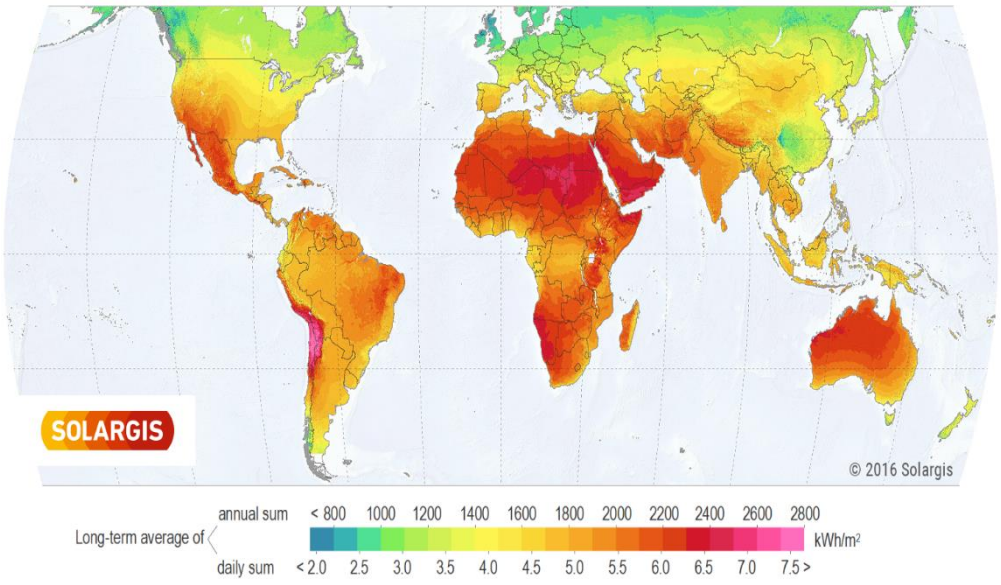

Figure 1.3. Daily average of global horizontal irradiation

1.2.1 Solar Thermal Technologies

Basically solar thermal technologies can be classified into 4 types.

1. Flat Plate Collectors (Non-concentrating)
2. Concentrating Collectors
3. Solar Thermal Energy Storage (E.g. Packed bed & Phase change Energy storage)
4. Solar Process Loads (E.g. Space heating and cooling)

Apart from the above 4 types, many hybrid solar thermal systems may include any combination of these technologies to enhance the efficiency.

1.2.2 Solar Thermal Applications

The thermal energy utilized from solar energy has the following applications.

1. Water heating
2. Air heating
3. Space heating
4. Space cooling and refrigeration
5. Power generation
6. Distillation
7. Drying, and
8. Cooking.

1.3 Solar Chimney Power Plant

The Solar Chimney Power Plant (SCPP) [6] is a device, which is guided through natural draft utilizing solar radiant energy, to impart an ascending thrust on air to run a turbine. An SCPP is constructed by the combination of three traditional devices used for energy conversion, viz., a greenhouse, a lengthened chimney in the middle of the greenhouse, and a wind turbine placed inside the chimney. Such a setup allows the transformation of radiant energy from the sun into electrical energy, achieved in two steps. In the first step, the collector transforms radiant energy into thermal energy by the greenhouse effect, and the design of the collector allows the heated air to flow radially towards the chimney at its center. In the next step, the chimney transforms the thermal potential into kinetic energy, and the wind turbine converts the kinetic energy into electricity using a generator. A simple model of the SCPP consists of an area of the ground with a film of glass or plastic above it drawn evenly over the ground, allowing solar radiation to pass through, while preventing

radiation of shorter wavelength emanating from the heated surface of the ground to escape. Consequently, the temperature of the air between the ground and the cover above it rises. The height of the cover of the collector above the ground gradually increases towards the middle of the SCPP. This design allows the continuous smooth passage of heated air, which flows through the long tubular chimney without turbulence, thereby diminishing the eddy losses. A collector with these characteristics can transform a considerable fraction of the radiant energy into thermal energy.

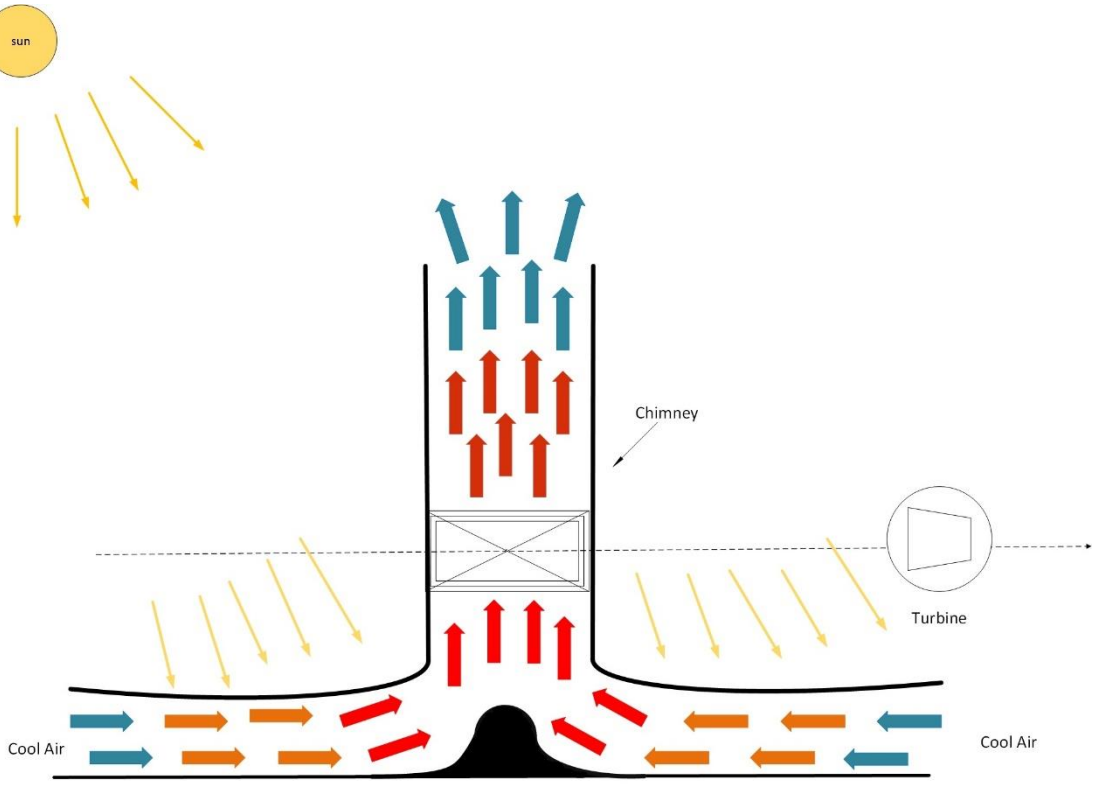

Figure 1.4. Illustrative representation of solar chimney power plant

The idea of an SCPP was conceived by Schlaich [7] in the 1970s. The very first operational 36 kW pilot plant was constructed in Manzanares near Madrid in Spain, 1982 under the sponsorship of Spanish government. The chimney had a height of 195 meters and the diameter of the collector was 240 meters. Although not achieving the maximum power as

designed, it was operated for 7 years, proving that the concept is technically feasible. The concept of the SCPP was further developed over the years, with several studies evaluating distinct facets of the SCPP, where the complex mechanism of heat transfer and fluid mechanics was considered. The most significant effort is being made for building large-scale plants in Australia, under a joint venture between an Australian based company, EnviroMission Ltd. and the German firm, Schlaich Bergermann und Partner.

1.3.1 Advantages of solar chimney power plant

- SCPP operates using simple technology, except the turbo-generator assembly, the technology of SCPP will not become outdated easily.
- Long operating life.
- Low maintenance cost.
- Construction materials used are inexpensive.

1.3.2 Disadvantages of solar chimney power plant

- The power output of the SCPP is not uniform.
- For SCPP to be efficient, very large scale SCPP has to be built. Owing to its huge size, the initial investment of the SCPP plant is high.
- Another challenge of SCPP is a huge land requirement. Though the abundant unhabituated land is available, the ground has to be leveled keeping the design of SCPP under consideration.

1.4 Motivation and significance

The world is facing a challenging time to fulfill its energy requirements with the depletion of fossil fuel resources. In these hard times, research is being carried out to effectively utilize sustainable energy resources to fulfill the increase in the energy demands.

Of all the known renewable energy technologies, solar thermal technology in the near future is expected to become the technology of choice. This is mainly due to the anticipated performance improvement and the cost reductions with innovations of technology associated with solar thermal energy. One such technology is solar chimney power plant.

Ever since the inception of the idea of SCPP in the 1970's, many research articles discussed distinct facets of SCPP. But, none of the work gives the complete insight about the detail performance of SCPP considering the intricate mechanism of heat transfer and fluid mechanics. In this thesis, an effort is made to present the detail thermodynamic modeling of SCPP considering all the losses and appropriate heat transfer correlations. Although SCPP seems to be economically feasible, few of the disadvantages associated with SCPP are low efficiency and power output.

With the quest of increasing the power output, a mathematical model for a novel method of enhancement of power output for SCPP is developed and analyzed thermodynamically. In this model, SCPP is aided with reflectors to increase the incident radiation on the floor of SCPP. All the reflectors are arranged in the similar pattern as heliostats of solar tower system reflecting towards the deck. The objective of the present study is to streamline the interpretative mathematical model of SCPP aided with reflectors and to present the comparative study with the conventional SCPP.

1.5 Objectives of the current study

The overall objective of this study is to perform thermodynamic analysis of solar chimney power plant. The specific objectives of the proposed work are as follows:

1. To develop the energy model of SCPP by control volume approach, thus forming the basis for energy analysis and to determine the energy efficiency.
2. To develop the exergy model of SCPP and to perform the exergy analysis and to determine the exergetic efficiency.
3. To develop the thermodynamic model of SCPP aided with reflectors and to perform the energetic and exergetic analysis.
4. To analyze the model of SCPP aided with reflectors and to identify the improvement in overall efficiency.
5. Experimental modeling of SCPP to perform the temperature analysis and to determine the comparative study with the analytical model.

The objectives are designed to provide the deliverables which are mainly related to the appropriate modeling of solar chimney power plant and a novel enhancement technique to improve the power output of the SCPP system. The results of this proposed work will be a valuable reference for both researchers and engineers in the area of solar thermal technology specifically solar chimney power plant.

1.6 Thesis outline

The objective of this thesis is to assess the thermodynamic model of solar chimney power plant and to model the novel design of SCPP with the aid of reflectors to enhance the power output. To evaluate the proposed model, Dhahran, Saudi Arabia is selected as an illustrative example.

This thesis contains seven chapters.

Chapter 1 introduces the fundamentals of solar thermal technology. It also discusses the challenges associated with trapping solar energy. The first chapter further discusses solar chimney power plant, its advantages, and disadvantages, and, defines the objective of this thesis work.

Chapter 2 reviews the literature related to solar chimney power plant. Summary of literature review presents a gist of previous work done in the area of solar chimney power plant. It also discusses the various methods employed to enhance the efficiency of solar chimney power plant.

Chapter 3 describes the approach and methodology for modeling of solar chimney power plant. It also mentions detail energy and exergy modeling of solar chimney power plant. In the last part, the validation results of the model are discussed.

Chapter 4 describes the novel method of enhancing the power output of solar chimney power plant with the aid of reflectors. Detailed energy and exergy modeling of solar chimney power plant with the aid of reflectors is presented.

Chapter 5 illustrates an effort for constructing the experimental models and the experimental analysis carried out is discussed in detail.

Chapter 6 presents detailed results and discussions of the solar chimney power plant. A comparative study of SCPP with the aid of reflectors is also presented.

Chapter 7 includes the conclusions of the study and also provides the directions in which this study can be extended in future.

CHAPTER 2

LITERATURE REVIEW

In this chapter, a detailed literature review is presented to identify the gap in the literature. The details of the literature review are organized as follows. It starts with the review of the studies on the solar chimney power plant (SCPP) system. Then, the review is presented on the technology incorporated to enhance the power output of SCPP. Lastly, the economic feasibility of SCPP system available in the literature is presented.

2.1 Solar Chimney Power Plant

The design of solar chimney power plant was conceived by Schlaich [7] in late 1970's. The very first operational 36kW pilot plant was constructed in Manzanares near Madrid in Spain, 1982. The chimney had a height of 195 meters and the diameter of the collector was 240 meters. The concept of the SCPP was further developed over the years with several studies evaluating the distinct facets of the SCPP, where the complex mechanism of heat transfer and fluid mechanics were considered.

After the construction of the experimental model of SCPP in Manzanares, Haaf et al. [6] discussed the basic principles behind the operation, construction and power generation of a solar chimney power plant. Following his publication in 1983, Haaf [8] documented the preliminary test results from the Manzanares prototype plant, with the experimental findings which correspond well with model calculations.

Mullett [9] performed an analysis to develop a formula for determining the overall efficiency. From his studies, it was concluded that overall efficiency is directly related to the height of the chimney and was found to be 1% for a height of 1000 m. It was also evident that solar chimney power plant is essentially a power generator of large scale. Hence, for a small unit of SCPP, say, 100 kW, the system is not efficient economically.

Pasumarthi and sheriff [10] developed a mathematical model to estimate the air temperature and power output of SCPP. Effect of surrounding conditions and geometry on the overall power output were examined. The model was justified for humid climate of Florida, which is almost the same in terms of climate with Saudi Arabia. Following their publication [10], in [11] they demonstrated a model of solar chimney power plant to inspect the experimental and theoretical performance. Also, an economic assessment of the system costs was presented.

Gannon and Von Backstrom [12] presented an ideal air standard cycle analysis of the SCPP to determine the limiting performance, ideal efficiencies, and relationships between main variables. Their analysis included the chimney friction and considered all losses into account. This cycle was used to predict the performance and operating range of a large-scale plant. The work was validated by comparing the simulation of a small scale plant with the experimental data of Manzanares plant. This work on ideal air standard cycle analysis of the SCPP acts as a powerful tool to quickly determine the upper limit of cycle performance, initial feasibility, and operating range. Also, Von Backstrom and Gannon [13] presented a one-dimensional compressible flow approach for calculations of the thermodynamic variables as dependent on the chimney height, wall friction and internal drag. It was concluded that pressure drop associated with the vertical acceleration of the

air is about three times the pressure drop associated with wall friction. Backstrom and Fluri [14], determined the maximum fluid power condition of an SCPP analytically and found that the turbine pressure drop to pressure potential ratio is 2/3.

Pastohr et al. [15] carried out an analysis to improve the description of the operational model and efficiency. They found that the pressure drop across the chimney and the mass flow rate have the decisive influence on the efficiency of SCPP. Using the CFD program FLUENT, they developed the numerical model of SCPP. The numerical results are in consensus with the analytical model and suggested the use of the analytical model for parametric studies.

Hedderwick [16] in his thesis, presented the performance evaluation of SCPP. In that model, the relevant discretized energy and draught equations were deduced and solved numerically subject to boundary conditions to determine the performance of a specific plant which is to be located in the Northern Cape of South Africa. The performance characteristics were presented using meteorological data of 21st December as an example. Air temperatures throughout the plant, temperature distribution along the ground, pressure variation across the SCPP model were presented and discussed.

Pretorius [17], Pretorius and Kroger [18] evaluated the performance of a large-scale solar chimney power plant numerically. Their study demonstrated the daily and seasonal power output variations. From their analysis, it was concluded that plant power production is a function of the collector roof shape and inlet height. Following their publication [17], in [18] they evaluated the influence of developed heat transfer equation and realistic turbine inlet loss coefficient. Their study concluded that due to use of new heat transfer equations

annual power output was reduced by 11.7% and realistic turbine inlet loss coefficient only accounted for a 0.6% rise in annual power production of the plant. The authors [19] also performed the sensitivity analysis on the influence of the quality, thickness, reflectance, emissivity, shape, and insulation of the collector roof glass, the cross-section of the collector roof supports, various ground types, ground surface roughness, absorptivity and emissivity, turbine inlet and bracing wheel loss coefficients, and the ambient pressure and lapse rate on the performance of large-scale solar chimney power plant. The above all mentioned parameters have major effect on the efficiency of the SCPP.

Hamdan [20] performed the analysis of a solar chimney power plant for the Arabian Gulf region. The author developed an analytical model to determine the impact of geometric parameters on SCPP. The height of chimney and turbine pressure head were found to be vital physical variables for the design of SCPP. The results of the analytical model were found to be in consensus with numerical and experimental results available in the literature. The model was analyzed for climatic conditions of UAE, which possess the same climatic conditions of Gulf peninsula.

Zhou et al. [21] determined the maximum chimney height for SCPP, to avoid the negative buoyancy. Optimum chimney height for maximum power output was determined and validated with the model of Manzanares. Their results concluded that maximum height gradually increases with the lapse rate increasing and go to infinity at a value of around 0.0098 Km^{-1}. The maximum height for convection and optimal height for maximum power output increase with larger collector radius and determined the variation of power produced as a function of the chimney height and the collector radius. The optimum height for the chimney was defined as 19.15 times the cross section of chimney.

Dehghani and Mohammadi [22] conducted a multi-objective optimization method using an evolutionary algorithm to determine the optimum configuration of solar chimney power plant. Two prime objective functions which were considered simultaneously are power output and capital cost. Collector diameter, chimney height, and chimney diameter were the concerned design parameter. Keeping the power output maximum and capital cost on the minimum, design parameters was varied and an optimal solution method was determined. Their analysis indicated that the height and diameter of the chimney are the most significant physical variables for solar chimney power plant design.

Von Backstrom and Fluri [14] presented an analytical approach to determine the maximum pressure drop across the turbine to obtain maximum fluid power. From the assumption of power-law model, the pressure potential is proportional to volume flow to the power *m*, where *m* is typically a negative number between 0 and -1. The pressure drop across the turbine is proportional to power *n*, where $n = 2$. Thus the analysis shows that the optimum pressure drop as a fraction of pressure potential $(n-m)/(n+1)$, which is equal to 2/3 when $m = 0$. Guo et al. [23] evaluated the optimum pressure drop across the turbine by 3D numerical solutions and validated the results numerically. For the Manzanares prototype, the optimum ratio ranges from 0.90 to 0.95 under the normal climatic conditions. Results indicated that the solar radiation and ambient temperature have a larger influence on pressure drop ratio.

Kasaeian et al. [24] performed an analytical and numerical study for geometrical optimizing of a solar chimney power plant prototype. The numerical predictions were validated with the experimental setup which was constructed with chimney height of 2m, collector radius of 3m and chimney diameter of 10 cm. By varying the chimney height, an

increase of 4% in the velocity was observed, whereas, by varying the chimney diameter, the velocity was increased by 25%.

Xu et al. [25] conducted the numerical analysis on the performance of SCPP system. They established a mathematical model of flow and heat transfer for SCPP to determine the numerical simulations of airflow, heat transfer and power output characteristics with energy storage layer. For the Manzanares plant, with solar radiation and efficiency of the turbine being 600W/m^2 and 80%, respectively, the power output of the system was found to be 120kW. A major source of energy losses is found to be from chimney, collector and pressure losses across the turbine.

Gholamalizadeh and Kim [26] presented a CFD study of an SCPP. A 3D model using RNG K-ε turbulence closure was simulated. To implement solar irradiation discrete ordinates model with non-gray behaviour was used, and solar tracing algorithm of the solar load model was employed. A parametric study was performed to determine the effect of the collector configuration on the performance of the Manzanares plant. Results yielded that with the increase in collector inclination, an increase in the mass flow rate of the system was observed.

Mehrpooya et al. [27] conducted the case study of solar chimney power plant for climatic conditions of Tehran. In their study, 3D model of SCPP was solved by CFD method. The geometry of the model selected was similar to the geometry of Manzanares plant. Results of the numerical study were validated with the analytical results of Petela [28]. By variation of solar radiation, the output electrical power changed from 180 W in the winter to 64 kW in the peak summer.

Nizetic et al. [29] performed the analytical and feasibility study of implementing SCPP in the Mediterranean region. Two locations in Croatia were selected having the typical climatic characteristics of Mediterranean region. It was concluded that a SCPP with a chimney height of 550m and a collector of 1250 diameter would produce 2.8-6.2 MW of power. The annual electric power production of SCPP would range from 5.0-6.0 GWh/year.

Using simplifying assumptions Petela [28] presented the thermodynamic analysis of an SCPP model, with the set of established geometrical parameters used in Manzanares SCPP. In this study, responsive trends of varying input parameters of geometry and radiation were studied. However, the formula suggested for effective diameter of the collector was inconsistent. Also, the heat transfer coefficient was determined using the forced convection correlations, whereas the operation of an SCPP is based on natural convection only.

2.2 Selected Experimental Works on SCPP

2.2.1 Spanish Model

After the oil crisis of the 1970s, Prof. Schlaich [7] along with his colleagues designed a working model of SCPP in Manzanares near Madrid, Spain in 1982. The project was funded by the German Ministry of Research and Technology, on a site provided by Spanish Utility Union Electrica Fenosa. The chimney had a height of 195 meters and the diameter of the chimney was 10 meters, the collector had a diameter of 240 m approximating an area of 45,000 m^2.The designed maximum power output of the model was 50 kW, but the model during its operation produced only up to 36 kW. The average increase in temperature of the air was observed to be 17K above the ambient and average air velocity at the inlet of

turbine reached up to 12 m/s. The plant was operated between 1982 and 1989, and then later decommissioned. As far as, materials are concerned, the chimney was made up of concrete, the deck was made up of transparent glass and collectors were installed in a normal vegetative ground. The bottom of the chimney housed a 4-bladed vertical axis single wind turbine to harness the energy from the buoyant air.

2.2.2 Chinese Model

Zhou et al. [30] conducted an experimental study of temperature field of SCPP. A pilot setup of collector 10 m in diameter and a 8 m tall chimney was built at HUST, in China. The temperature difference between the air at the inlet of the turbine to an inlet of SCPP was found to be 24.1 ^{0}C. The inlet height of the collector was chosen as 0.05 m, standard PVC pipes of 0.3 m diameter were used as a chimney. The collector was covered with the glass made up of reinforced fiberglass plastic and was set on framework constructed of angle iron. Unlike, the Manzanares plant, this plant had an absorber ground made up of mixed asphalt and black gravel placed above the insulating material, to increase the efficiency.

2.2.3 Brazilian Model

Maia and co-workers [31] conducted an experiment to evaluate the thermodynamic study of an SCPP setup. A pilot setup of collector 25 m in diameter and a 12.3 m high chimney was built at Belo Horizonte, Brazil. The experiments were conducted for 4 days in late autumn with maximum and minimum air temperatures of around 27.3^{0}C and 8.4^{0}C, respectively. They also evaluated the model for drying agricultural products by determining the dryness fraction of humid air flow. An effort was made to determine the

improvement potential of SCPP by exergy analysis. At higher temperatures, higher exergy losses were observed compared to the lower temperatures of the daylight hours.

2.2.4 Iran Model

Kasaeian et al. [24] performed an analytical and numerical study for geometrical optimization of a solar chimney power plant. The numerical predictions were validated with the experimental setup which was constructed with chimney height of 2m, collector radius of 3m and chimney diameter of 10 cm. The deck was made up of glass, the chimney was made up of polycarbonate 4 mm thick, and was put above the ground to increase the efficiency 2 mm thick steel absorber plate along with 8 mm thick wood was placed as insulation. By varying the chimney height, an increase of 4% in the velocity was observed, whereas, by varying the chimney diameter, the velocity was increased by 25%.

2.2.5 Egyptian Model

Mekhail et al. [32] studied the experimental and theoretical performance of mini solar chimney power plant. A very small model of chimney height of 6 m, collector diameter of 6 m and chimney diameter of 0.15 m was built at Aswan, Egypt. A mathematical model was developed to validate the experimental results with the analytical model. As far as, construction is concerned chimney was made up of PVC pipe, the deck was made up of a thin sheet of transparent plastic and was set upon steel beams with the wooden network. The efficiency of the mini setup was found to be 0.267%.

2.3 Geometrical Specifications

Table 2-1 presents the geometrical specifications of the various experimental models discussed in the above section.

Table 2-1. Geometrical Specifications for Various Experimental Models

Model / Parameter	Spanish [8]	Chinese [30]	Brazilian [31]	Iran [24]	Egyptian [32]
Collector Diameter (m)	240	10	25	3	6
Chimney Height (m)	195	8	12.3	2	6
Chimney Diameter (m)	17.86	0.3	1	0.40	0.15

2.4 Material Specification

Table 2-2 presents the materials used in the various experimental models discussed in the above sections.

Table 2-2. Material Specifications for Various Experimental Models

Model / Part	Spanish [8]	Chinese [30]	Iranian [24]	Egyptian [32]
Deck	Glass	Transparent glass fiber reinforced plastic	Glass Roof	Thin sheet of transparent plastics
Chimney	Concrete	PVC pipe	Poly carbonate	PVC pipe
Absorber	Not used	Mixed asphalt and black gravel	Steel with wood as insulation	Not used
Frame	Iron Frame	Angle Iron	Not available	Steel beams with wooden network

2.5 SCPP Enhancement Technologies

Ever since the inception of the idea of SCPP in Manzanares [8], Spain many research articles mentioned in the above literature discussed the operation of SCPP in detail by performing the analytical, numerical and experimental analysis. But very few attempts have been reported to enhance the performance of the SCPP system. Below are the few techniques available in the literature used to enhance the performance of the SCPP system.

One of the technique was to introduce water-filled tubes for thermal storage as reported by Kreetz [33]. Water-filled tubes were placed on the ground upon which radiation is incident. Thermal energy was stored during daytime and retracted during the night when there is no solar radiation as the temperature of air in the collector drops. Then water inside the tubes releases the heat that is stored during the sunshine hours. But in the extended study of Bernardes [34], Bernardes et al. [35] it is reported that the power produced during the peak hours of sunshine is decreased as the heat is absorbed by the water-filled tubes. Anyhow, uniform power is produced during day and night i.e. approximately 40% of the peak power of a conventional SCPP without water tubes is produced depending upon the depth of water stored. Thus an effort has been made to make an SCPP operational for 24 hours.

Pasumarthi and sheriff [10,11,36] proposed a mathematical model to estimate the air temperature and power output of an SCPP, where the effects of the ambient conditions and the geometry on the overall power output were examined. They also performed an experimental analysis of an SCPP and proposed the following designs to enhance the power

output; (i) a larger sloped collector, and (ii) introduction of an absorber plate between the ground and the glass cover. Both the designs were found to enhance the power output by 10-15% compared with the conventional SCPP. Pretorius [17,37] extended their work to the second design suggested by Pasumarthi and Sherif. He introduced the regulating mechanism to control the air mass flow rate between the absorbing plate and floor. It was introduced to regulate and store the energy released from ground depending upon the power output demand of the plant.

Bilgen and Rheault [38] designed a sloped SCPP for a hill at high latitudes and evaluated its performance. As natural hills are used as collector field, the chimney height was reduced by 90%, which reduces the construction and maintenance cost. The construction of sloped collector increases the cost as it involves more civil work. However, the authors claimed an efficiency of 0.48%, which is slightly better than the conventional SCPP.

Papageorgiou [39–41] proposed a new idea for the construction of chimney, as it is the only component of SCPP which involves huge construction cost. He initiated the cost-effective idea of floating solar chimneys (FSC). These FSC is made up of successive balloon tubes, filled with gases lighter than air, and this allows the chimney to float in the air. As in conventional SCPP chimney height is limited taking into consideration construction and its cost. For the same power output of SCPP, the height of FSC can be reduced by three times and power produced could be 5 to 6 times cheaper. He also stated that using 5% of the existing desert land in all the continents can cater up to 50% of the global electricity demand.

Zhou et al. [42] proposed a novel concept for producing power by integrating a solar collector with a man-made mountain hollow. The mountain hollow, formed by an excavation in a large elevation mountain, can avoid the issues of concrete chimneys which could reduce the use of material and construction cost.

Alrobaei [43] proposed hybrid geothermal/SCPP/PV system in the south region of Libya to enhance the production of powerhouse and overcome the zero production of energy of the SCPP/PV unit during night time by combining it with geothermal technology. Hot water obtained from underground, by a geothermal unit was circulated through the floor of SCPP to generate artificial wind and run the SCPP.

Zuo et al. [44,45] integrated SCPP with seawater desalination and performed analytical and numerical analyses. The design suggested by the authors was similar to water-filled tubes placed on the ground by Kreetz [33]. In this design, a water still was placed as a ground to SCPP and sea water is vaporized and cooled on still and collected as fresh water. Though the combined solar energy conversion was not much, it was claimed to be economical by authors.

Islamuddin et al. [46,47] proposed a new idea of providing an external heat source to the SCPP by placing the hollow rectangular channels beneath the collector cover and passing the exhaust gases (flue gases) through it. They developed the mathematical model and investigated the numerical simulation and validated their result with the analytical model of Petela [28]. But increase in overall efficiency of the system was found to be 1.14%. Anyhow, the shortcoming of this hybrid technique is that flue gas is to be transported to the location of SCPP or thermal power plant should be in the vicinity of SCPP.

Nizetic et al. [48,49] proposed the implementation of convective gravitational vortices in the SCPP, they developed the mathematical model and performed the numerical simulation. This model was based on the idea of tornado funnel. They placed the short diffuser at the bottom of chimney i.e., below the turbine, which would create the vortex in the air, which is a desirable input for a turbine for obtaining the higher efficiency by increasing the pressure difference across the turbine.

All the above enhancement techniques increases the power output by utmost 15% and most of the techniques involve hybrid systems. Hence, there is a need to find an alternative technology to enhance the power output of the SCPP.

2.6 Economic Study of an SCPP Model

From the above literature review, it was observed that the efficiency of the SCPP is very small. In this section, an effort is put to show that the SCPP technology is a feasible option and works from available literature is presented in terms of economic feasibility.

Beerbaum and Weinrebe [50], performed the techno-economic analysis of solar thermal power generation in India. They analysed the potential and the cost-effectiveness of centralized and decentralised solar thermal electricity generating systems. For solar chimney power plants especially in the areas with high insolation levels, calculations predicted that the levelized electricity cost (LEC) varies from 4.6 cents/kWh to 15.8 cents/kWh. As far as, other decentralised solar thermal electricity generation is concerned LEC varies from 11.7 cents/kWh to 39.9 cents/kWh.

Nizetic et al. [29] analysed the feasibility of SCPP for the Croatian climatic condition by approximating cost analysis, which included the estimation of total investment. For an annual electricity production of 5.0 to 6.0 GWh by SCPP, the levelized mean price of

electricity was within a range of 0.31-0.68 €/kWh. However, the other side electricity price in EU is 0.15 €/kWh. Electricity production price by SCPP was found to be higher as it did not consider the grant subventions for renewable energy production which most of the countries provide. Finally, SCPP was considered to be viable over a long-term period (60 years) unlike conventional plants with the shelf life of fewer than 30 years.

Zhou et al. [51] performed the detailed economic analysis of power generation from floating solar chimney power plant (FSCPP) with the power output of 100 MW. Keeping in view, the minimum attractive rate of return of 8% for the investors, the minimum price was found to be 0.83 yuan/kWh. Under financial incentives, loans at a low-interest rate of 2% and free income tax were considered. From [39] it was also evident that FSCPP, in reality, is more economical than the conventional SCPP.

Fluri et al. [52] performed the cost analysis and investigated the impact of carbon credits on the LEC of solar chimney power plant. The assumed model of 100 MW capacity, had a chimney height of 850 m with the collector diameter 4950 m. The annual power output was found to be 281 GWh and levelized electricity cost was found to be 0.0370 €/kWh. Here the LEC is found to be much lower than the previous models, as the previous models included superfluous construction cost.

Pretorius and Kroger [53], performed the thermo-economic optimization of a large-scale SCPP. An approximate cost model is then developed by determining the optimum plant dimensions. It was found that the larger SCPP's are economical and cost-effective than the smaller plants. For the chimney height of 1500 m and collector of 720 m diameter, specific plant cost was found to be 1931 C/GWh, where C is the term defined for a currency

unit dependent upon the cost of one cubic material of chimney, for determining the specific plant cost in the local currency, C can be suitably replaced.

Gholamalizadeh and Mansouri [54] presented a comprehensive approach of SCPP by optimising the geometrical parameters, construction cost, and power output. For a collector of 100 m and a chimney with a height of 105 m and 5 m diameter, specific expenditure of the plant was found to be less than 0.05 U/kWh. Specific expenditures for various configuration of SCPP were presented.

Li et al. [55] performed the cost-benefit analysis of conventional SCPP built with concrete chimney considering Chinese economic model. For a service period of 120 years divided into 4 phases of 30 years each and a repayment period of 30 years, with an interest rate and inflation rate of 3% each, LEC by SCPP was found to be on average of 0.912 Yuan/kWh for over a period of 120 years. All the above calculations are made for a 100MW SCPP plant with the chimney height and diameter of 1000 m and 110 m and 4300 m collector diameter.

Gholamalizadeh and Kim [56] developed a triple-objective design method for SCPP to optimize the expenditure, the efficiency of SCPP setup, and power output. A multi-objective genetic algorithm was developed to determine the best combination of geometric parameters keeping in the loop the power output and the construction cost. The results concluded that the increment of the power output was higher than the increment of the expenditure in the optimal configuration.

From the reviews summarised in the literature above, it can be concluded that SCPP technology is an economically viable option and cheaper than the conventional

technologies used today. Hence, a serious effort is in need to establish the potential use of SCPP technology in the times to come.

2.7 Summary

A detailed literature review of the solar chimney power plant, the economic feasibility and the enhancement technologies associated with the SCPP models are presented. It can be observed that only a few studies have been conducted in the modeling of solar chimney power plants. Hence, a proper modeling of solar chimney power plant is required taking all the losses into account. The enhancement technologies of SCPP models are not efficient, all the enhancement techniques mentioned in the literature increases the power output by utmost 15% and most of the techniques involved hybrid systems. Hence, there is a need to find an alternative technology to enhance the power output of the SCPP. The current study deals with proper modeling of SCPP and presents a new technology to enhance the power output of SCPP, with the aid of reflectors.

CHAPTER 3

MATHEMATICAL MODELING OF SOLAR CHIMNEY POWER PLANT

A mathematical model is developed to achieve the objectives of the present study. The first part of the mathematical model deals with geometric modeling of SCPP. Once the geometric parameters are set, energy and exergy modeling of SCPP is carried out. The thermodynamic equations are derived by equaling the solar input energy with the energy losses at various locations and the final output power. After establishing the correlations between the energy input and final output, all the equations are solved simultaneously using engineering equation solver (EES) software. The SCPP model is analyzed for the solar irradiation conditions prevailing in Dhahran.

Energy modeling is followed by exergy modeling of SCPP, by considering the exergy associated with each of the energy term obtained in energy modeling, including the irreversibility (i.e., exergy destruction). After establishing the correlations between the qualities of input, output and associated irreversibility's, all the equations are solved simultaneously using EES. Then, the SCPP model is used for determining the scope of improvement by performing the exergy analysis.

Last part of the chapter, elucidates the validation of the model developed for the present study.

3.1 Geometric Modeling of SCPP

In the model discussed here, the deck is made of glass or plastic film, which is at an inclination and is raised above the ground level. In this arrangement, the cover traps the radiation emitted from the ground. The deck blocks the short wavelength of the solar radiation emitted from the ground (below the upper limit of the visible spectrum) and allows the radiation of a longer wavelength to pass (above the upper limit of the visible spectrum). Thus, the ground below the deck/cover gets hot.

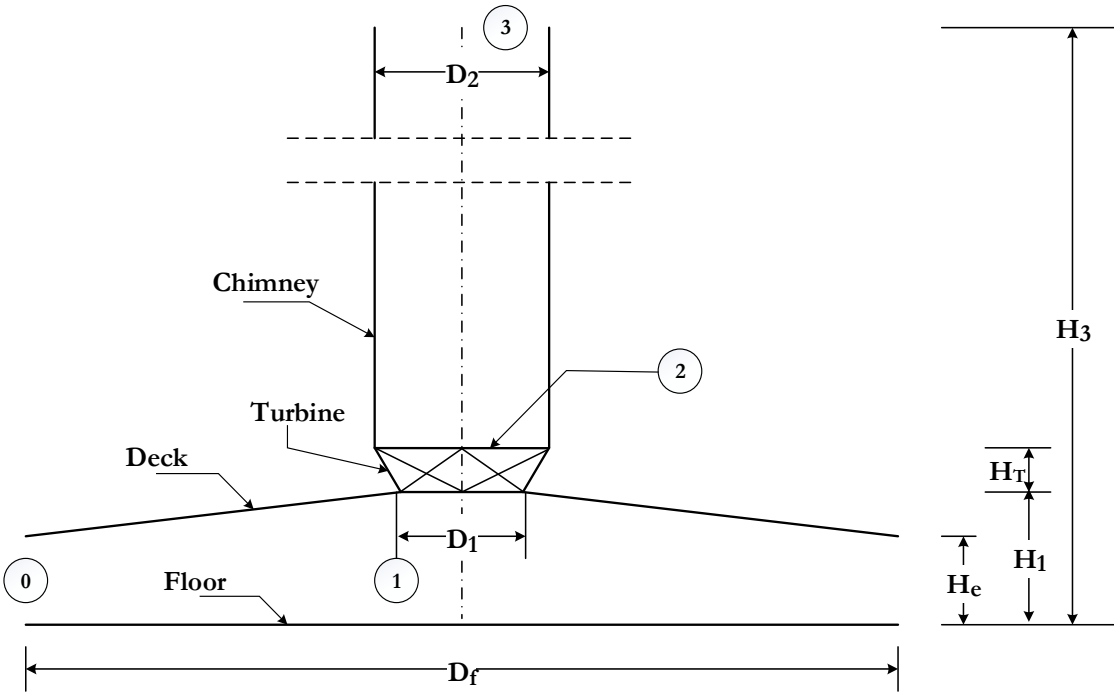

Figure 3.1. A schematic diagram of an SCPP

Figure 3.1 depicts a schematic diagram of the SCPP evaluated in this study. The air enters the collector through point 0 with a gap of H_e. The floor of the collector under the transparent cover has a diameter of D_f, the deck is at an inclination to ensure a constant radial cross-sectional area of flow of the radially directed air. The constant radial cross-section implies the following equation (3.1).

$$\pi \times D_f \times H_e = \pi \times D_1 \times H_1 = \pi \times D_1^2/4 \quad (3.1)$$

The known values of H_e and D_f allow the determination of the inlet turbine diameter and height at location 1 using the Equations (3.2) and (3.3):

$$D_1 = \left(4 \times D_f \times H_e\right)^{1/2} \quad (3.2)$$

$$H_1 = D_1/4 \quad (3.3)$$

Radiation from the floor heats the air from state 0 to state 1. Heated air expands in the turbine reaching state 2. The inlet and outlet diameters of the turbine are D_1 and D_2, respectively, which are related by Equation (3.4).

$$D_1 = 0.95 \times D_2 \quad (3.4)$$

Here, the height of the turbine is H_T; ($H_1 + H_T = H_2$). Air after expansion leaves the SCPP through the top of the chimney, which has a height of H_3. Although the chimney height H_3 can vary between 10.5 and 22 times of the outlet diameter of the turbine, Zhou et al. [21] states that the maximum power that can be obtained is 19.15 times the outlet diameter of the turbine. The dimensions of the SCPP model evaluated in this study are those described by Petela [28] and are provided in Table 3-1.

Table 3-1. The dimensions of the SCPP under evaluation [28]

Geometric Parameter	Dimensions (meter)
D_f	240
D_1	16.97
D_2	17.86
H_1	4.243
H_e	0.3
H_3	195

3.2 Energy Modeling of SCPP

The energy conservation principle was applied to each part of the SCPP. All energy components are represented by *E*. Six energy balance equations based on the control volume approach to the surface of the floor, air in the collector, collector, turbine, chimney, and air in the chimney are used as described by Petela [28] with a few adjustments, which are described in detail in the following sections.

Table 3-2. Line representation for the various modes of energy transfer

Line Representation	Mode of Energy
	Radiation
	Convection
	Enthalpy, Kinetic & Potential Energy

3.2.1 Energy Modeling of the Floor

The energy exchange at the floor is depicted in Figure 3.2 and described by Equation (3.5), where $E_{s\text{-}f}$ is the solar radiation energy absorbed by the floor, $E_{f\text{-}a}$ is the convection heat transfer between the floor and air, and $E_{f\text{-}d}$ is the radiation energy exchange between the floor and the deck.

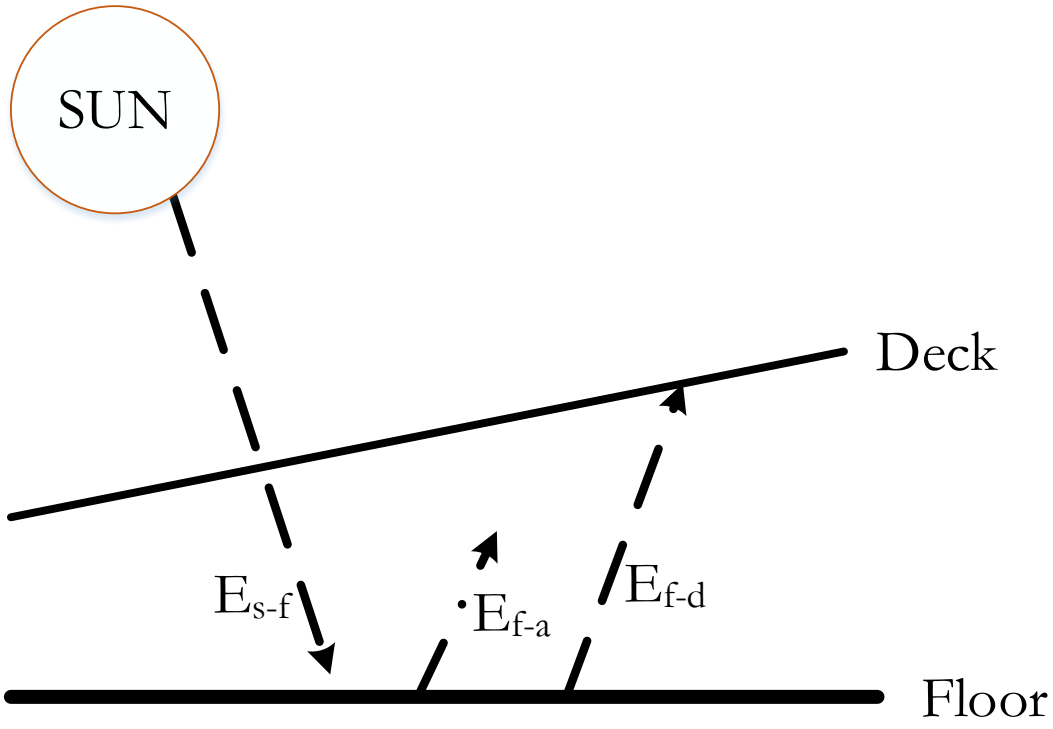

Figure 3.2. Energy Exchange at Floor

$$E_{S-f} = E_{f-a} + E_{f-d} \tag{3.5}$$

3.2.2 Energy Modeling of the Air Flowing Between the Floor and the Deck

The energy components received by the air between the floor and the deck are depicted in Figure 3.3 and the energy balance is described by Equation (3.6), where $E_{d\text{-}a}$ and $E_{f\text{-}a}$ are energies absorbed by air due to convective heat transfer from the deck and the floor, respectively. E_{a1}, E_{w1}, and E_{p1} are the respective gain in the enthalpy of air, and the kinetic and potential energy at location 1 when compared to the atmospheric conditions, i.e., location 0. E_{a0}, E_{w0}, and E_{p0} are respective enthalpy and kinetic and potential energy of air at location 0.

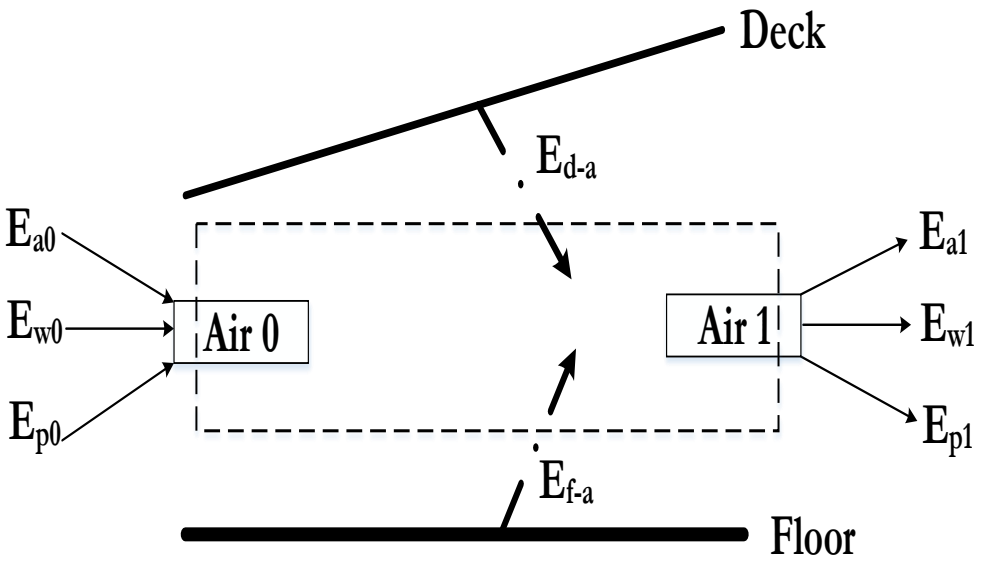

Figure 3.3. Energy components of the air flowing between the floor and the deck

$$E_{f-a} + E_{d-a} + E_{a0} + E_{w0} + E_{p0} = E_{a1} + E_{w1} + E_{p1} \quad (3.6)$$

3.2.3 Energy Modeling of the Collector

The energy balance for the collector (floor, deck, and air combined) is depicted in Figure 3.4 and described by Equation (3.7), where $E_{d\text{-}sky}$ is the exchange of radiation energy between the deck and the sky, $E_{d\text{-}amb}$ is the loss of energy from the deck to the atmosphere by convection heat transfer, and $E_{d\text{-}ch}$ is the loss of energy from the deck due to radiation exchange between the deck and the outer chimney surface.

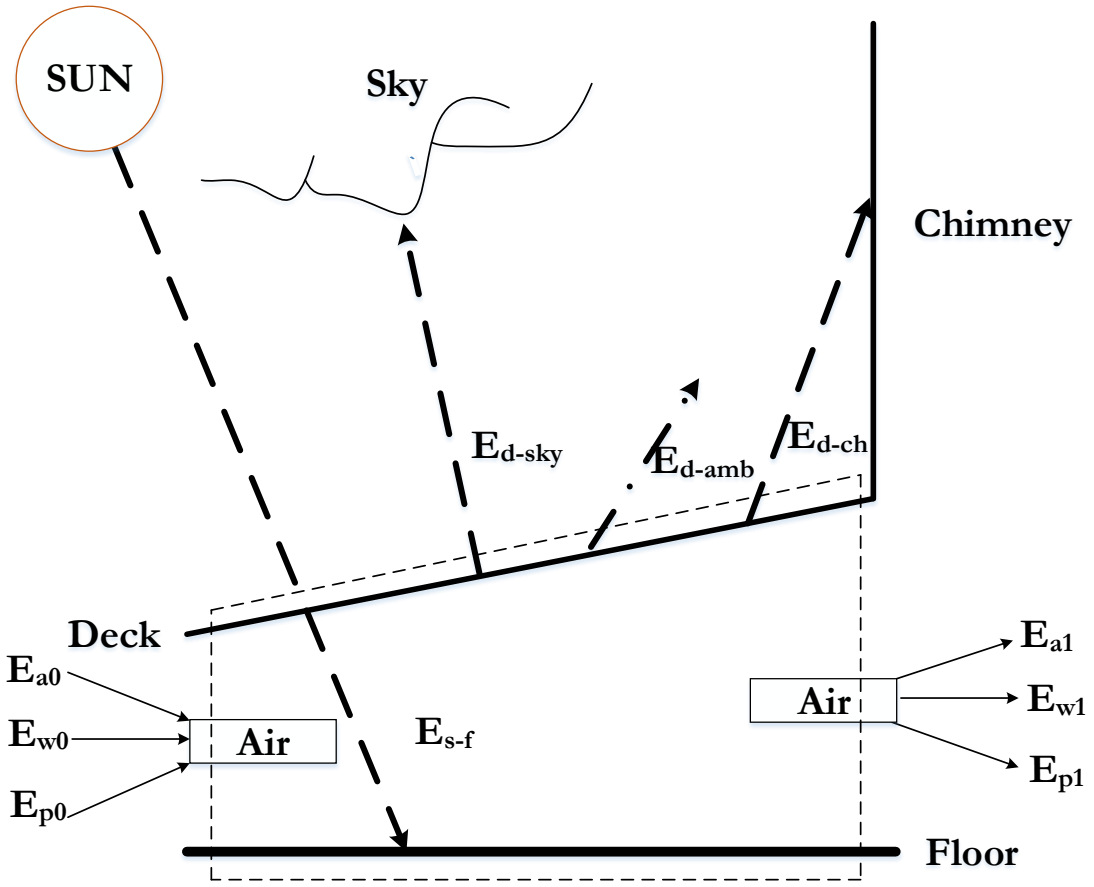

Figure 3.4. Energy exchange at the collector

$$E_{s-f} + E_{a0} + E_{w0} + E_{p0} = E_{a1} + E_{w1} + E_{p1} + E_{d-sky} + E_{d-amb} + E_{d-ch} \quad (3.7)$$

3.2.4 Energy Modeling of the Turbine

The energy balance across the turbine is depicted in Figure 3.5 and described by Equation (3.8), where E_{power} is the power generated by the turbine, and E_{a2}, E_{w2}, and E_{p2} are the respective gain or loss in enthalpy of air, and kinetic and potential energy at location 2, i.e., at the exit of the turbine.

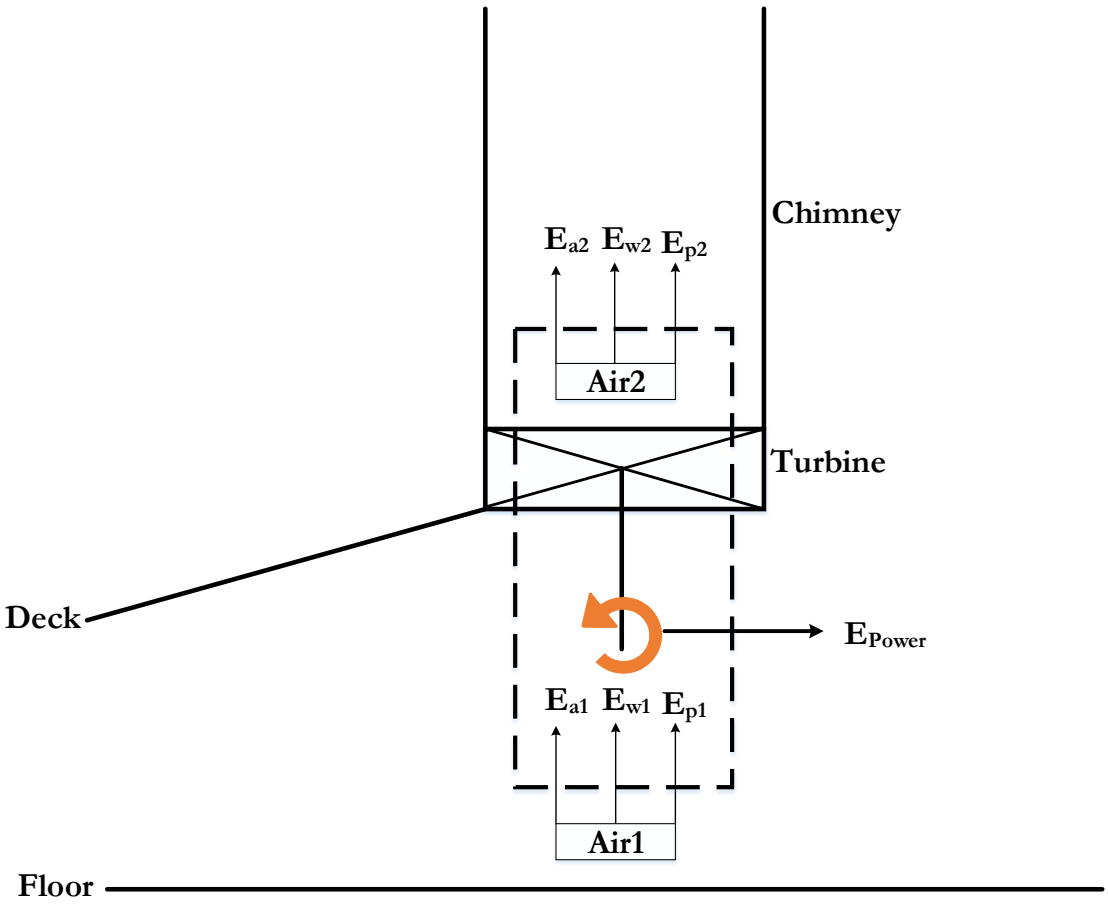

Figure 3.5. Energy exchange at the turbine

$$E_{a1} + E_{w1} + E_{p1} = E_{a2} + E_{w2} + E_{p2} + E_{Power} \quad (3.8)$$

3.2.5 Energy Modeling along the Chimney Surface

The energy exchange at the chimney is depicted in Figure 3.6 and described by Equation (3.9), where E_{a3}, E_{w3}, and E_{p3} are the respective gain or loss in enthalpy of air, and kinetic and potential energy at location 3, i.e., at the exit of the chimney, $E_{ch\text{-}sky}$ is the radiation exchange between the chimney and the sky, $E_{ch\text{-}gr}$ is the radiation heat transfer from the chimney to the ground, and $E_{ch\text{-}amb}$ is the gain in energy by air surrounding the chimney by

convection heat transfer. Heat gained through solar radiation incident on the chimney surface is negligible owing to the chimney being vertical and cylindrical in shape.

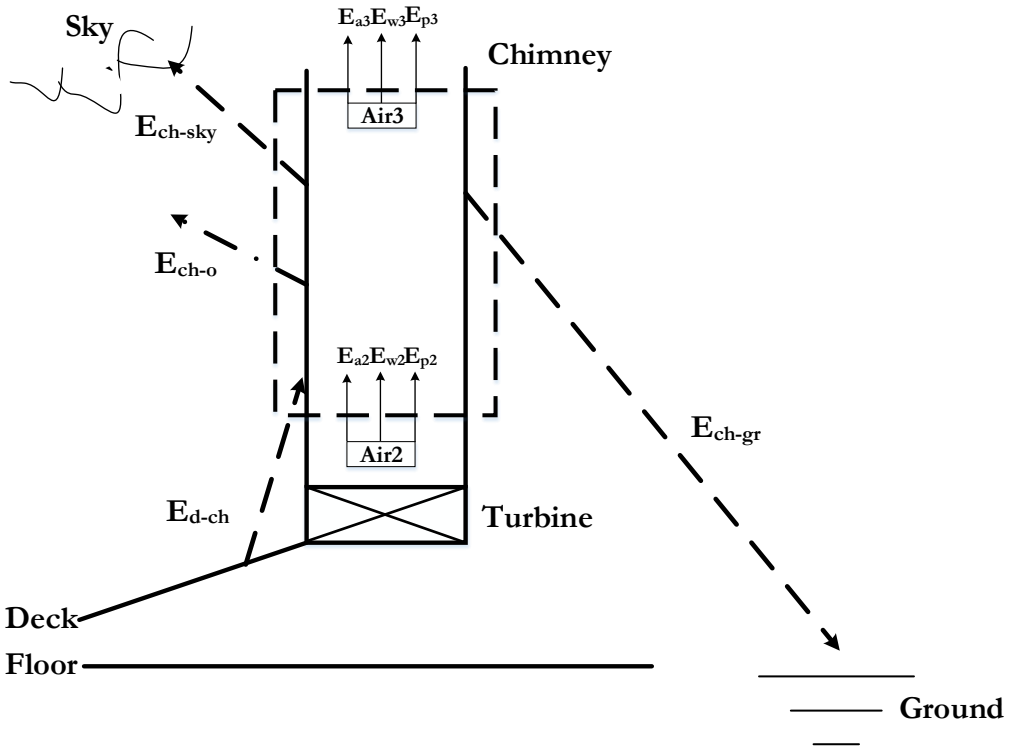

Figure 3.6. Energy exchange along the chimney surface

$$E_{a2} + E_{w2} + E_{p2} + E_{d-ch} = E_{a3} + E_{w3} + E_{p3} + E_{ch-amb} + E_{ch-sky} + E_{ch-gr} \quad (3.9)$$

3.2.6 Energy Modeling for Air Flowing in the Chimney

The energy balance for the air flowing in the chimney is depicted in Figure 3.7 and described by Equation (3.10), where $E_{a\text{-}ch}$ is the convection heat transfer between the inner surface of the chimney and the air flowing across locations 2 and 3.

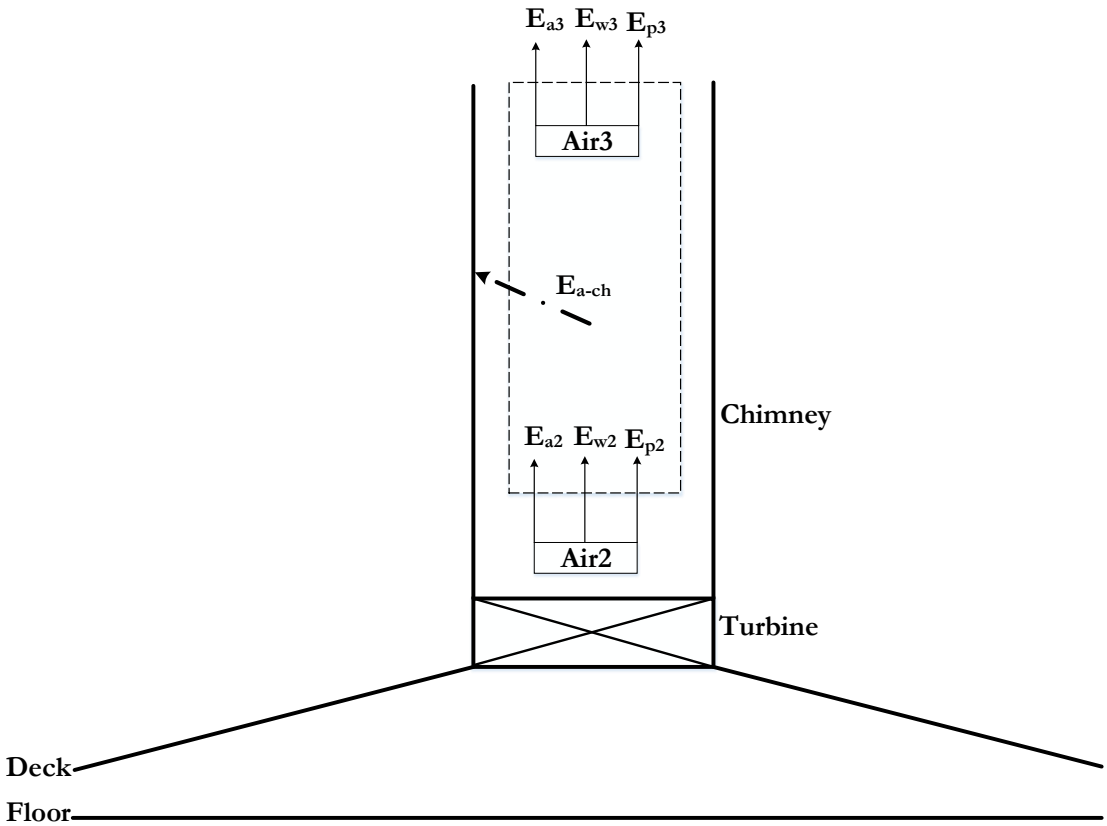

Figure 3.7. Energy distribution of the air flowing in the chimney

$$E_{a2} + E_{w2} + E_{p2} = E_{a-ch} + E_{a3} + E_{w3} + E_{p3} \quad (3.10)$$

3.2.7 Brief on Energy Terms of the Modeling

This section explains, each of the term associated with the above-discussed model.

The Kinetic energies at locations 1, 2, and 3 are calculated using the well-known formula Equation (3.11) using their respective velocities.

$$E_w = m \times w^2/2 \quad (3.11)$$

The mass flow rate *m* is calculated using Equation (3.12).

$$m = 0.25 \times \pi \times D_1^2 \times w_1 \times \rho_{a1} \tag{3.12}$$

Enthalpy of air at locations 1, 2, and 3 are calculated using the respective air temperatures using Equation (3.13).

$$E_a = m \times c_p \times (T_a - T_0) \tag{3.13}$$

The potential energies of air at locations 1, 2, and 3 are calculated using the formula Equation (3.14) derived by Petela [57]:

$$E_p = m\left\{-\frac{1}{\rho d}\left[\frac{b}{6d}(\rho - e)^3 + \frac{a}{2}(\rho - e)^2\right]\right\} \tag{3.14}$$

where, *a*, *b*, *d*, and *e* are constants, as defined by Equations (3.15), (3.16), (3.17), and (3.18) according to Petela [57–59].

$$a = 9.7807 \ {}^{m}/_{s^2} \tag{3.15}$$

$$b = -3.806 * 10^{-6} \ {}^{1}/_{s} \tag{3.16}$$

$$d = -9.973 * 10^{-5} \ {}^{kg}/_{m^4} \tag{3.17}$$

$$e = 1.217 \ {}^{kg}/_{m^3} \tag{3.18}$$

The overall solar energy received by the floor of the collector is defined by Equation (3.19).

$$E_{S-f} = \tau_d \varepsilon_f I A_f \tag{3.19}$$

where *I* is the incident solar radiation on the earth surface, τ_d is the transmissivity of the deck, ε_f is the emissivity of the collector floor, and $A_f$is the surface area of the floor calculate from Equation (3.20).

$$A_f = \pi(D_f^2 - D_1^2)/4 \tag{3.20}$$

Energy radiated from the floor to the deck is described by Equation (3.21).

$$E_{f-d} = \varepsilon_f A_f \sigma(T_{fE}^4 - T_{dE}^4) \tag{3.21}$$

where, T_{fE} and T_{dE} are the effective temperature of the floor and the deck, respectively.

Energy transfer from the floor to the air by convection is given by Equation (3.22).

$$E_{f-a} = A_f h_{f-a}(T_{fE} - T_{aE}) \tag{3.22}$$

where, T_{aE} is the effective temperature of air in the collector.

Energy transfer from the deck to the air by convection is given by Equation (3.23).

$$E_{d-a} = A_d h_{d-a}(T_{dE} - T_{aE}) \tag{3.23}$$

The energy radiated by the deck to the chimney is calculated by Equation (3.24).

$$E_{d-ch} = \varepsilon_d \, \phi_{d-ch} A_d \sigma(T_{dE}^4 - T_{ch}^4) \tag{3.24}$$

where, T_{dE} and T_{ch} are the effective temperature of the deck and chimney surface, respectively, and σ is the Stefan-Boltzmann constant. The shape factor for radiation from the deck to the chimney ϕ_{d-ch}can be calculated by Equation (3.25).

$$\phi_{d-ch} A_d = \phi_{ch-d} A_{ch} \tag{3.25}$$

where the lateral surface area of the deck is similar to the frustum of a cone and area of the deck A_d is defined by Equation (3.26).

$$A_d = \frac{\pi}{2}\left(D_f^2 - D_1^2\right)\sqrt{\left(\frac{H_1 - H_e}{D_f - D_1}\right)^2 + \frac{1}{4}} \tag{3.26}$$

The surface area of the chimney is defined by Equation (3.27).

$$A_{ch} = \pi \times c_D \times D_2 \times (H_3 - H_2) \tag{3.27}$$

where, c_D is a factor used to account for the thickness of the chimney wall.

The value of ϕ_{ch-d}can be determined by Equation (3.28).

$$\phi_{ch-d} = 0.5 \times (90 - \beta)/90 \tag{3.28}$$

The value for β is found from Equation (3.29).

$$\tan\beta = 2 \times H_3/D_f \tag{3.29}$$

Energy transfer from the deck to the ambient air by convection is given by Equation (3.30).

$$E_{d-amb} = A_d h_{d-amb}(T_{dE} - T_{amb}) \tag{3.30}$$

where, T_{amb} is the ambient temperature and h_{d-amb} is the convective heat transfer coefficient between the deck and the atmosphere.

Energy radiated from the deck to the sky is given by Equation (3.31).

$$E_{d-sky} = \varepsilon_d \phi_{d-sky} A_d \sigma(T_{dE}^4 - T_{sky}^4) \tag{3.31}$$

Energy transfer from the chimney to the environment by convection is given by Equation (3.32).

$$E_{ch-amb} = A_{ch} h_{ch-amb} (T_{ch} - T_{amb}) \tag{3.32}$$

where, T_{ch} is the effective temperature of the surface of the chimney and h_{ch-amb} is convective heat transfer coefficient between the outer surface of the chimney and the atmosphere.

Energy radiated from the chimney to the sky is given by Equation (3.33).

$$E_{ch-sky} = \varepsilon_{ch} \phi_{ch-sky} A_{ch} \sigma (T_{ch}^4 - T_{sky}^4) \tag{3.33}$$

Energy radiated from the chimney to the ground, which is not a part of the collector is given by Equation (3.34).

$$E_{ch-gr} = \varepsilon_{ch} \phi_{ch-gr} A_{ch} \sigma (T_{ch}^4 - T_{gr}^4) \tag{3.34}$$

The formula suggested by Swinbank [60] described by Equation (3.35) is used to determine the temperature of the sky.

$$T_{sky} = 0.0552 * T_0^{1.5} \tag{3.35}$$

The shape factor relationships are described by Equations (3.36) and (3.37).

$$\phi_{d-sky} + \phi_{d-ch} = 1 \tag{3.36}$$

$$\phi_{ch-sky} + \phi_{ch-d} + \phi_{ch-gr} = 1 \tag{3.37}$$

where, $\phi_{ch-sky} = 0.5$ and the other shape factors are calculated using Equations (3.25), (3.28), (3.36), and (3.37).

Energy transfer from the air inside the chimney to the chimney wall by convection is given by Equation (3.38).

$$E_{a-ch} = \pi D_2 (H_3 - H_2) h_{a-ch} \left(\frac{T_{a2} + T_{a3}}{2} - T_{ch} \right) \quad (3.38)$$

where, T_{a2} and T_{a3} are temperature of air the at location 2 and 3.

In the above equations, $h_{a\text{-}ch}$ is the convective heat transfer coefficient for air flowing through the chimney.

The convective heat transfer coefficient h_{a-ch} can be determined using Equation (3.39).

$$h_{a-ch} = Nu \times k/D_2 \quad (3.39)$$

The Energy transfer $E_{a\text{-}ch}$ from air to the chimney is by forced convection due to the external agency effect from the turbine, seated at the bottom of the chimney. Hence, Dittus-Boelter equation for heating of fluids (Equation (3.40)) is used to determine the Nusselt number for turbulent internal flow through a tube, using the Reynolds number (Re).

$$Nu = 0.023 \times Re^{0.8} \times Pr^{0.4} \quad (3.40)$$

The Reynolds number is calculated using Equation (3.41).

$$Re = w_2 D_2 / \nu \quad (3.41)$$

The Prandtl number (Pr) is considered as a constant for air (Pr = 0.7).

The convective heat transfer coefficient h_{f-a} is determined for free convection where the flow is turbulent. Nusselt number can be determined using Equation (3.42) described by Hollands et al. [61] for heat transfer to a fluid flowing between two extended parallel plates.

The deck and the floor are assumed to be parallel and horizontal as the inclination of the deck is only about 2^0.

$$Nu = 1 + 1.44\left[1 - \frac{1708(sin\ 1.8\theta)^{1.6}}{Ra\ cos\ \theta}\right]\left[1 - \frac{1708}{Ra\ cos\ \theta}\right]^{+} + \left[\left(\frac{Ra\ cos\ \theta}{5830}\right)^{\frac{1}{3}} - 1\right]^{+} \tag{3.42}$$

where, θ is the inclination angle, with the floor horizontal and the deck inclined about 2^0. The values of the cosine and the sine are not much different from those for an angle of zero. Hence, θ is assumed to be 0^0. *Ra* is the Rayleigh number which is the product of the Grashoff number and the Prandtl number.

Grashoff number is calculated using Equation (3.43).

$$Gr = \frac{g\beta\Delta T D_E^3}{\upsilon^2} \tag{3.43}$$

where g=9.81 m/s^2 is acceleration due to gravity,

$\beta = 1/T_{aE}$ (1/K) is volumetric coefficient of expansion for an ideal gas,

$\Delta T = T_{fE} - T_{dE}$ (K) is the temperature difference between the plates,

D_E is the characteristic length (m), and

υ is the kinematic viscosity of fluid (m^2/s).

The characteristic length for 3D flow can be calculated as the cube root of the volume of flow (*V*) between deck and floor under consideration, which can be described by Equation (3.44).

$$V = \left[\frac{\pi}{12}\left(\frac{H_1 - H_e}{D_f - D_1}\right)\left(D_f^3 - D_1^3\right)\right] + \frac{\pi}{4}D_f^2 H_e \tag{3.44}$$

The effective diameter or characteristic length is defined by Equation (3.45).

$$D_E = \sqrt[3]{V} \tag{3.45}$$

Hence the formula for heat transfer coefficient between the floor and the air, and the deck and the air is given by Equation (3.46).

$$h_{f-a} = h_{d-a} = \frac{Nu * k}{D_E} \tag{3.46}$$

Convective heat transfer coefficient between the deck and the atmosphere is described by Equation (3.47) according to McAdams [62] and Duffie and Beckman [63].

$$h_{d-amb} = 5\frac{W}{m^2}K \tag{3.47}$$

Convective heat transfer coefficient between the chimney and the atmosphere is described by Equation (3.48) according to McAdams [62] and Duffie and Beckman [63].

$$h_{ch-amb} = 7\frac{W}{m^2}K \tag{3.48}$$

Temperature T_{a2} is calculated using the equation for isentropic expansion in a turbine described by Equation (3.49).

$$\frac{T_{a2}}{T_{a1}} = \left(\frac{p_2}{p_1}\right)^{\frac{\kappa}{\kappa-1}} \tag{3.49}$$

Isentropic expansion coefficient, κ for air is 1.4. Internal efficiency of the turbine is η_T. Further, the temperature drop in the chimney can be estimated using Equation (3.50) proposed by Petela [58].

$$T_{a2} - T_{a3} = 0.154 \times D_2 \times H_3/m \tag{3.50}$$

For the maximum fluid power condition, the ratio between the turbine pressure drop and pressure potential is 2/3 as described in [7,13,14], and described by Equation (3.51).

$$\frac{P_1 - P_2}{P_1 - P_3} = \frac{2}{3} \tag{3.51}$$

The variation of pressure P_3 is described by Equation (3.52) according to Petela [59].

$$P_3 = P_0 - \frac{g_0 + g_3}{2}\frac{\rho_0 + \rho_3}{2} H_3 \tag{3.52}$$

where, P_3, g_3, and ρ_3 are the pressure, acceleration due to gravity, and the density at location 3, respectively. Here the acceleration due to gravity and the density is described by Equations (3.53) and (3.54) according to Petela [57,59]

$$g_3 = g_0 - 3.086 * 10^{-6} * H_3 \tag{3.53}$$

$$\rho_3 = \rho_0 - 9.973 * 10^{-5} * H_3 \tag{3.54}$$

The momentum conservation for the air flowing between the deck and the floor is described by Equation (3.55).

$$P_0 - P_1 = \rho_1 w_1^2 \tag{3.55}$$

Air distribution inside the collector was assumed to be linear. Therefore, the average temperature of the air inside the collector was calculated by Equation (3.56).

$$T_{aE} = (T_{amb} + T_{a1})/2 \tag{3.56}$$

The energetic efficiency of an SCPP is described by Equation (3.57).

$$\eta_{energy} = \frac{E_{power}}{E_{s-f}} * 100 \tag{3.57}$$

The following constants given in [28] are used for the calculations:

$T_{gr} = T_{amb} = T_0,\ c_D = 1.015$, $c_p = 1000 \frac{J}{kg} K$, $\kappa = 1.4$, $\eta_T = 0.7$, $H_T = 1\ m\ \tau_d = 0.95$, $\varepsilon_f = 1$, R = 287.04 $^{J}/_{kg\ K}$, $P_0 = 101.235\ kPa,\ g_0 = 9.81\ ^{m}/_{s^2}$.

3.3 Exergy Modeling of SCPP

Data from energy analysis can be used to interpret the results of exergy analysis performed using exergy balance equations. Exergy is represented by *X* and an exergy equation each was formulated for the floor, air within the collector, collector, turbine, and the chimney. The exergy balance equations are similar to energy balance equations but differ by an additional term of irreversibility or available work destroyed, which is represented by *ΔX*. Exergy exchange at the floor is analogous to the energy exchange as represented in Figure 3.2 and is described by Equation (3.58), where $X_{s\text{-}f}$ is the exergy associated with the solar radiation absorbed by the floor, $X_{f\text{-}a}$ is the exergy associated with the convection heat exchange between the floor and the air, $X_{f\text{-}d}$ is the exergy associated with the radiation

exchange between the floor and the deck, and ΔX_f is the exergy destruction associated with the floor.

$$X_{S-f} = X_{f-a} + X_{f-d} + \Delta X_f \tag{3.58}$$

The exergy exchange of air with the floor and the deck is analogous to the energy exchange as represented in Figure 3.3 and is described by Equation (3.59), where $X_{d\text{-}a}$ and $X_{f\text{-}a}$ are the exergies associated with air due to convective heat exchange with the deck and the floor, respectively. X_{a1}, X_{w1}, and X_{p1} are the respective exergies associated with the enthalpy of air, and the kinetic and potential exergy at location 1 when compared to atmospheric conditions, i.e., those at location 0. X_{a0}, X_{w0}, and X_{p0} are the respective exergies associated with the enthalpy of air, and the kinetic and potential exergy at location 0, and ΔX_a is the exergy destruction associated with the air between the floor and the deck.

$$X_{f-a} + X_{d-a} + X_{a0} + X_{w0} + X_{p0} = X_{a1} + X_{w1} + X_{p1} + \Delta X_a \tag{3.59}$$

The exergy exchange at the deck is analogous to the energy exchange for the collector as represented in Figure 3.4 and is described by Equation (3.60), where $X_{d\text{-}sky}$ is the exchange of radiation exergy between the deck and the sky, $X_{d\text{-}amb}$ is the loss of exergy from the deck to the atmosphere by convection heat transfer, $X_{d\text{-}ch}$ is the loss of exergy from the deck due to the radiation exchange between the deck and outer surface of the chimney, and ΔX_d is the exergy destruction associated with the collector.

$$\begin{aligned} X_{s-f} + X_{a0} + X_{w0} + X_{p0} \\ = X_{a1} + X_{w1} + X_{p1} + X_{d-sky} + X_{d-amb} + X_{d-ch} + \Delta X_d \end{aligned} \tag{3.60}$$

The exergy balance across the turbine is analogous to the energy balance as represented in Figure 3.5 and is described by Equation (3.61), where X_{power} is the exergy associated with

the work done or power generated by the turbine, X_{a2}, X_{w2}, and X_{p2} are the respective exergies associated with the gain or loss in the enthalpy of air, and the kinetic and potential exergy at location 2, i.e., at the exit of the turbine, and ΔX_T is the exergy destruction associated with the turbine.

$$X_{a1} + X_{w1} + X_{p1} = X_{a2} + X_{w2} + X_{p2} + X_{Power} + \Delta X_T \tag{3.61}$$

The exergy exchange across the chimney is analogous to the energy exchange across the chimney as represented in Figure 3.6 and is described by Equation (3.62), where X_{a3}, X_{w3}, and X_{p3} are the respective exergies associated with the gain or loss in the enthalpy of air, and the kinetic and potential exergy at location 3, i.e., at the exit of the chimney, $X_{ch\text{-}sky}$ is the exergy associated with the radiation exchange between the chimney and the sky, $X_{ch\text{-}gr}$ is the exergy associated with the radiation heat transfer from the chimney to the ground, $X_{ch\text{-}amb}$ is the gain in exergy by the air surrounding the chimney by convection heat transfer, and ΔX_{ch} is the exergy destruction associated with the chimney.

$$\begin{aligned} X_{a2} + X_{w2} + X_{p2} + X_{d-ch} & \\ = X_{a3} + X_{w3} + X_{p3} + X_{ch-amb} + X_{ch-sky} + X_{ch-gr} & \\ + \Delta X_{ch} & \end{aligned} \tag{3.62}$$

Exergy of solar radiation, X_s, as described by Petela [64] is 90% of the radiation energy.

$$X_S = 0.9 \times E_s \tag{3.63}$$

The radiation exergy X of a surface with a surface area of A, the emissivity of ε, and temperature of T is expressed by Equation (3.64) according to Petela [64–66] and Szargut et al. [67].

$$X = \varphi A \varepsilon \frac{\sigma}{3}(3T^4 + T_0^4 - 4T_0T^3) \quad (3.64)$$

Where, φ is the shape factor which depends on the geometry of the surface under study and with respect to the black surface at which considered radiation would arrive. Radiation exergy swapped between any two surfaces at different temperature T_x and T_y can be determined by Equation (3.64) for both surfaces, which leads to Equation (3.65).

$$X_{x-y} = \varphi_{x-y} A_x \varepsilon_{x-y} \frac{\sigma}{3}\left[3\left(T_x^4 - T_y^4\right) - 4T_0\left(T_x^3 - T_y^3\right)\right] \quad (3.65)$$

where, $\varepsilon_{x\text{-}y}$ is the effective emissivity which depends on the emissivities ε_x and ε_y of respective surfaces and formulated similarly to the equations of radiation exergy exchange. The effective emissivity reduces to $\varepsilon_{x\text{-}y}=1$ when the emissivities $\varepsilon_x = \varepsilon_y = 1$. Equation (3.65) is used to calculate radiation exergies: $X_{d\text{-}sky}$, $X_{f\text{-}d}$, $X_{d\text{-}ch}$, $X_{ch\text{-}sky}$ and $X_{ch\text{-}gr.}$

Exergy associated with the radiation energy exchange between the floor and the deck is given by the Equation (3.66).

$$X_{f-d} = \varphi_{f-d} A_f \varepsilon_{f-d} \frac{\sigma}{3}\left[3\left(T_{fE}^4 - T_{dE}^4\right) - 4T_0\left(T_{fE}^3 - T_{dE}^3\right)\right] \quad (3.66)$$

The shape factor between the floor and the deck is 1, as they are assumed parallel considering that the slope of the deck is less than 2^0.

Exergy associated with the radiation energy exchange between the deck and the chimney is given by Equation (3.67).

$$X_{d-ch} = \varphi_{d-ch} A_d \varepsilon_{d-ch} \frac{\sigma}{3}\left[3(T_{dE}^4 - T_{ch}^4) - 4T_0\left(T_{dE}^3 - T_{ch}^3\right)\right] \quad (3.67)$$

Exergy associated with the radiation energy exchange between the deck and the sky is given by Equation (3.68).

$$X_{d-sky} = \varphi_{d-sky} A_d \varepsilon_{d-sky} \frac{\sigma}{3}\left[3\left(T_{dE}^4 - T_{sky}^4\right) - 4T_0\left(T_{dE}^3 - T_{sky}^3\right)\right] \quad (3.68)$$

Exergy associated with the radiation energy exchange between the chimney and the sky is given by Equation (3.69).

$$X_{ch-sky} = \varphi_{ch-sky} A_{ch} \varepsilon_{ch-sky} \frac{\sigma}{3}\left[3\left(T_{ch}^4 - T_{sky}^4\right) - 4T_0\left(T_{ch}^3 - T_{sky}^3\right)\right] \quad (3.69)$$

Exergy associated with the radiation energy exchange between the chimney and the ground is given by Equation (3.70).

$$X_{ch-gr} = \varphi_{ch-gr} A_{ch} \varepsilon_{ch-gr} \frac{\sigma}{3}\left[3\left(T_{ch}^4 - T_{gr}^4\right) - 4T_0\left(T_{ch}^3 - T_{gr}^3\right)\right] \quad (3.70)$$

The physical exergy of air at locations 1, 2, and 3 are calculated by Equation (3.71) substituting the respective temperature and pressure at the three locations.

$$X_a = m\left[c_p(T_a - T_0) - T_0\left(C_p\, ln\frac{T_a}{T_0} - R\, ln\frac{P_a}{P_0}\right)\right] \quad (3.71)$$

where, C_p and R are the specific heat and gas constant of air. Apparently, the exergy of air entering the collector is zero, given that the air is at ambient conditions. Exergy X associated with a surface at temperature T in contact with air, where energy transfer is by convective heat transfer, depends on energy E, and is given by the orthodox Equation (3.72) of thermodynamics.

$$X = E\left(1 - \frac{T_0}{T}\right) \quad (3.72)$$

Equation (3.72), is used for calculations of the four exergies $X_{f\text{-}a}$, $X_{d\text{-}a}$, $X_{d\text{-}amb}$, and $X_{ch\text{-}amb}$. Exergy associated with the energy transfer between the floor and the air flowing through the collector is given by Equation (3.73).

$$X_{f-a} = E_{f-a}\left(1 - \frac{T_0}{T_{fa}}\right) \tag{3.73}$$

where, $T_{f\text{-}a}$ is the mean of effective temperature of the floor and air flowing through the collector.

$$T_{f-a} = \frac{T_{fE} + T_{aE}}{2} \tag{3.74}$$

Exergy associated with the energy transfer between the deck and the air flowing through the collector is given by Equation (3.75).

$$X_{d-a} = E_{d-a}\left(1 - \frac{T_0}{T_{da}}\right) \tag{3.75}$$

$T_{d\text{-}a}$ is the mean effective temperature of the deck and the air flowing through the collector.

$$T_{d-a} = \frac{T_{dE} + T_{aE}}{2} \tag{3.76}$$

Exergy associated with the energy transfer between the deck and the atmosphere is given by Equation (3.77).

$$X_{d-amb} = E_{d-amb}\left(1 - \frac{T_0}{T_{d-amb}}\right) \tag{3.77}$$

$T_{d\text{-}amb}$ is the mean of the effective temperature of the deck and the atmosphere.

$$T_{d-amb} = \frac{T_{amb} + T_{dE}}{2} \tag{3.78}$$

Exergy associated with the energy transfer between the chimney and the atmosphere is given by Equation (3.79).

$$X_{ch-amb} = E_{ch-amb}\left(1 - \frac{T_0}{T_{ch-amb}}\right) \tag{3.79}$$

$T_{ch\text{-}amb}$ is the mean effective temperature of the chimney and the atmosphere.

$$T_{ch-amb} = \frac{T_{amb} + T_{ch}}{2} \tag{3.80}$$

In our analysis, kinetic exergies of air are equal to the kinetic energies, ($X_{w1}=E_{w1}$, $X_{w2}=E_{w2}$, $X_{w3}=E_{w3}$). Potential exergies of air are also equal to their respective energies ($X_{p1}=E_{p1}$, $X_{p2}=E_{p2}$, $X_{p3}=E_{p3}$).

The exergetic efficiency of an SCPP is given by Equation (3.81).

$$\eta_{exergy} = \frac{X_{power}}{X_{s-f}} * 100 \tag{3.81}$$

3.4 Model Validation

This section presents the analytical, numerical and experimental validation of the model developed in the previous section. Using simplifying assumptions Petela [28] presented a thermodynamic analysis of an SCPP model, with the set of established geometrical parameters used in the Manzanares SCPP. However, the formula used by Petela [28], is inconsistent for determining the effective diameter of a collector. Also, the heat transfer coefficient was determined using the forced convection correlations, whereas the operation of the SCPP is based on natural convection only. However, in the model developed, a detailed method for determining the effective diameter of a 3D flow and an appropriate heat transfer relations are used, which were clearly elucidated in the sections above. Results of the improved model are validated with the analytical case study of Petela [28], a numerical model of Mehrpooya et al. [27], and experimental model of Guo et al. [68].

3.4.1 Analytical Validation

All the equations of the improvised model, presented in the above sections are solved simultaneously using EES software, taking all losses into account. The equations are used to determine the theoretical final power output, and hence the theoretical efficiency. Table 3-3 shows a comparison of the results obtained in this study with those obtained by five case studies of Petela [28].

Table 3-3. Comparison of the results from present study and by Petela [28]

	Parameter	**Units**	**Case 1**	**Case 2**	**Case 3**	**Case 4**	**Case 5**
	Input						
1	S	W/m²	800	850	800	800	800
2	H_3	m	195	195	200	195	195
3	D_f	m	240	240	240	250	240
4	H_e	m	0.3	0.3	0.3	0.3	0.35
	Results obtained by Petela						
5	$eP\ (\eta)$	%	0.64	0.53	0.65	0.57	1.18
6	E_P	kW	229	203	234	222	423
	Results of the Present Study						
7	$eP\ (\eta)$	%	0.4325	0.3543	0.428	0.3815	0.8365
8	E_P	kW	147.962	128.789	146.402	141.63	285.923

Figure 3.8 depicts the variation of the heat transfer coefficient (h_{fa}) for the transfer of heat between the floor and the air, for the cases described by Petela [28], calculated using the approach proposed in this study. The values calculated by Petela [28] randomly vary due to the use of a dimensionally inconsistent formula to determine the effective diameter of a 3D flow. Also, a formula based on forced convection is used to determine the associated

Nusselt number, while the flow between the floor and the deck is due to free convection. This inconsistency was corrected in the approach proposed in this study by approximating the formula (Equation (3.42)) as suggested by Hollands et al. [61]. Variation in the values obtained by Petela [28] is due to the dependence of the Nusselt number on the Reynolds number, which depends on the velocity, and thus varies owing to changes in the velocity of air flow between the deck and the floor. However, in the proposed approach the Nusselt number is calculated based on the Grashoff number, which is a function of the volume expansion coefficient and the temperature difference between the floor and the deck. The average heat transfer coefficient (h_{fa}) for all the cases is approximately 2.544 W/m^2K with a slight variation, due to the change in solar irradiation and geometric parameters of the five cases. Heat transfer coefficient is nearly constant because for all the cases, Petela [28] assumed that the atmospheric temperature is 288.14K.

Figure 3.9 shows a comparison of the mass flow rate through the SCPP model for the five cases evaluated by Petela [28] and using the new approach. The variation of the mass flow rate determined by the new approach is deviating much with the results of Petela [28]. However, the values of the flow rate determined by the new approach are on the average lower by 32.91% owing to the increase in temperature of air in the collector, which is evident from Figure 3.10.

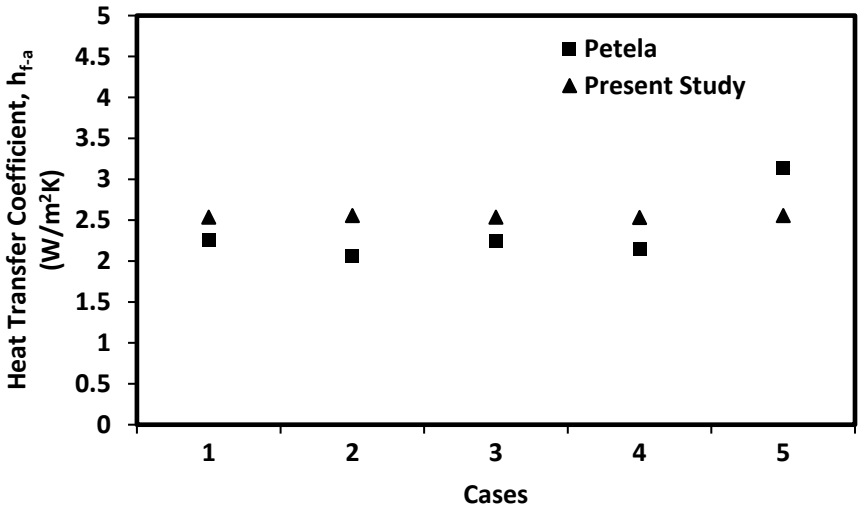

Figure 3.8. Variation of the heat transfer coefficient between the floor and the air

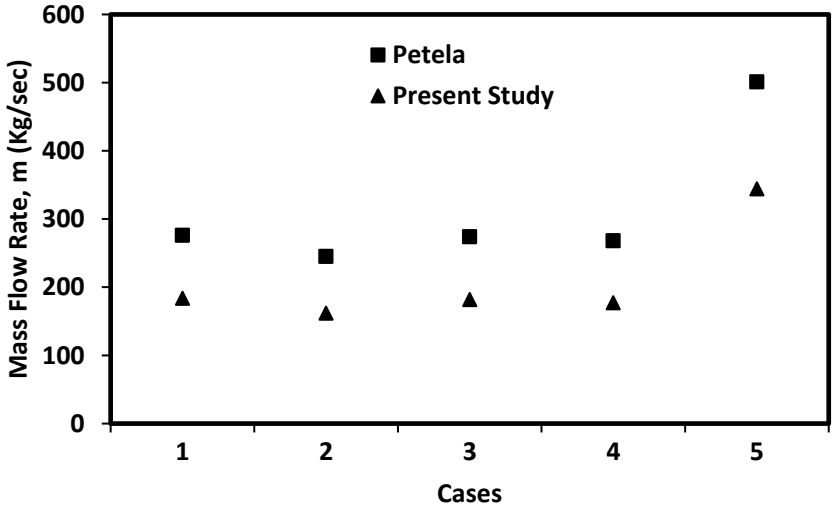

Figure 3.9. Variation of the mass flow rate

Figure 3.10 depicts a comparison of the variation of the temperature of the floor, deck, and air in the collector, determined in this study and by Petela [28]. The temperature of the floor and deck determined in the present study is lower owing to the increased heat transfer rate between the floor and air, and the deck and air, which is evident from the results shown

in Figure 3.8. Increase in the heat transfer rate translates into an increase of the temperature of the air between the floor and the deck. The average increase in the temperature of the air is 2.98%, while the average decrease in the temperature of the floor and the deck is 1.52% and 1.78%, respectively.

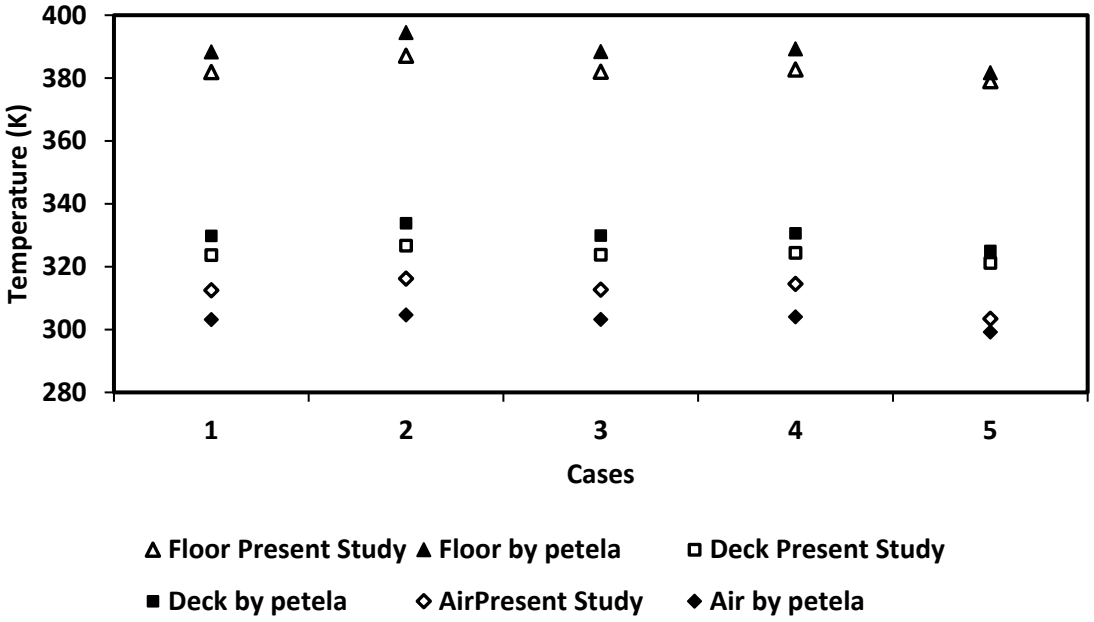

Figure 3.10. Variation of average temperatures of the floor, deck, and air

Figure 3.11 depicts a comparison of the variation of the energetic and exergetic efficiency and the power produced by the SCPP model, determined in this study and by Petela [28]. The results are also tabulated in Table 3-3. All the parameters determined by the proposed approach are lower owing to the decrease in the mass flow rate, evident from Figure 3.9. The rational efficiency, i.e., the ratio of the energetic efficiency to the exergetic efficiency, is 0.9 owing to the assumption that the radiation exergy from the sun is 0.9 of the solar energy (Equation (3.63)). The average decrease in the energetic and exergetic efficiency is

31.85% and 31.74%, respectively, whereas the average decrease in the power produced by the SCPP model is 35.11%.

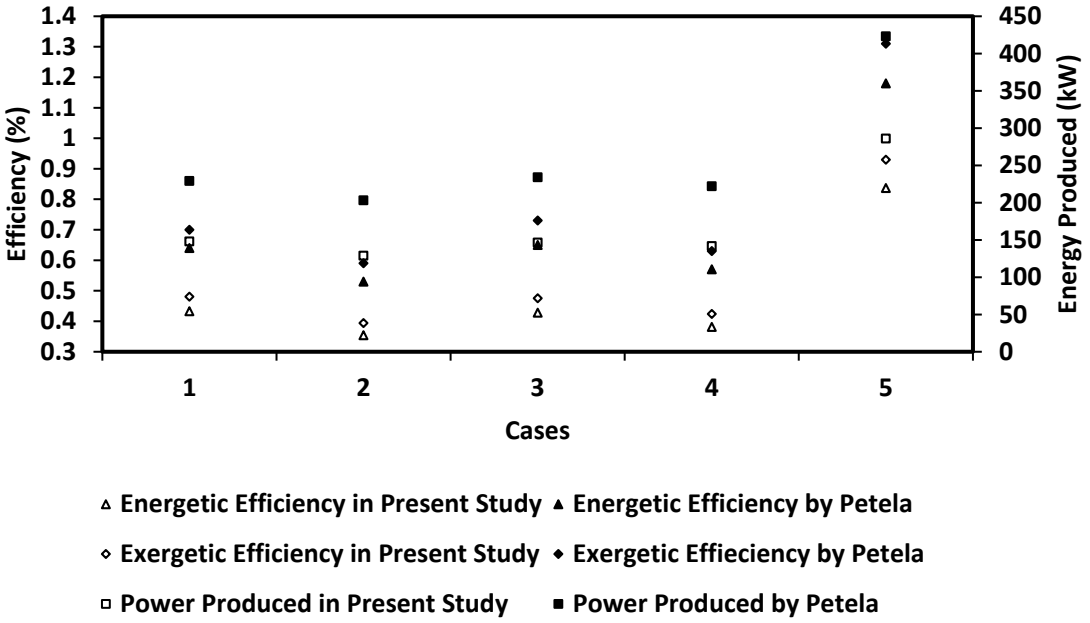

Figure 3.11. Variation of the power output and efficiencies

The increase in the temperature of air flowing through the collector as indicated by the results depicted in Figure 3.10, is expected to correspond to a higher power output and efficiency. However, as the density of air decreases with increasing temperature, there is a decrease in the mass flow rate. Hence, a lower energy output and efficiency are observed in this study, when compared to the results obtained by Petela [28]. From the above validation results, it is clear that the Petela model is over estimating the values of mass flow rate and efficiency.

3.4.2 Numerical Validation

To validate the improved model, its obtained results were compared with the 3D numerical model of Mehrpooya et al. [27] and analytical model of Petela [28]. The geometry of the 3D model is same as considered in the present study. Table 3-4 and Table 3-5 presents the comparison between the results of the improved model, 3D numerical model, and cases of an analytical model of Petela [28] for solar insolation of 800 Wm^{-2} and 850Wm^{-2} respectively.

Validation for Case1 at S = 800 Wm^{-2}

Table 3-4. Comparison of present study with numerical model at 800 Wm^{-2}

Parameter	Units	Present Study	Numerical Comparative Study Mehrpooya et al. [27]		Analytical Comparative Study Petela [28]		Relative Error between the results of Mehrpooya et al. [27] and Petela [28]
			Results by Numerical Study	Relative Error	Results by Analytical Study	Relative Error	
P_1	Pa	101234	98996	2.26	101233.66	0.00	2.21
P_2	Pa	99686	98993	0.70	99686.13	0.00	0.70
P_3	Pa	98912	98965	0.05	98912	0.00	0.05
w_1	m/s	0.7765	0.83	6.45	1.1	29.41	24.55
m	Kg/s	183.9	255	27.88	276	33.37	7.61
T_{fE}	K	381.9	364	4.92	388.3	1.65	6.26
T_{dE}	K	323.7	331	2.21	329.8	1.85	0.36
T_{a1}	K	336.9	338	0.33	318.19	5.88	6.23
T_{ch}	K	314.4	292	7.67	292.43	7.51	0.15

Validation for Case2 at S = 850 Wm^{-2}

Table 3-5. Comparison of present study with the numerical model at 850 Wm^{-2}

Parameter	Units	Present Study	Numerical Comparative Study Mehrpooya et al. [27]		Analytical Comparative Study Petela [28]		Relative Error between the results of Mehrpooya et al. [27] and Petela [28]
			Results by Numerical Study	Relative Error	Results by Analytical Study	Relative Error	
P_1	Pa	101234	98875	2.39	101233.93	0.00	2.33
P_2	Pa	99686	98875	0.82	99686.22	0.00	0.81
P_3	Pa	98912	98861	0.05	98912	0.00	0.05
w_1	m/s	0.6989	0.73	4.26	0.99	29.40	26.26
m	Kg/s	162	200	19.00	245	33.88	18.37
T_{fE}	K	387.1	409	5.35	394.5	1.88	3.68
T_{dE}	K	326.7	345	5.30	333.8	2.13	3.36
T_{a1}	K	344.2	331	3.99	321.08	7.20	3.09
T_{ch}	K	316.8	292	8.49	292.9	8.16	0.31

The average relative error for two cases between the results of the present study and 3D numerical model is less than 5.6%, almost all the results are in consensus with one another. There exists a wide relative error for the velocity of air at location1 (w_1) and mass flow rate (m). The pressure at location 3 (constraint with chimney height) is assumed too low in the numerical model which leads to high-density variation, thus predicting the higher values for velocity and mass flow rate. The deviation in temperature of the floor (T_{fE}) and temperature of the deck (T_{dE}) is due to incorrect Nusselt number correlation used in the later models for determining the heat transfer coefficient ($h_{f\text{-}a}$) and inconsistent formula for determining the effective diameter (D_E). The error for chimney surface temperature (T_{ch})

is 7%, this is due to inappropriate modeling for losses of chimney surface, which is corrected in the present study. The results of the model in the present study are in good agreement with the 3D numerical model of Mehrpooya et al. [27], when compared to the analytical model of Petela [28]. When the results of simplified models are in consensus with the numerical models, simplified models get an edge of an economic advantage as it requires little computation time and saves man-hours.

3.4.3 Experimental Validation

The SCPP model developed in the present study is validated with an experimental model of Guo et al.[68]. They built a laboratory model of SCPP and simulated it in an artificial environment to study the experimental behavior. By varying irradiation, the gain in temperature of air and updraft velocity were measured. Table 3-6 shows the dimensions of the experimental setup under evaluation. By varying the radiation intensities from 250 to 500 W/m^2 for the same set of geometry as experimental setup, results were obtained for the Petela model [28] and proposed model which are as shown below.

Table 3-6. The dimensions of the experimental model of SCPP [68]

Geometric Parameter	Dimensions (meter)
D_f	1.22
D_1	0.05
H_3	1

The variation of updraft velocity by Petela approach, proposed approach, and experimental model is shown in Figure 3.12. The values of updraft velocity (*w1*) predicted by proposed approach are 18% higher than the experimental values, whereas the Petela model predicts the updraft velocity with a higher variance of 70%. The higher variance for Petela[28] is due to the improper modeling of air flowing through the chimney which is corrected in

Equation (3.10). For the proposed model the values of updraft velocity are closer to experimental model when compared with Petela model.

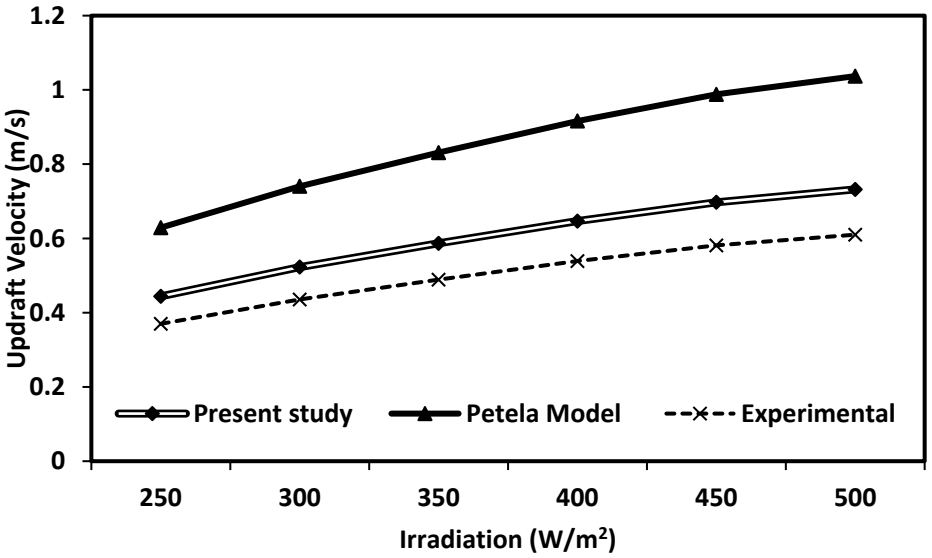

Figure 3.12. Validation of Updraft Velocity

Figure 3.13 depicts the variation of gain in temperature of air flowing through the collector. It is evident that as the radiation intensity increases, gain in temperature of air increases because of the increase in the thermal potential of the floor. The rise in temperature for the proposed model under consideration is 6.8% higher than the experimental rise, whereas the Petela model predicts the values 124% higher. The large deviation in a rise in temperature of the air by Petela model is due to incorrect Nusselt number correlation used for determining the heat transfer coefficient between floor, deck, and air. Also, due to an inconsistent formula for determining the effective diameter (D_E). The appropriate equations for determining the heat transfer coefficient and effective diameter are clearly elucidated in the above study.

Figure 3.14 shows the variation of collector efficiency. The values of collector efficiency predicted by Petela model are 184% higher than the experimental model, whereas the

proposed model under consideration predicts the values with the variance of 5.8% only. The higher values for Petela model are due to large temperature difference which is evident from Figure 3.13.

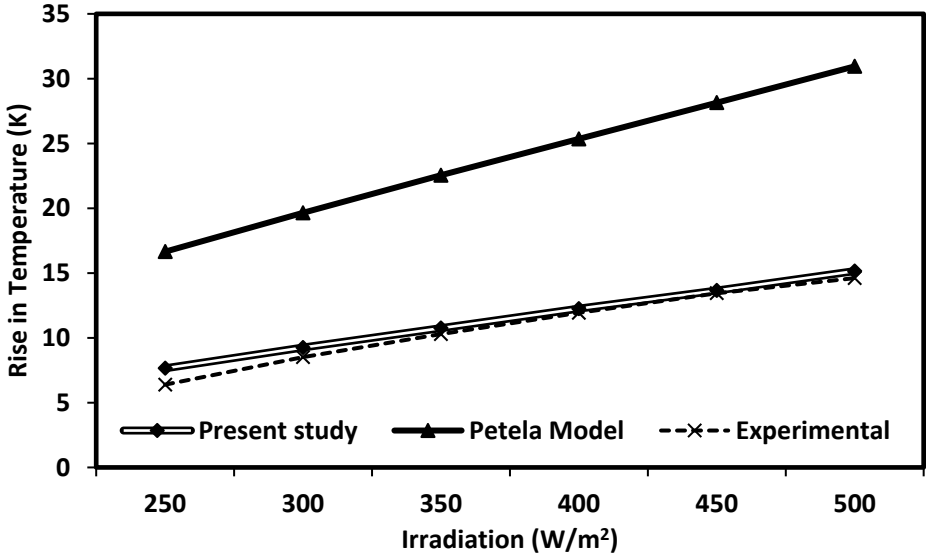

Figure 3.13. Validation of gain in temperature of air

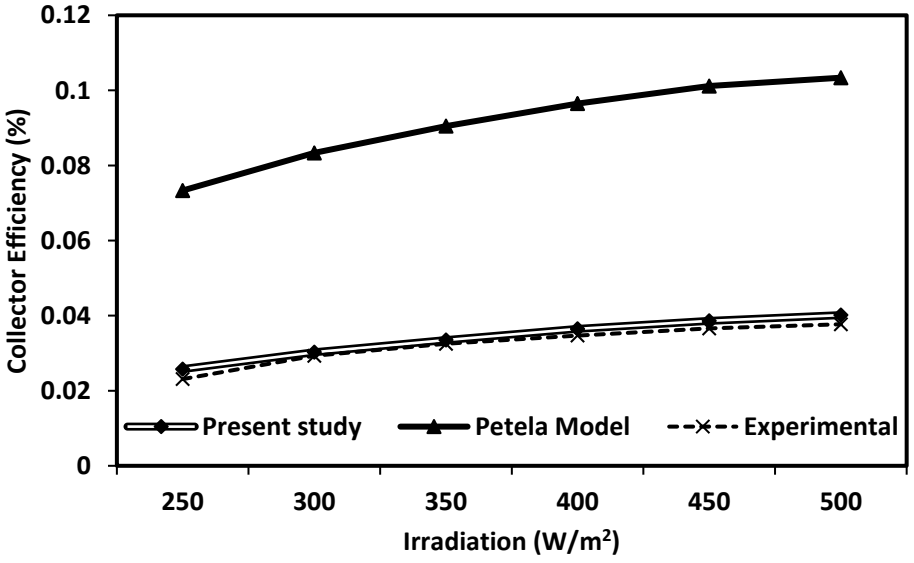

Figure 3.14. Validation of collector efficiency

It is evident from Figure 3.8 to Figure 3.11 that there exist high variance between the results of an analytical model of Petela [28] and the analytical model proposed in the present study. From Figure 3.12, Figure 3.13, and Figure 3.14, it is evident that there exists a fair agreement between the values obtained by the proposed model and the experimental setup, than the analytical model of Petela[28]. Moreover, the results of the 3D numerical model are complying with the results of the present study. Hence, the proposed model can be adopted for the analytical study of SCPP which predicts the real values of temperature and efficiency with the variance of 5-6%.

CHAPTER 4

MATHEMATICAL MODELING OF SOLAR CHIMNEY POWER PLANT AIDED WITH REFLECTORS

A mathematical model is developed to achieve the objectives of the present study. The first part of the mathematical model deals with geometric modeling of SCPP aided with reflectors. Once the geometric parameters are set, energy and exergy modeling of SCPP is carried out. The thermodynamic equations are derived by equaling the solar input energy from sun and reflectors, with the energy losses at various locations and the final output power. After establishing the correlations between the energy input and final output, all the equations are solved simultaneously using engineering equation solver (EES) software. Then, the SCPP model aided with reflectors is analyzed for the solar irradiation conditions prevailing in Dhahran.

Energy modeling is followed by exergy modeling of SCPP, by considering the exergy associated with each of the energy term obtained in energy modeling, including the irreversibility (i.e., exergy destruction). After establishing the correlations between the qualities of input, output and associated irreversibility's, all the equations are solved simultaneously using EES. Then, the SCPP model is analyzed for determining the scope of improvement by performing the exergy analysis.

In the model discussed here, SCPP is aided with reflectors to increase the radiation incident on the floor of SCPP. All the reflectors are arranged in the similar pattern as heliostats of

solar tower reflecting towards the deck. The study conducted by Petela [28] , Hussain and Al-Sulaiman [69] is the basis for the analysis of SCPP. However, detail analysis for the reflectors is clearly elucidated in the study below. Few assumptions are taken into account while considering the analysis of reflectors, such as shape factors with respect to the mirror are determined considering the mean location of reflector field. The reflectors need constant tracking, to simplify our study, the angle of the reflector is assumed to be constant. The position of the reflector (i.e., the height of pole and dimensions of the reflector) should be optimized, for the sake of convenience it is assumed to be constant. The present study involves the simplified model to determine the varying trends of power output and efficiency if all the above assumptions are not considered it would incur huge computation time. The objective of the present study is to streamline the interpretative mathematical model of the SCPP aided with reflectors and to present the comparative study with the conventional SCPP.

4.1 Geometric Modeling of SCPP aided with reflectors

Figure 4.1 depicts a schematic diagram of an SCPP aided with reflectors, geometric parameters of the SCPP without reflectors are clearly elucidated in the previous chapter. All the mirrors are placed around the deck, in the circular pattern such that it resembles the field of heliostats uniformly directing towards the deck. They are placed in such a way that all the radiation falling onto the mirror is reflected onto the deck. The deck receives the direct radiation from the mirror in the form of reflection, diffuse radiation from the mirror is lost to sky and ground, a little amount of it is lost from the mirror by convective heat transfer to the atmosphere i.e., due to absorption of the mirror.

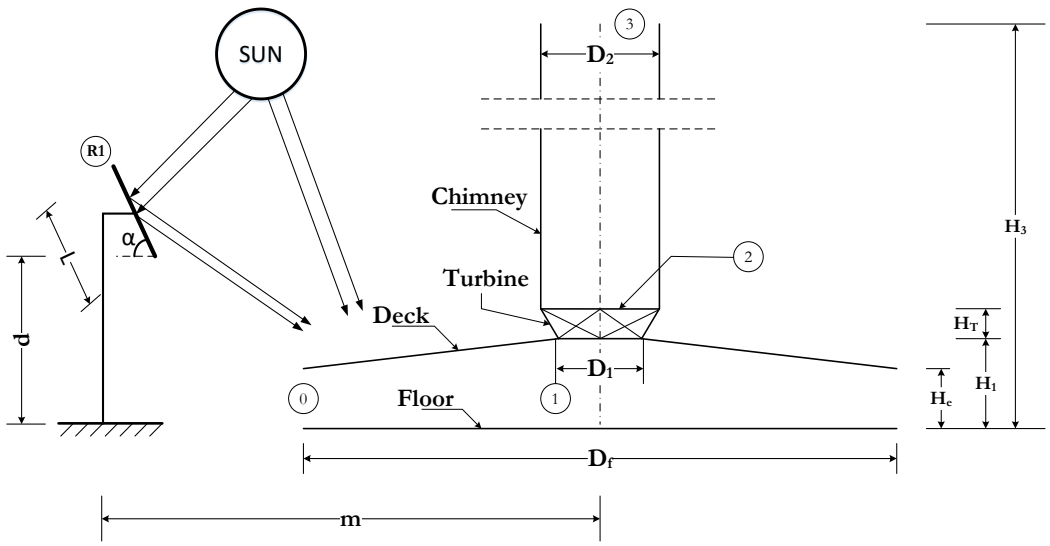

Figure 4.1. A Schematic diagram of an SCPP aided with reflectors

Here, *m* denotes the distance of mirror from the center of SCPP, *d*, denotes the height between lower edges of the mirror to the ground, *L*, denotes the length of a mirror placed at an angle *α*. Since the mirrors are placed around the deck in a concentric pattern, in the present analysis, we consider the location of the mirror along the mean position of the mirror field.

The ratio of reflection of the mirror on deck to each mirror area is assumed to be one, which implies a total area of mirrors required is equal to the area of the deck.

$$Number\ of\ mirrors = \frac{Total\ area\ of\ deck}{Area\ of\ each\ mirror} \tag{4.1}$$

The dimensions of SCPP and positioning of the mirror with respect to SCPP evaluated in this study are provided in Table 4-1.

Table 4-1. The dimensions of the SCPP aided with reflectors under evaluation

Geometric Parameter	Quantity
D_f	240 m
D_1	16.97 m
D_2	17.86 m
H_1	4.243 m
H_e	0.3 m
H_3	195 m
Area of each mirror	4 m^2
Number of mirrors	11260
m	150 m
L	2 m
d	10 m
Alpha (α)	70^0

4.2 Energy Modeling of SCPP aided with reflectors

The energy conservation principle was applied to each part of the SCPP including mirrors. All energy components are represented by *E*. Seven energy balance equations based on the control volume approach to the surface of the floor, air in the collector, collector, turbine, chimney, the air in the chimney and mirror are used, and are described in detail in the following sections.

Table 4-2. Line representation for the various modes of energy transfer

Line Representation	Mode of Energy
	Radiation
	Convection
	Enthalpy, Kinetic & Potential Energy

4.2.1 Energy Modeling of the Floor

The energy exchange at the floor is depicted in Figure 4.2 and described by Equation (4.2), where E_{s-f} is the solar radiation energy absorbed by the floor, E_{m-f} is the reflected solar radiation from mirror to floor, E_{f-a} is the convection heat transfer between the floor and air, and E_{f-d} is the radiation energy exchange between the floor and the deck.

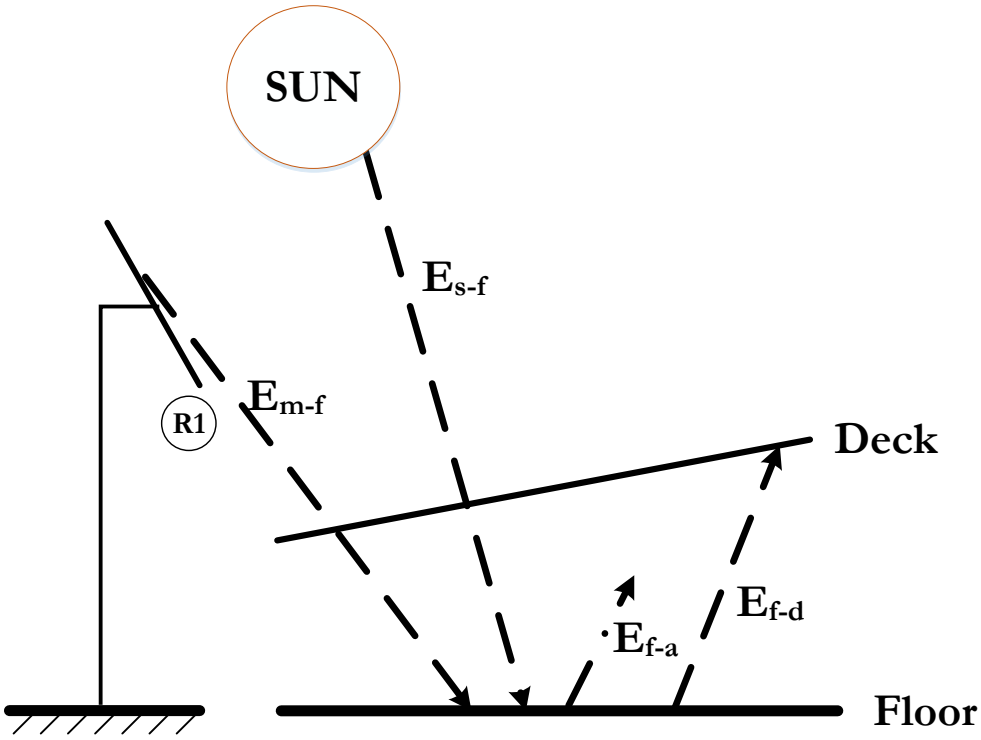

Figure 4.2. Energy exchange at the floor

$$E_{S-f} + E_{m-f} = E_{f-a} + E_{f-d} \tag{4.2}$$

4.2.2 Energy Modeling of the Air Flowing Between the Floor and the Deck

The energy components received by the air between the floor and the deck are depicted in Figure 4.3 and the energy balance is described by Equation (4.3), where $E_{d\text{-}a}$ and $E_{f\text{-}a}$ are energies absorbed by air due to convective heat transfer from the deck and the floor, respectively. E_{a1}, E_{w1}, and E_{p1} are the respective gain in the enthalpy of air, the kinetic and, the potential energy at location 1 when compared to the atmospheric conditions, i.e., location 0. E_{a0}, E_{w0}, and E_{p0} are respective enthalpy and kinetic and potential energy of air at location 0.

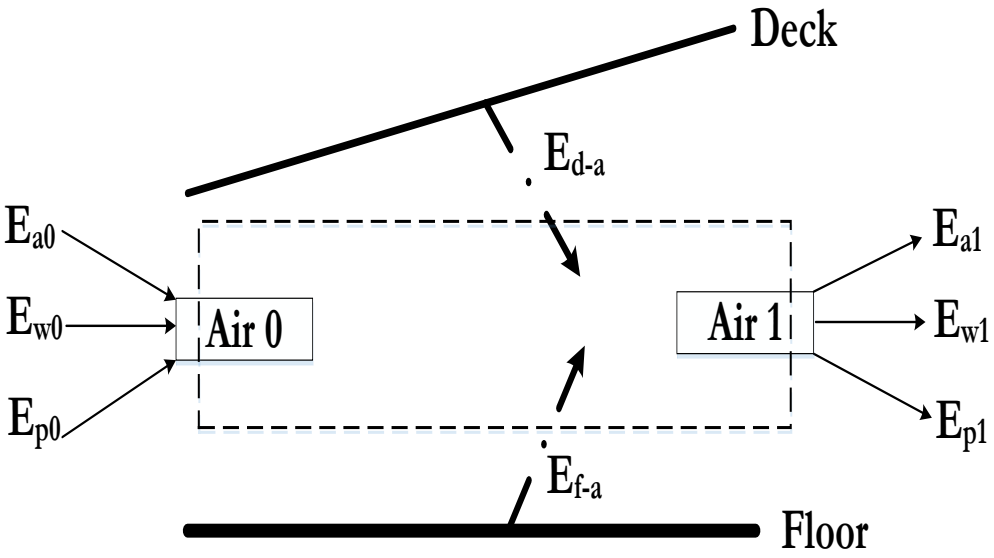

Figure 4.3. Energy components of the air flowing between the floor and the deck

$$E_{f-a} + E_{d-a} + E_{a0} + E_{w0} + E_{p0} = E_{a1} + E_{w1} + E_{p1} \quad (4.3)$$

4.2.3 Energy Modeling of the Collector

The energy balance for the collector (floor, deck, and air combined) is depicted in Figure 4.4 and described by Equation (4.4), where $E_{d\text{-}sky}$ is the exchange of radiation energy

between the deck and the sky, $E_{d\text{-}amb}$ is the loss of energy from the deck to the atmosphere by convection heat transfer, $E_{d\text{-}ch}$ is the loss of energy from the deck due to radiation exchange between the deck and the outer chimney surface, and $E_{d\text{-}m}$ is the exchange of radiation energy between the deck and the mirror.

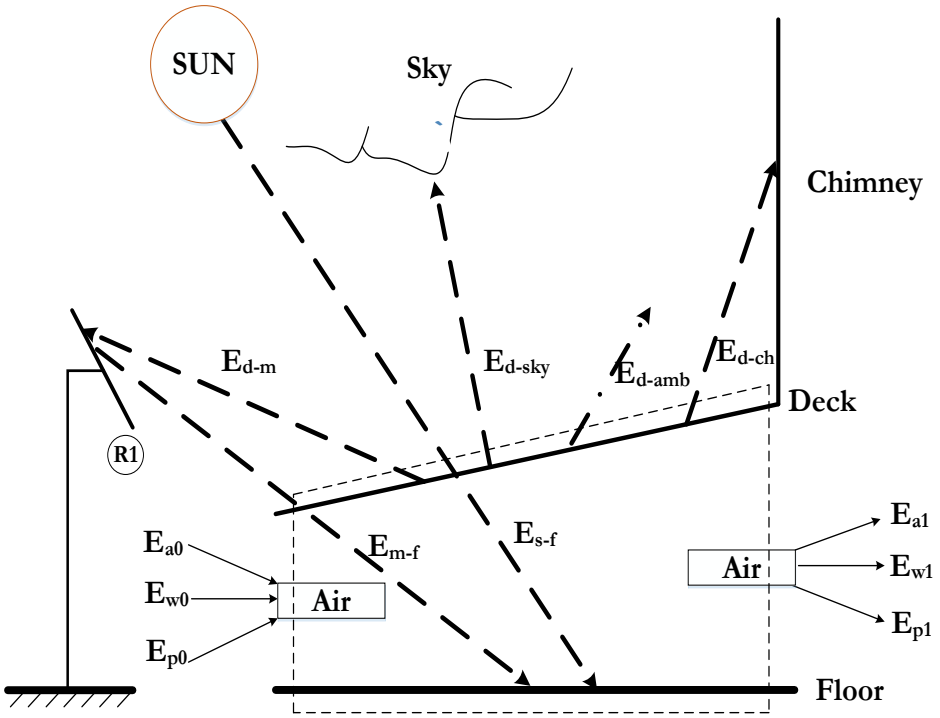

Figure 4.4. Energy exchange at the collector

$$E_{s-f} + E_{m-f} + E_{a0} + E_{w0} + E_{p0} = E_{a1} + E_{w1} + E_{p1} + E_{d-sky} + E_{d-amb} + E_{d-ch} + E_{d-m} \quad (4.4)$$

4.2.4 Energy Modeling of the Turbine

The energy balance across the turbine is depicted in Figure 4.5 and described by Equation (4.5), where E_{power} is the power generated by the turbine, and E_{a2}, E_{w2}, and E_{p2} are the

respective gain or loss in enthalpy of air, the kinetic and, the potential energy at location 2, i.e., at the exit of the turbine.

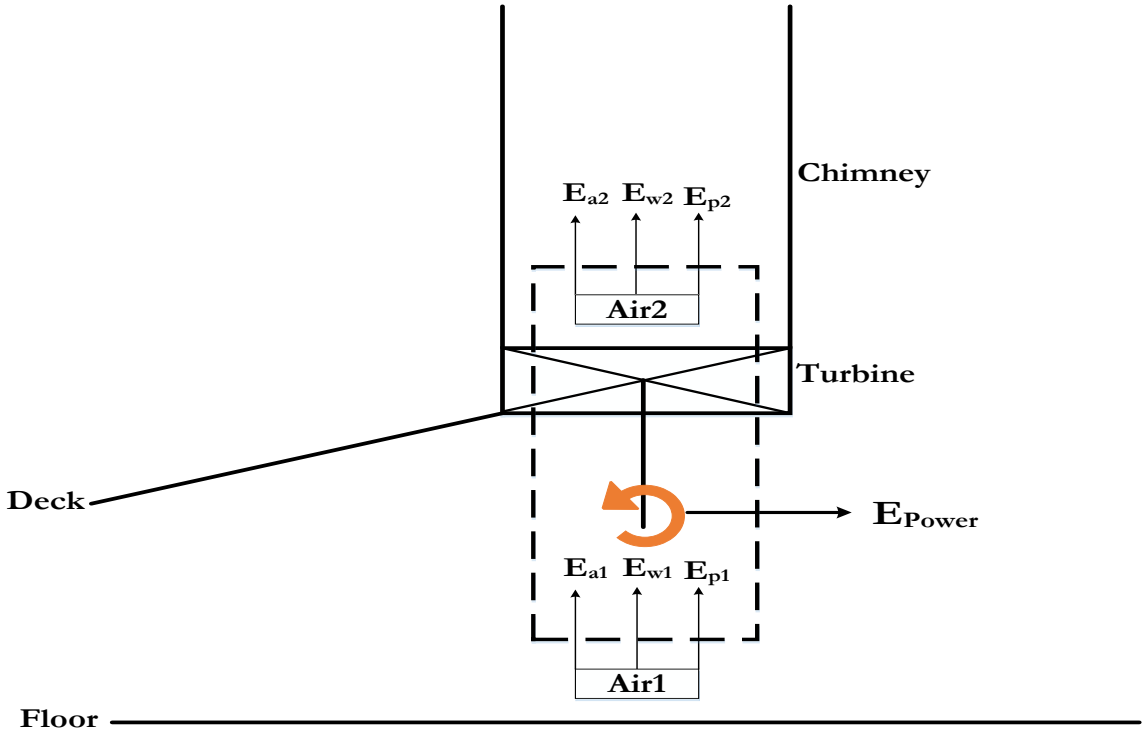

Figure 4.5. Energy exchange across the turbine

$$E_{a1} + E_{w1} + E_{p1} = E_{a2} + E_{w2} + E_{p2} + E_{Power} \quad (4.5)$$

4.2.5 Energy Modeling along the Chimney Surface

The energy exchange at the chimney surface is depicted in Figure 4.6 and described by Equation (4.6), where E_{a3}, E_{w3}, and E_{p3} are the respective gain or loss in enthalpy of air, the kinetic and, the potential energy at location 3, i.e., at the exit of the chimney, $E_{ch\text{-}sky}$ is the radiation exchange between the chimney and the sky, $E_{ch\text{-}gr}$ is the radiation heat transfer from the chimney to the ground, $E_{ch\text{-}amb}$ is the gain in energy by air surrounding the chimney by convection heat transfer, and $E_{ch\text{-}m}$ is the radiation exchange between mirror

and chimney surface. Heat gained through solar radiation incident on the chimney surface is negligible owing to the chimney being vertical and cylindrical in shape.

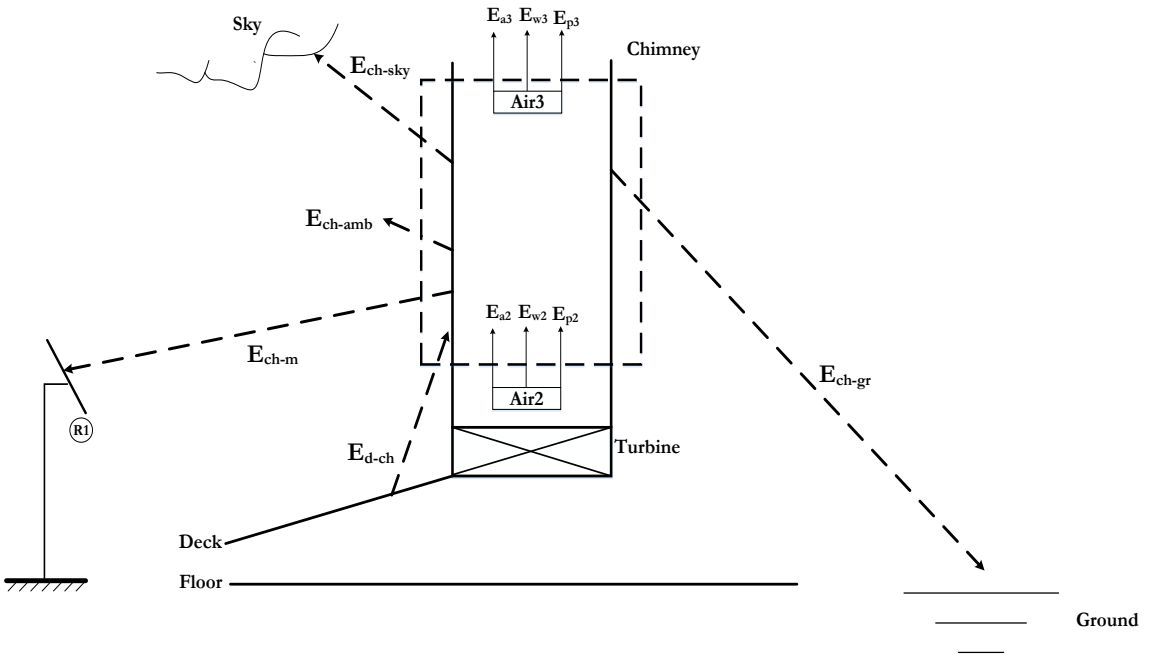

Figure 4.6. Energy exchange along the chimney surface

$$E_{a2} + E_{w2} + E_{p2} + E_{d-ch} = E_{a3} + E_{w3} + E_{p3} + E_{ch-amb} + E_{ch-sky} + E_{ch-gr} + E_{ch-m} \quad (4.6)$$

4.2.6 Energy Modeling for Air Flowing through the Chimney

The energy balance for the air flowing in the chimney is depicted in Figure 4.7 and described by Equation (4.7), where $E_{a\text{-}ch}$ is the convection heat transfer between the inner surface of the chimney and the air flowing across locations 2 and 3.

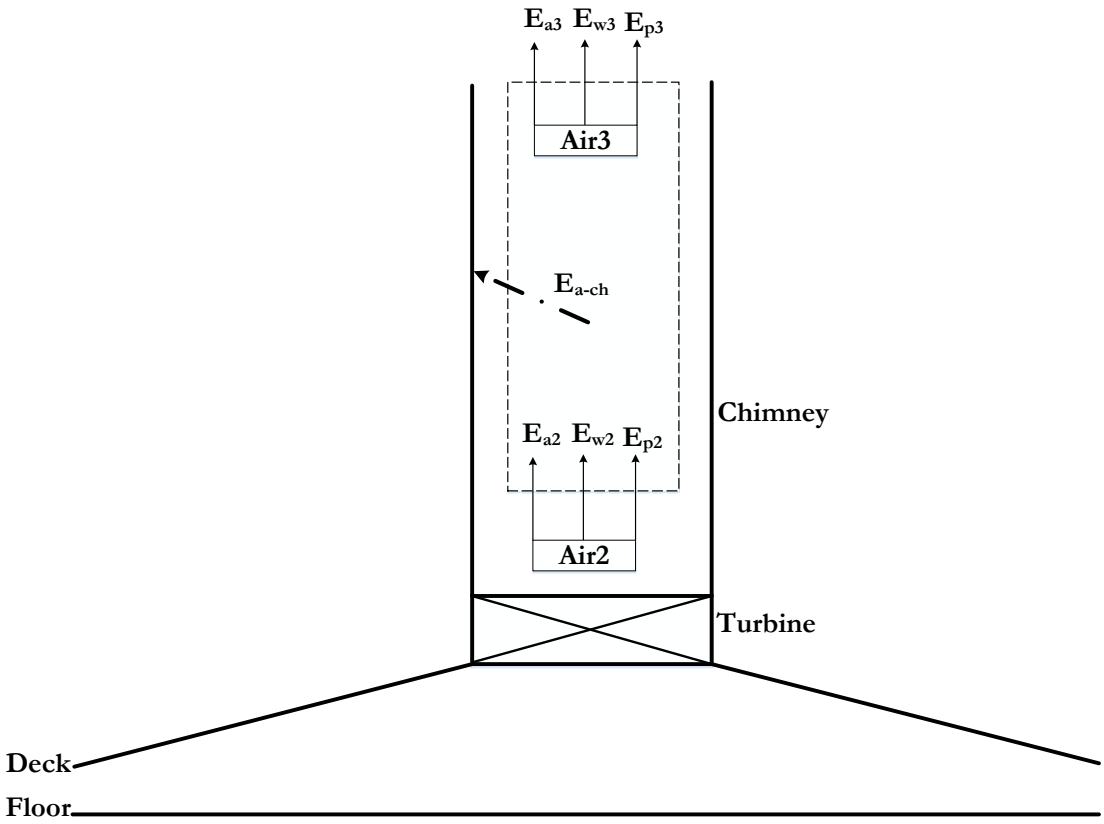

Figure 4.7. Energy distribution for the air flowing in the chimney

$$E_{a2} + E_{w2} + E_{p2} = E_{a-ch} + E_{a3} + E_{w3} + E_{p3} \quad (4.7)$$

4.2.7 Energy Modeling of the Mirror

The energy balance across the mirror surface is depicted in Figure 4.8 and described by Equation (4.8), where $E_{s\text{-}m}$ is the radiant energy incident on the mirror, $E_{m\text{-}sky}$ is the radiation exchange between the mirror and the sky, $E_{m\text{-}gr}$ is the radiation heat transfer from the mirror to the ground, and, $E_{m\text{-}amb}$ is the gain in energy by air surrounding the mirror by convection heat transfer.

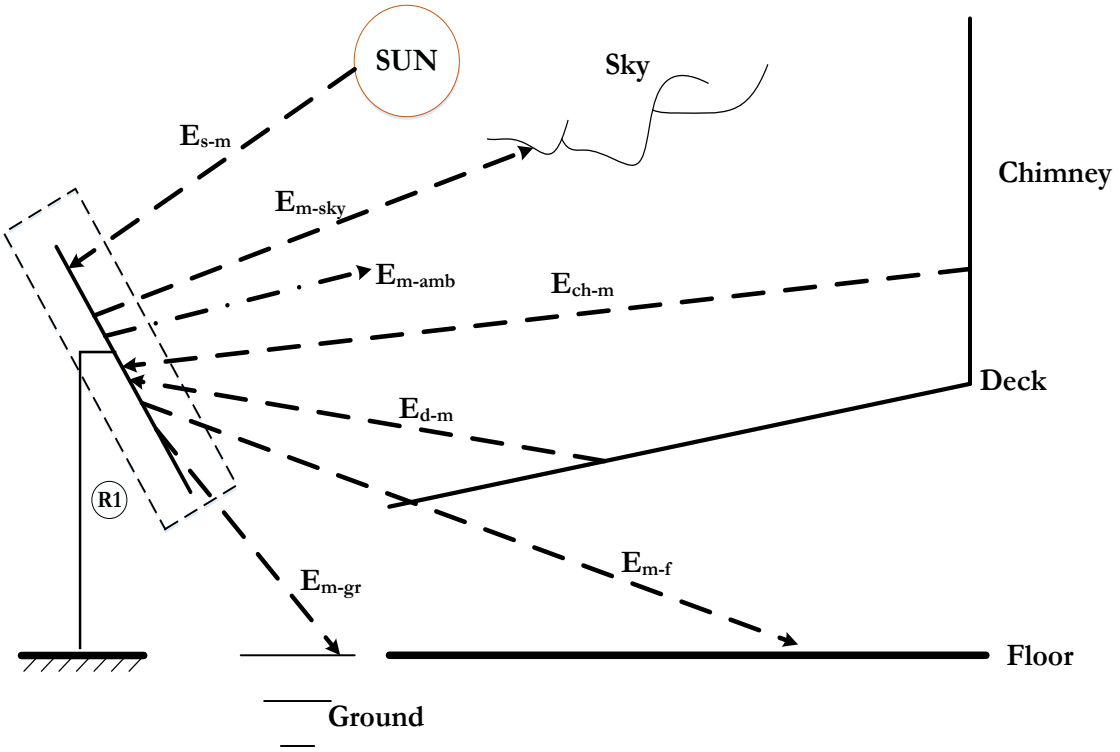

Figure 4.8. Energy exchange over the mirror surface

$$E_{s-m} + E_{d-m} + E_{ch-m} = E_{m-f} + E_{m-amb} + E_{m-sky} + E_{m-gr} \quad (4.8)$$

4.2.8 Brief on Energy Terms of the Modeling

All the terms in the Equations (4.2)-(4.7) are clearly explained in the previous chapter except the mirror modeling which is described as below.

The solar energy received by the mirror, E_{s-m} is defined by Equation (4.9).

$$E_{s-m} = IA_m \quad (4.9)$$

Where, I is the incident solar radiation on the earth surface, and A_m is the area of the mirror.

Solar energy reflected from mirror to floor, E_{m-f} is defined by Equation (4.10)

$$E_{m-f} = \rho_m \tau_d \varepsilon_f I A_m \quad (4.10)$$

Where, ρ_m is the reflectivity of mirror, τ_d is the transmissivity of the deck, ε_f is the emissivity of the collector floor.

Energy radiated from deck to mirror, $E_{d\text{-}m}$ is given by Equation (4.11).

$$E_{d-m} = \varepsilon_d \phi_{d-m} A_d \sigma (T_{dE}^4 - T_m^4) \tag{4.11}$$

Where, ε_d is the emissivity of the deck, $\varphi_{d\text{-}m}$ is the fraction of energy radiated from deck to mirror, A_d is the area of the deck, σ is the Stefan-Boltzmann constant, T_{dE} and T_m are the effective temperature of the deck and mirror surface, respectively.

Energy radiated from deck to mirror, $E_{ch\text{-}m}$ is given by Equation (4.12)

$$E_{ch-m} = \varepsilon_{ch} \phi_{ch-m} A_{ch} \sigma (T_{ch}^4 - T_m^4) \tag{4.12}$$

Where, ε_{ch} is the emissivity of the chimney, $\varphi_{ch\text{-}m}$ is the fraction of energy radiated from the chimney to mirror, A_{ch} is the area of outer chimney surface, and, T_{ch} is the effective temperature of the chimney surface.

Energy radiated from mirror to sky, $E_{m\text{-}sky}$ is given by Equation (4.13).

$$E_{m-sky} = \varepsilon_m \phi_{m-sky} A_m \sigma (T_m^4 - T_{sky}^4) \tag{4.13}$$

Where, ε_m is the emissivity of the mirror, $\varphi_{m\text{-}sky}$ is the fraction of energy radiated from mirror to sky, A_m is the area of the mirror, and, T_{sky} is the effective temperature of the sky.

Energy radiated from mirror to ground, $E_{m\text{-}gr}$ is given by Equation (4.14).

$$E_{m-gr} = \varepsilon_m \phi_{m-gr} A_m \sigma (T_m^4 - T_{gr}^4) \quad (4.14)$$

Where $\varphi_{m\text{-}gr}$ is the fraction of energy radiated from mirror to ground, and, T_{gr} is the effective temperature of the ground.

Energy transfer from the mirror to the environment by convection is given by Equation (4.15).

$$E_{m-amb} = A_m h_{m-amb} (T_m - T_{amb}) \quad (4.15)$$

Where T_{amb} is the ambient temperature, and, $h_{m\text{-}amb}$ is convective heat transfer coefficient between the mirror and the atmosphere.

Convective heat transfer coefficient between the mirror and the atmosphere is described by Equation (4.16) according to McAdams [62], and Duffie and Beckman [63].

$$h_{m-amb} = 5 \frac{W}{m^2 K} \quad (4.16)$$

The shape factor relationships by summation, for deck, mirror, and chimney, are presented in Equations (4.17), (4.18), and (4.19), respectively.

$$\phi_{d-m} + \phi_{d-ch} + \phi_{d-sky} = 1 \quad (4.17)$$

$$\phi_{ch-m} + \phi_{ch-d} + \phi_{ch-gr} + \phi_{ch-sky} = 1 \quad (4.18)$$

$$\phi_{m-d} + \phi_{m-ch} + \phi_{m-gr} + \phi_{m-sky} = 1 \quad (4.19)$$

The shape factors $\varphi_{d\text{-}m}$, $\varphi_{m\text{-}ch}$, $\varphi_{m\text{-}d}$, and, $\varphi_{ch\text{-}m}$ are determined by Hottel's crossed-strings method [70]. The shape factors $\varphi_{m\text{-}sky}$ and $\varphi_{ch\text{-}sky}$ are assumed to be 0.3 and 0.5 respectively. And, the determination of shape factors $\varphi_{ch\text{-}d}$ and $\varphi_{d\text{-}ch}$ is clearly explained in the previous

chapter.

The energetic efficiency of an SCPP aided with reflectors is described by Equation (4.20)

$$\eta_{energy} = \frac{E_{power}}{E_{sf} + E_{mf}} * 100 \tag{4.20}$$

4.3 Exergy Modeling of SCPP aided with reflectors

Data from energy analysis can be used to interpret the results of exergy analysis performed using exergy balance equations. Exergy is represented by *X* and an exergy equation each was formulated for the floor, air within the collector, collector, turbine, chimney, and the mirror. The exergy balance equations are similar to energy balance equations but differ by an additional term of irreversibility or available work destroyed, which is represented by ΔX.

Exergy exchange at the floor is analogous to the energy exchange as represented in Figure 4.2 and is described by Equation (4.21), where $X_{m\text{-}f}$ is the exergy associated with the reflected solar radiation absorbed by the floor, $X_{s\text{-}f}$ is the exergy associated with the incident solar radiation absorbed by the floor, $X_{f\text{-}a}$ is the exergy associated with the convection heat exchange between the floor and the air, $X_{f\text{-}d}$ is the exergy associated with the radiation exchange between the floor and the deck, and ΔX_f is the exergy destruction associated with the floor.

$$X_{s-f} + X_{m-f} = X_{f-a} + X_{f-d} + \Delta X_f \tag{4.21}$$

The exergy exchange of air between the floor and the deck is analogous to the energy exchange as represented in Figure 4.3 and is described by Equation (4.22), where $X_{d\text{-}a}$ and $X_{f\text{-}a}$ are the exergies associated with air due to convective heat exchange with the deck and

the floor, respectively. X_{a1}, X_{w1}, and X_{p1} are the respective exergies associated with the enthalpy of air, and the kinetic and potential exergy at location 1 when compared to atmospheric conditions, i.e., those at location 0. X_{a0}, X_{w0}, and X_{p0} are the respective exergies associated with the enthalpy of air, and the kinetic and potential exergy at location 0, and ΔX_a is the exergy destruction associated with the air between the floor and the deck.

$$X_{f-a} + X_{d-a} + X_{a0} + X_{w0} + X_{p0} = X_{a1} + X_{w1} + X_{p1} + \Delta X_a \qquad (4.22)$$

The exergy exchange at the deck is analogous to the energy exchange for the collector as represented in Figure 4.4 and is described by Equation (4.23), where $X_{d\text{-}sky}$ is the exchange of radiation exergy between the deck and the sky, $X_{d\text{-}amb}$ is the loss of exergy from the deck to the atmosphere by convection heat transfer, $X_{d\text{-}ch}$ is the loss of exergy from the deck due to the radiation exchange between the deck and outer surface of the chimney, $X_{d\text{-}m}$ is the loss of exergy from deck due to radiation exchange between the deck and the mirror, and ΔX_d is the exergy destruction associated with the collector.

$$\begin{aligned} X_{s-f} + X_{m-f} + X_{a0} + X_{w0} + X_{p0} & \\ = X_{a1} + X_{w1} + X_{p1} + X_{d-sky} + X_{d-amb} + X_{d-ch} & \\ + X_{d-m} + \Delta X_d & \end{aligned} \qquad (4.23)$$

The exergy balance across the turbine is analogous to the energy balance as represented in Figure 4.5 and is described by Equation (4.24), where X_{power} is the exergy associated with the work done or power generated by the turbine, X_{a2}, X_{w2}, and X_{p2} are the respective exergies associated with the gain or loss in the enthalpy of air, and the kinetic and potential exergy at location 2, i.e., at the exit of the turbine, and ΔX_T is the exergy destruction associated with the turbine.

$$X_{a1} + X_{w1} + X_{p1} = X_{a2} + X_{w2} + X_{p2} + X_{Power} + \Delta X_T \quad (4.24)$$

The exergy exchange across the chimney is analogous to the energy exchange across the chimney as represented in Figure 4.6 and is described by Equation (4.25) , where X_{a3}, X_{w3}, and X_{p3} are the respective exergies associated with the gain or loss in the enthalpy of air, and the kinetic and potential exergy at location 3, i.e., at the exit of the chimney, $X_{ch\text{-}sky}$ is the exergy associated with the radiation exchange between the chimney and the sky, $X_{ch\text{-}gr}$ is the exergy associated with the radiation heat transfer from the chimney to the ground, $X_{ch\text{-}amb}$ is the gain in exergy by the air surrounding the chimney by convection heat transfer, $X_{ch\text{-}m}$ is the exergy associated with the radiation heat transfer from the chimney to the mirror, and ΔX_{ch} is the exergy destruction associated with the chimney.

$$\begin{aligned} X_{a2} + X_{w2} + X_{p2} + X_{d-ch} & \\ = X_{a3} + X_{w3} + X_{p3} + X_{ch-amb} + X_{ch-sky} + X_{ch-gr} & \\ + X_{ch-m} + \Delta X_{ch} & \end{aligned} \quad (4.25)$$

The exergy exchange along the mirror is analogous to the energy exchange along the mirror as represented in Figure 4.8 and is described by Equation (4.26), where $X_{m\text{-}sky}$ is the exergy associated with the radiation exchange between the mirror and the sky, $X_{m\text{-}gr}$ is the exergy associated with the radiation heat transfer from the mirror to the ground, $X_{m\text{-}amb}$ is the gain in exergy by the air surrounding the chimney by convection heat transfer, and ΔX_m is the exergy destruction associated with the chimney.

$$\begin{aligned} X_{s-m} + X_{d-m} + X_{ch-m} & \\ = X_{m-f} + X_{m-amb} + X_{m-sky} + X_{m-gr} + \Delta X_m & \end{aligned} \quad (4.26)$$

All the terms in the Equations (4.21)-(4.25) are clearly explained in the previous chapter except the mirror modeling which is described as below.

Exergy of solar radiation, X_{s-m} as described by Petela [64] is 90% of the radiation energy.

$$X_{s-m} = 0.9 \times E_{s-m} \tag{4.27}$$

Similarly exergy associated with the reflection of incident radiation on mirror to the floor can be determined from the Equation (4.28).

$$X_{m-f} = 0.9 \times E_{m-f} \tag{4.28}$$

The radiation exergy X of a surface with a surface area of A, emissivity of ε, and temperature of T is expressed by Equation (4.29) according to Petela [64–66] and Szargut et al. [67].

$$X = \varphi A \varepsilon \frac{\sigma}{3}(3T^4 + T_0^4 - 4T_0T^3) \tag{4.29}$$

Where, φ is the shape factor which depends on the geometry of the surface under study and with respect to black surface at which considered radiation would arrive. Radiation exergy swapped between any two surfaces at different temperature T_x and T_y can be determined by Equation (4.29) for both surfaces, which leads to Equation (4.30).

$$X_{x-y} = \varphi_{x-y} A_x \varepsilon_{x-y} \frac{\sigma}{3}\left[3\left(T_x^4 - T_y^4\right) - 4T_0\left(T_x^3 - T_y^3\right)\right] \tag{4.30}$$

Where, $\varepsilon_{x\text{-}y}$ is the effective emissivity which depends on the emissivities ε_x and ε_y of respective surfaces and formulated similar to the equations of radiation exergy exchange. The effective emissivity reduces to $\varepsilon_{x\text{-}y} = 1$, when the emissivities $\varepsilon_x = \varepsilon_y = 1$. Equation (4.30) is used to calculate radiation exergies: $X_{d\text{-}m}$, $X_{ch\text{-}m}$, $X_{m\text{-}sky}$ and $X_{m\text{-}gr.}$

Exergy associated with the radiation energy exchange between the deck and the mirror is given by Equation (4.31).

$$X_{d-m} = \varphi_{d-m} A_d \varepsilon_{d-m} \frac{\sigma}{3} [3(T_{dE}^4 - T_m^4) - 4T_0 (T_{dE}^3 - T_m^3)] \quad (4.31)$$

Exergy associated with the radiation energy exchange between the chimney and the mirror is given by Equation (4.32).

$$X_{ch-m} = \varphi_{ch-m} A_{ch} \varepsilon_{ch-m} \frac{\sigma}{3} [3(T_{ch}^4 - T_m^4) - 4T_0 (T_{ch}^3 - T_m^3)] \quad (4.32)$$

Exergy associated with the radiation energy exchange between the mirror and the sky is given by Equation (4.33).

$$X_{m-sky} = \varphi_{m-sky} A_m \varepsilon_{m-sky} \frac{\sigma}{3} \left[3\left(T_m^4 - T_{sky}^4\right) - 4T_0 \left(T_m^3 - T_{sky}^3\right)\right] \quad (4.33)$$

Exergy associated with the radiation energy exchange between the mirror and the ground is given by Equation (4.34).

$$X_{m-gr} = \varphi_{m-gr} A_m \varepsilon_{m-gr} \frac{\sigma}{3} \left[3\left(T_m^4 - T_{gr}^4\right) - 4T_0 \left(T_m^3 - T_{gr}^3\right)\right] \quad (4.34)$$

Exergy associated with the convective heat transfer between the chimney and the atmosphere is given by Equation (4.35).

$$X_{m-amb} = E_{m-amb} \left(1 - \frac{T_0}{T_{m-amb}}\right) \quad (4.35)$$

$T_{ch\text{-}amb}$ is the mean effective temperature of the chimney and the atmosphere.

$$T_{m-amb} = \frac{T_{amb} + T_m}{2} \quad (4.36)$$

The exergetic efficiency of an SCPP is given by Equation (4.37).

$$\eta_{exergy} = \frac{X_{power}}{X_{s-f} + X_{m-f}} * 100 \quad (4.37)$$

CHAPTER 5

EXPERIMENTAL SETUP AND ANALYSIS

In this section, an effort for constructing the experimental models and the analysis carried out is discussed in detail. This experiment was carried out by making three models.

5.1 Model I

A frame for the proposed SCPP model is designed and built as shown in Figure 5.1. The frame of the experimental setup was constructed with the 7mm iron bars to balance the weight of the chimney and to place the collector easily. Within the frame, the arrangement of nut and bolt as shown in Figure 5.3 was made to erect the chimney with the help of flanges. In this arrangement, 1.5m diameter absorber plate made up of the 3mm thick Aluminum plate was used and painted black, to increase the absorbance. The bottom of the absorber plate was insulated with the fiber sheet to reduce the heat losses towards the ground. Clear plastic used in automotive applications was used as a collector, to transmit the solar radiation onto the absorber plate and to direct the air towards the center i.e., chimney. The chimney is made up of 0.11m diameter and 0.9m long, black carbon steel. Turbine used in the Model-I as shown in Figure 5.3 is basically a fan used in cooling of computer appliances. The tip diameter of the turbine is 9cm, it was selected as such to avoid the striking of the tip with the internal wall of the chimney. The geometrical and material specifications of the model I are as shown in Table 5-1 and Table 5-2, respectively.

Table 5-1. Geometrical Specifications of Model I

Geometric Parameter	Dimensions (meter)
Diameter of Absorber Plate (D_f)	1.5
Inner Diameter of Chimney(D_1)	0.106
Height of Collector Inlet (H_e)	0.002
Height of Collector Outlet (H_1)	0.342
Height of Chimney (H_3)	0.9

Table 5-2. Material Specifications of Model I

Part	Material
Absorber Plate	Aluminum plate painted black (3mm thick)
Chimney	Black Carbon Steel (2mm thick)
Collector	Clear plastic used in automotive applications
Insulation	Fiber

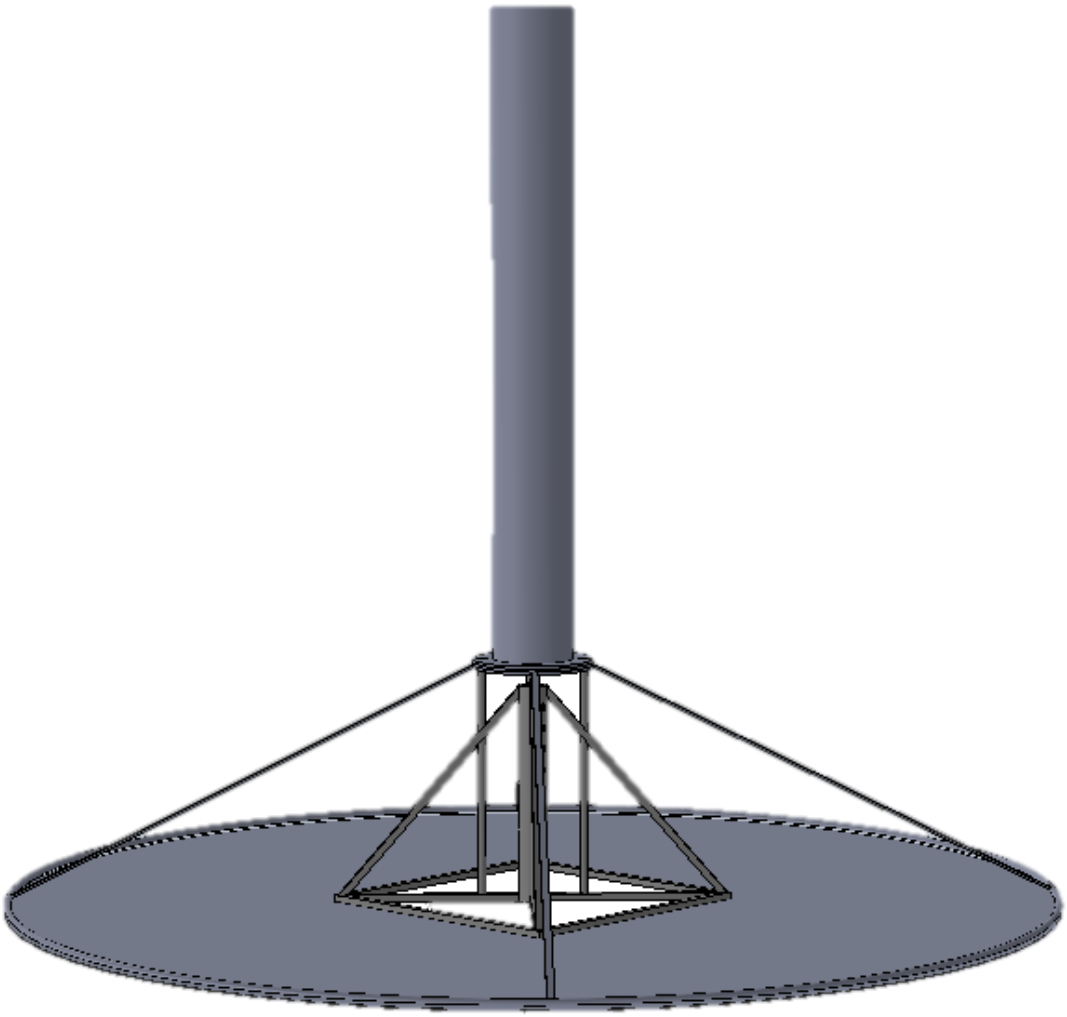

Figure 5.1. 3-D design of SCPP Model I

Figure 5.2. Experimental Model 1

Figure 5.3. Turbine used in Model 1

All the parts were manufactured as per the required design and dimensions. Final assembly of the SCPP Model I is as shown in Figure 5.2. After assembling the parts and sealing everything to prevent leakages, the turbine placed at the bottom of the chimney failed to rotate continuously. The reasons for failure were examined and were helpful for carrying out our research further.

5.1.1 Reasons for Failure of Model I

The reasons for failure are as follows:

- The area under the collector was too big to allow for continuous supply of warmed air to pass through the chimney. During the design stage, we made the slope of the collector to be around 24^0, which is the nearly the latitude angle, expecting this would increase the amount of radiation incident on the collector. Unfortunately, this design leads to backflow of air through an inlet of collector due to the presence of higher dense air in large quantity in the collector.
- The other issue which affected the performance was the collector material. Clear plastic was used, which was translucent. It did not allow all the radiation onto the absorber plate.
- One more issue was improper insulation at the bottom through which absorber plate was losing heat continuously.

5.1.2 Conclusions from Design of Model I

The conclusions from the failures of Model I are as follows:

- Re-design collector such that, the cross flow area remains constant throughout the flow.

- A search of other collector material which has high transmissivity.
- Proper insulation for the bottom of the absorber plate.

5.2 Model II

Model II was designed avoiding all the flaws made in Model I and bigger in size to obtain high power output. In this Model II, as shown in Figure 5.5, the slope of the collector was kept at 2^0 to obtain the constant mass flow rate and ensuring constant flow area so that upon decreasing the density, air is accelerated towards the center of the chimney. Instead of clear plastic, in this model Plexiglas with high transmissivity was used as collector cover. As far as, Chimney is concerned CPVC (Chlorinated Polyvinyl Chloride) was used instead of carbon steel pipe which ensured smooth flow and withstand high temperatures. Moreover, a concrete foundation was used to erect the tall chimney and synthetic ropes were tied at the top of the chimney to further protect the chimney from strong winds.

A concrete base is designed and built as shown in Figure 5.4 to provide balance to SCPP system. The frame to place the Plexiglas is made up of 7mm iron bars. The concrete base consists of four threaded rods placed at a diagonal distance of 0.25m and an angle of 90^0 each to place a 4m long and 0.2m diameter chimney with the help of flanges and nuts. These nuts pass through the absorber plate as shown in the assembly. In this arrangement, 3m diameter absorber plate made up of 3mm thick Aluminum plate was used and painted black, to increase the absorbance. The absorber plate at the bottom was insulated with high-quality fiber to reduce the bottom losses. To increase the transmissivity Plexiglas was used as collector cover. To ensure that absorber plate is perfectly horizontal, pneumatic levelers were used. Turbine used in the Model-II is 180mm PC fan that had brushless magnet DC motor that was converted as a generator by welding two wires at the winding to generate

power and in case of providing a starting torque, a provision was made to input power with the help of battery. The geometrical and material specifications of model II are as shown in Table 5-3 and Table 5-4, respectively.

Table 5-3. Geometrical Specifications of Model II

Geometric Parameter	Dimensions (meter)
Diameter of Absorber Plate (D_f)	3
Inner Diameter of Chimney(D_1)	0.203
Height of Collector Inlet (H_e)	0.003
Height of Collector Outlet (H_1)	0.048
Height of Chimney (H_3)	4

Table 5-4. Material Specification of Model II

Part	Material
Absorber Plate	Aluminum plate painted black (3mm thick)
Chimney	CPVC pipe Schedule-40 8 inches
Collector	Plexiglas (3mm thick)
Concrete Base	Concrete (Height 20cm, Diameter 60cm)
Insulation	Fiber

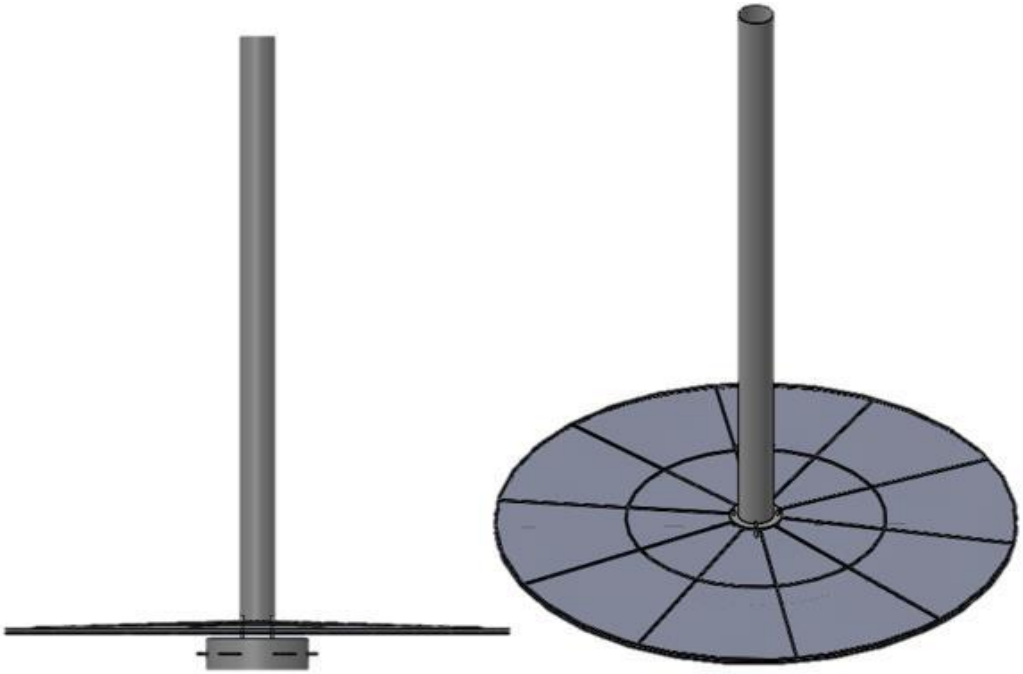

Figure 5.4. 3-D design of SCPP Model II

Figure 5.5. Experimental Model II

All the parts were manufactured as per the required design and dimensions. After assembling the parts, silica was used to cover up the gaps between the Plexiglas pieces.

Final assembly of the SCPP model II is as shown in Figure 5.5. Due to difficulties in handling the Plexiglas and its fragile nature lead to failure of Model II. The reasons for failure were examined and were helpful for carrying out our research further.

5.2.1 Reasons for Failure of Model III

The reasons for failure are as follows:

- After assembly, one of the four parts of the Plexiglas broke due to mishandling.
- Moreover, the location between chimney and collector cover were sealed improperly which led to the leakage.
- Iron frame absorbs heat from the absorber plate due to the high conductivity of Iron.

5.2.2 Conclusions from Design of Model II

The conclusions from the failures of Model II are as follows:

- A search of other collector material, which is easy to handle and possess high transmissivity.
- Need to find another alternative to properly insulate the bottom of the absorber plate.
- Search for an alternative frame material.

5.3 Model III

Taking into account, failures associated with Model I and Model II. SCPP was re-designed to a smaller scale compared to the Model II to reduce the cost of materials and to obtain easiness in handling. In Model III cardboard was used as an insulating material instead of fiber. As far as, the frame is concerned iron frame was replaced by wooden frame and

chimney was supported with the help of steel bars as shown in Figure 5.6. The geometrical and material specifications of model III are as shown in Table 5-5 and Table 5-6, respectively.

Figure 5.6. Experimental Model III

A cardboard base 10mm thick is placed below the SCPP system as shown in Figure 5.6. Absorber plate of 1.6m diameter and 3mm thick Aluminum plate is fixed to the Cardboard. Wooden arms to place the collector cover and to erect the chimney are drilled and bolted

to the base of absorber plate. Neatly cut Clear glass with 0.85 transmissivity is used as collector cover and are fixed to the wooden arms placed on the absorber plate. The 0.15m diameter and 2m long Chimney is erected with the help of steel bars fixed on the wooden frame with the bolt assembly. Turbine used in the Model-III is 140mm PC fan that had brushless magnet DC motor that was converted as a generator by welding two wires at the winding to generate power and in case of providing a starting torque, a provision was made to input power with the help of battery.

Table 5-5. Geometrical Specifications of Model III

Geometric Parameter	Dimensions (meter)
Diameter of Absorber Plate (D_f)	1.6
Inner Diameter of Chimney(D_1)	0.14
Height of Collector Inlet (H_e)	0.003
Height of Collector Outlet (H_1)	0.048
Height of Chimney (H_3)	2

Table 5-6. Material Specification of Model III

Part	Material
Absorber Plate	Aluminum plate painted black (3mm thick)
Chimney	CPVC pipe Schedule-40 8 inches
Collector	Clear Glass (3mm thick)
Frame	Wooden frame with iron supports
Insulation	Cardboard

5.3.1 Experimental Procedure

The Schematic diagram of the experimental model III along with the installed instrumentation is as shown in Figure 5.7.

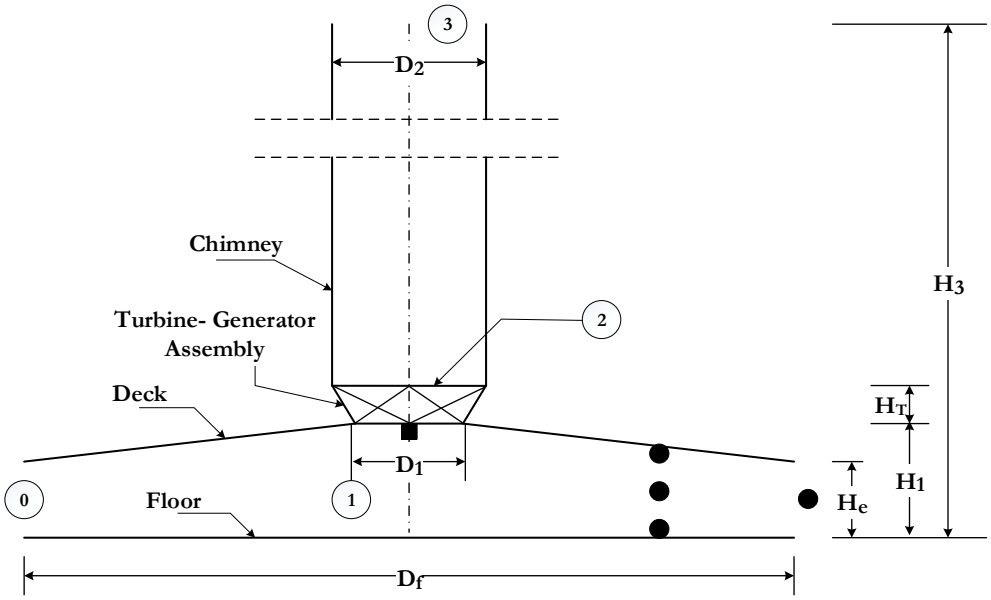

Figure 5.7. Schematic diagram of experimental setup

(i) 0, Collector Inlet, (ii) 1, Collector Outlet & Turbine Inlet, (iii) 2, Turbine Outlet, (iv) 3, Chimney Outlet, (v) ● , Thermocouples, (vi) ■ , DC power Measurement source

The air enters the collector through point 0 with a gap of H_e. The floor of the collector under the transparent cover has a diameter of D_f, the deck is at an inclination to ensure a constant radial cross-sectional area of flow of the radially directed air. Radiation from the floor heats the air from state 0 to state 1. Heated air expands in the turbine reaching state 2. The inlet and outlet diameters of the turbine are D_1 and D_2, respectively. Heated air leaves the SCPP from location 3 after gaining atmospheric pressure at height H_3 to avoid the negative draft.

5.3.2 Instrumentation

K-type thermocouples are used to measure temperatures of the floor, glass, and air, as well as ambient temperature. Thermocouple probes are calibrated before installing them in the experimental setup. A data acquisition consisting of four thermocouple input modules installed in an OMEGA HH1384 data logger where thermocouple measurements are displayed and stored. Real-time processed thermocouple readings are measured every 60 seconds and the average temperatures of every 5 minutes were recorded. Fluke 233/A remote digital multimeter was used to record the power rating of turbine-generator assembly. Solar radiation data was recorded from KFUPM-RI services for particular days.

5.3.3 Error and Uncertainty

All the instruments are calibrated before installing them in the experimental setup. Errors in the measurement devices are calculated as the ratio of the device least count to the minimum value of the output measured by that instrument.

Table 5-7. Measurement devices with their range, accuracy, error, and uncertainty

Parameter	Instruments	Range	Accuracy	Error	Uncertainty
Temperature	Thermocouple	-267 – 316 °C	± 0.1 °C	0.5 %	0.05 °C
Solar radiation	Pyranometer	0-2000 W/m^2	±0.02W/m^2	2 %	0.01 W/m^2
Current	Multimeter	0.01 mA-10 A	± 0.002mA	0.25%	0.001 mA
Voltage	Multimeter	0.1mV-1000V	±0.001mV	1%	0.5 mV

The uncertainty in the measurements is calculated as the root sum square of the fixed error of the instrumentation and the random error observed during different measurements. The measurement devices along with their range, accuracy, error, and uncertainty are summarized in Table 5-7.

5.3.4 Uncertainty Analysis for Power and Efficiency Calculation

Power produced by the SCPP is calculated by multiplication of voltage and current from DC-generator.

$$Power = Voltage\ X\ Current$$

Maximum error while recording power can be obtained by

$$Maximum\ Power = (Voltage + Voltage\ Accuracy)\ X\ (Current + Current\ Accuracy)$$

$$Maximum\ Error = Maximum\ Power - Power$$

Minimum error while recording power can be obtained by

$$Minimum\ Power = (Voltage - Voltage\ Accuracy)\ X\ (Current - Current\ Accuracy)$$

$$Minimum\ Error = Power - Minimum\ Power$$

Average Error while recording power can be obtained by mean of maximum and minimum.

$$Average\ Error = \frac{Maximum\ Error + Minimum\ Error}{2}$$

Combined Standard uncertainty for error in power calculation can be obtained by

$$\frac{Error\ in\ Power\ Calculation}{Power} = \sqrt{\left(\frac{Error\ in\ Voltage}{Voltage}\right)^2 + \left(\frac{Error\ in\ Current}{Current}\right)^2}$$

Efficiency obtained by the SCPP is calculated as an amount of power obtained over a radiant energy incident onto the absorber plate.

$$Efficiency = \frac{Power\ Produced}{Radiant\ Energy\ incident\ per\ unit\ Area\ X\ Area\ of\ absorber\ plate}$$

The area of absorber plate is fixed and considering no geometrical errors in the size of absorber plate leads to the conclusion that efficiency is a function of power and radiant energy only.

Maximum error while calculating efficiency can be obtained by

$$Maximum\ Efficiency = \frac{Power\ Output + error\ in\ power\ output\ calculation}{Incident\ Energy - error\ in\ pyranometer}$$

$$Maximum\ Error = Maximum\ Efficiency\ - Efficiency$$

Minimum error while recording power can be obtained by

$$Minimum\ Efficiency = \frac{Power\ Output - error\ in\ power\ output\ calculation}{Incident\ Energy + error\ in\ pyranometer}$$

$$Minimum\ Error = Efficiency - Minimum\ Efficiency$$

Average Error while recording power can be obtained by mean of maximum and minimum.

$$Average\ Error = \frac{Maximum\ Error + Minimum\ Error}{2}$$

Combined Standard uncertainty for error in efficiency can be obtained by

$$\frac{Error\ in\ Efficiency}{Efficiency} = \sqrt{\left(\frac{Error\ in\ Power}{Power}\right)^2 + \left(\frac{Error\ in\ Radiant\ Energy}{Energy}\right)^2}$$

5.4 Model III Aided with Reflectors

With the quest of higher power output, a model for a solar chimney power plant (SCPP) aided with reflectors is developed and a comparative study is conducted with an SCPP model without reflectors. Mirrors were placed along the Model III to increase the amount

of incident energy onto the absorber plate by tracing the light from the sun to the collector surface.

Figure 5.8. Model III aided with reflectors

Table 5-8. Geometrical Specifications of Model III aided with reflectors

Geometric Parameter	Dimensions (meter)
Diameter of Absorber Plate (D_f)	3
Inner Diameter of Chimney(D_1)	0.14
Height of Collector Inlet (H_e)	0.003
Height of Collector Outlet (H_1)	0.048
Height of Chimney (H_3)	4

Table 5-9. Material Specification of Model III aided with reflectors

Part	Material
Absorber Plate	Aluminum plate painted black (3mm thick)
Chimney	CPVC pipe Schedule-40 8 inches
Collector	Clear glass (3mm thick)
Frame	Wooden Frame with iron supports
Insulation	Card board
Reflectors	Mirrors 4 nos. (0.45m X 0.75m)

An experimental model with mirrors is as shown in Figure 5.8. The geometrical and material specifications of model III aided with reflectors are as shown in Table 5-8 and Table 5-9, respectively.

5.4.1 Experimental Procedure of SCPP aided with Reflectors

The Schematic diagram of the experimental model III aided with reflectors along with the installed instrumentation is as shown in Figure 5.9. All the mirrors are placed around the deck, in the circular pattern such that it resembles the field of heliostats uniformly directing towards the deck. They are placed in such a way that all the radiation falling onto the mirror is reflected onto the deck. The deck receives the direct radiation from the mirror in the form of reflection, diffuse radiation from the mirror is lost to sky and ground, a little amount of it is lost from the mirror by convective heat transfer to the atmosphere i.e., due to absorption of the mirror. The air enters the collector through point 0 with a gap of H_e. The floor of the collector under the transparent cover has a diameter of D_f, the deck is at an inclination to ensure a constant radial cross-sectional area of flow of the radially directed air. Radiation

from the floor heats the air from state 0 to state 1. Heated air expands in the turbine reaching state 2. The inlet and outlet diameters of the turbine are D_1 and D_2, respectively. Heated air leaves the SCPP from location 3 after gaining atmospheric pressure at height H_3 to avoid the negative draft. All the geometric specifications and material specifications are clearly mentioned in Table 5-8 and Table 5-9, respectively.

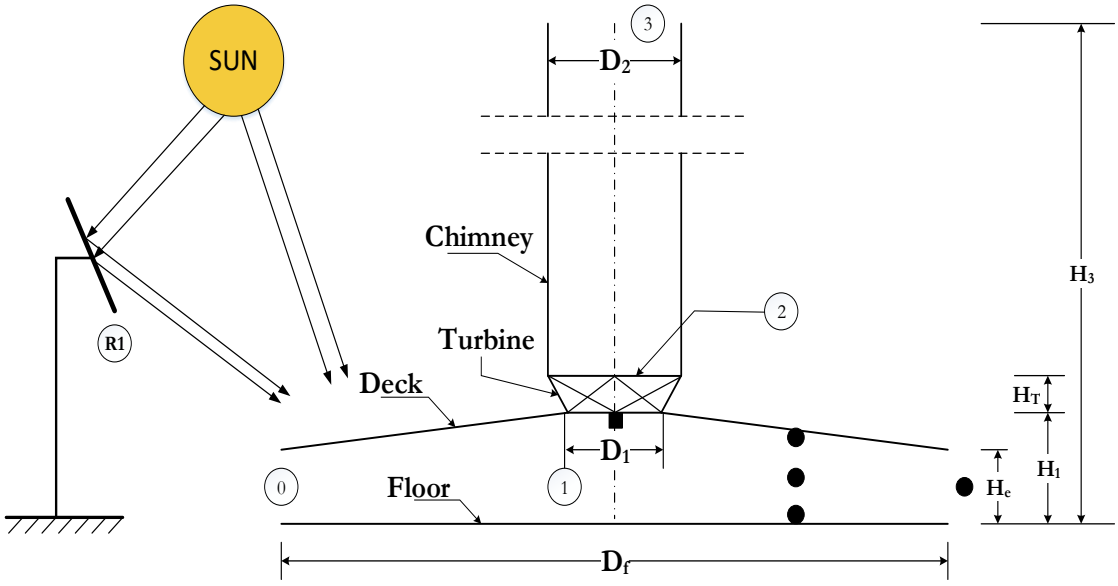

Figure 5.9. Schematic diagram of experimental setup with mirrors

(i) 0, Collector Inlet, (ii) 1, Collector Outlet & Turbine Inlet, (iii) 2, Turbine Outlet, (iv) 3, Chimney Outlet, (v) ● , Thermocouples, (vi) ■ , DC power Measurement source

5.5 Results and Discussion of Experimental Analysis

The experiment was carried out on Model III, with and without reflectors as described in the sections above. The temperature of ambient air, floor, collector surface and air flowing through the collector were recorded for two days on 24th and 25th January 2017 between 11:00 AM to 12:00 Noon. Simultaneously, the power output of SCPP system was also recorded. Solar radiation data was collected from KFUPM-RI Atlas services. On 24th

January 2017 experiments were conducted only on the SCPP system, whereas, on 25th January 2017 SCPP system was augmented with mirrors.

5.5.1 Variation of Temperature of Model III

Figure 5.10 depicts the variation of the average temperature of the ambient air and components of the SCPP during the experimental hours. The floor upon which the incident solar radiation falls has the highest temperature. The average ambient temperature during experimental hours is 19.12^0C, while the average temperature of the floor, collector cover (glass), and air in the collector are 41.22^0C, 32.83^0C, and 31.39^0C, respectively.

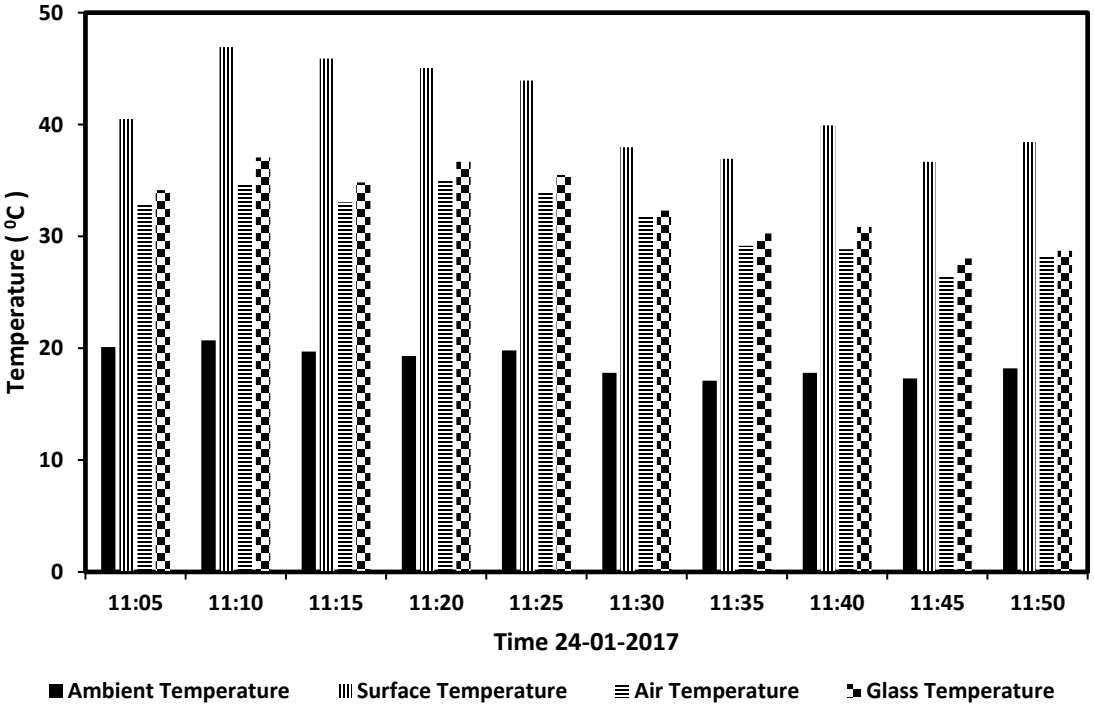

Figure 5.10. Temperature variation of SCPP Model III

5.5.2 Variation of Voltage and Current of Model III

Figure 5.11 depicts the variation of the voltage and current from the turbine-generator assembly of SCPP during the experimental hours. The absurd variation of current and voltage is due to dynamic variation of ambient temperature and amount of radiant energy incident on the absorber floor. The average DC voltage developed and current produced from the SCPP is 296.8 mV and 0.067 mA, respectively.

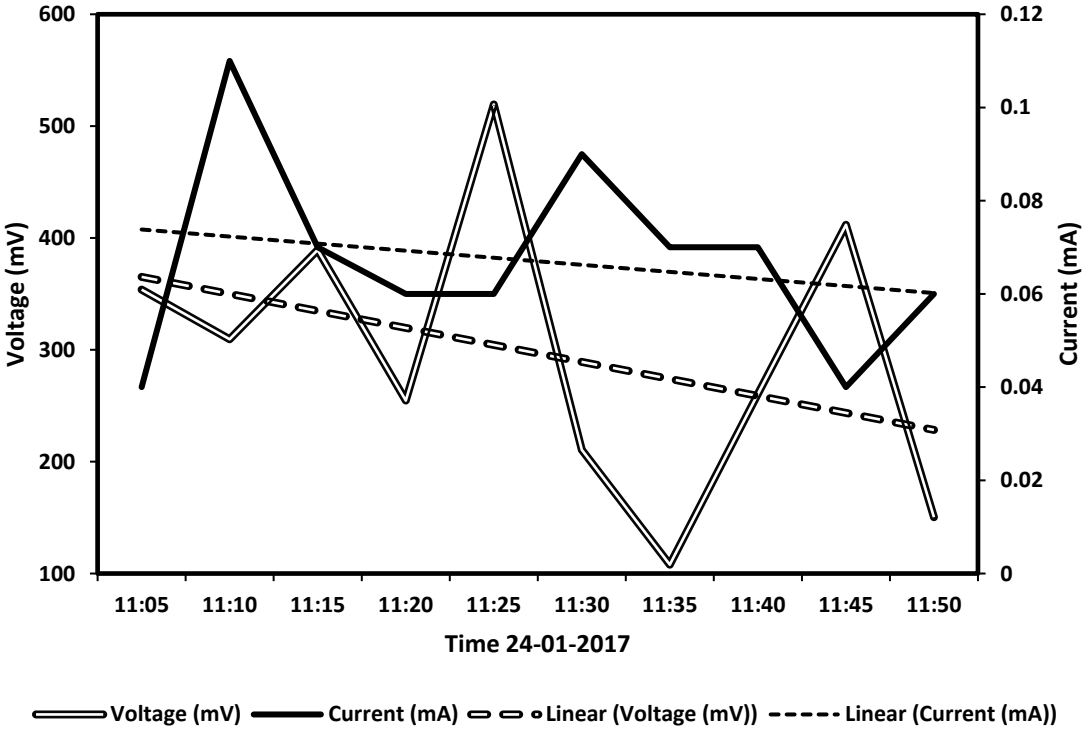

Figure 5.11. Voltage and Current Variation of SCPP model III

5.5.3 Variation of Power Produced and Efficiency of Model III

Figure 5.12 depicts the variation of power output and efficiency of the SCPP Model III during the experimental hours. The absurd variation of power output and efficiency is due to dynamic variation of ambient temperature and amount of radiant energy incident on the absorber floor. As evident from the results, power output and efficiency are directly dependent on each other. The average power output and efficiency of the SCPP are 19.214μW and 1.92E-06 %, respectively.

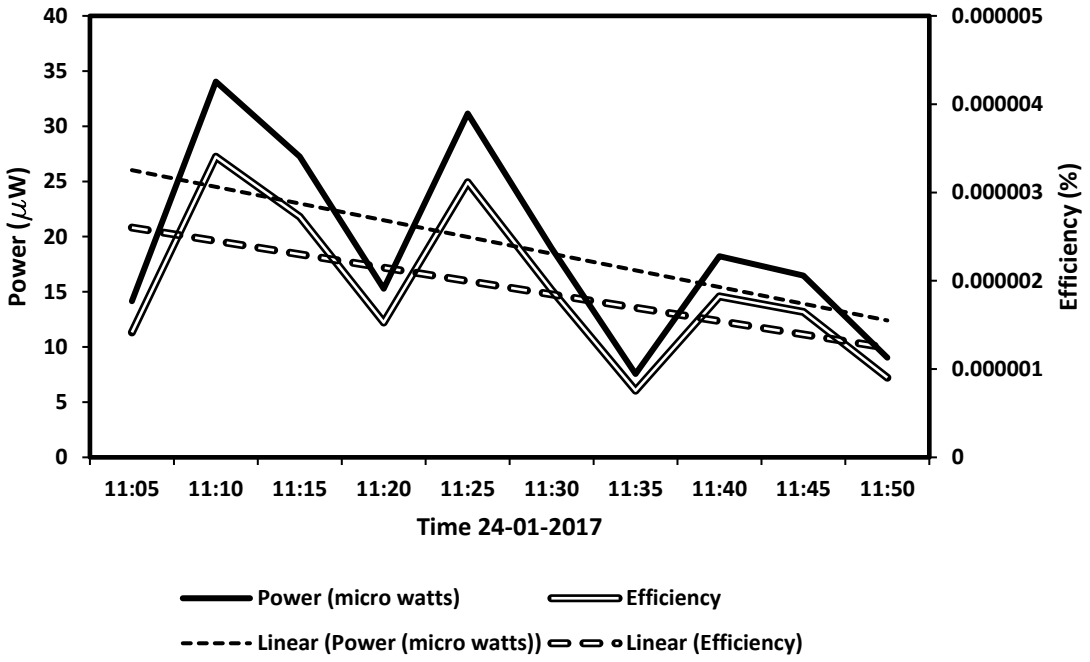

Figure 5.12. Variation of power produced and efficiency of Model III

5.5.4 Variation of Temperature of Model III aided with Reflectors

Figure 5.13 depicts the variation of the average temperature of the ambient air and components of the SCPP aided with reflectors during the experimental hours. The floor upon which the incident solar radiation falls has the highest temperature. The average ambient temperature during experimental hours is 18.78^0C, while the average temperature of the floor, collector cover (glass), and air in the collector are 44.19^0C, 33.85^0C, and 31.43^0C, respectively. With the aid of reflectors, increase in floor temperature and air in the collector is by 7.2% and 0.16%, respectively.

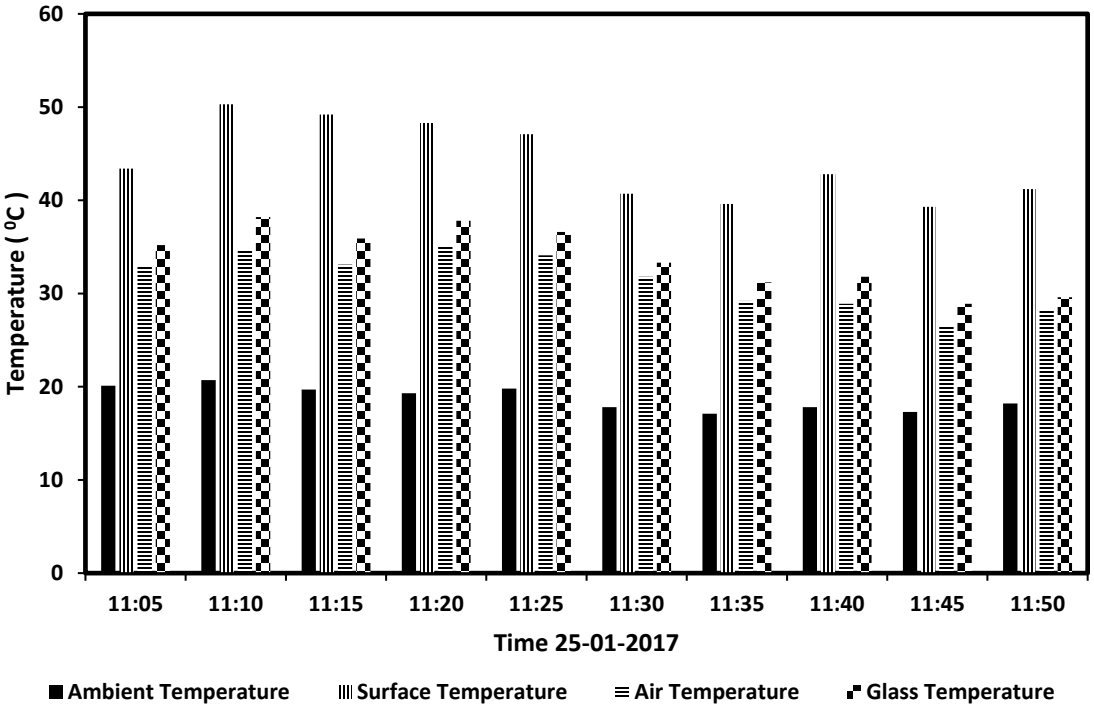

Figure 5.13. Temperature variation of SCPP Model III aided with reflectors

5.5.5 Variation of Voltage and Current of Model III aided with Reflectors

Figure 5.14 depicts the variation of the voltage and current from the turbine-generator assembly of SCPP during the experimental hours. The absurd variation of current and voltage is due to dynamic variation of ambient temperature and amount of radiant energy incident on the absorber floor. The average DC voltage developed and current produced from the SCPP is 314.3 mV and 0.126 mA, respectively. With the aid of reflectors, increase in voltage and current is by 5.89% and 88.06%, respectively.

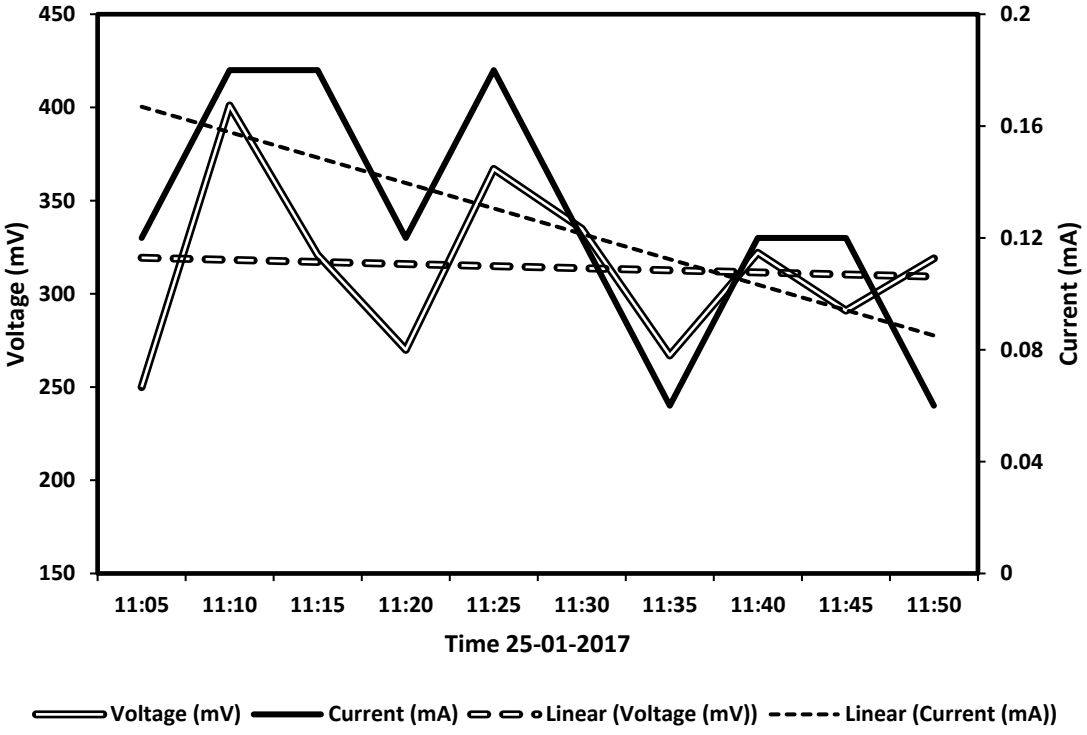

Figure 5.14. Voltage and Current Variation of SCPP model III aided with reflectors

5.5.6 Variation of Power Produced and Efficiency of Model III aided with Reflectors

Figure 5.15 depicts the variation of power output and efficiency of the SCPP Model III aided with reflectors during the experimental hours. The absurd variation of power output and efficiency is due to dynamic variation of ambient temperature and amount of radiant energy incident on the absorber floor. As evident from the results, power output and efficiency are directly dependent on each other. The average power output and efficiency of the SCPP aided with reflectors is 40.734 μW and 2.82E-06 %, respectively. With the aid of reflectors, power output is enhanced by 112%.

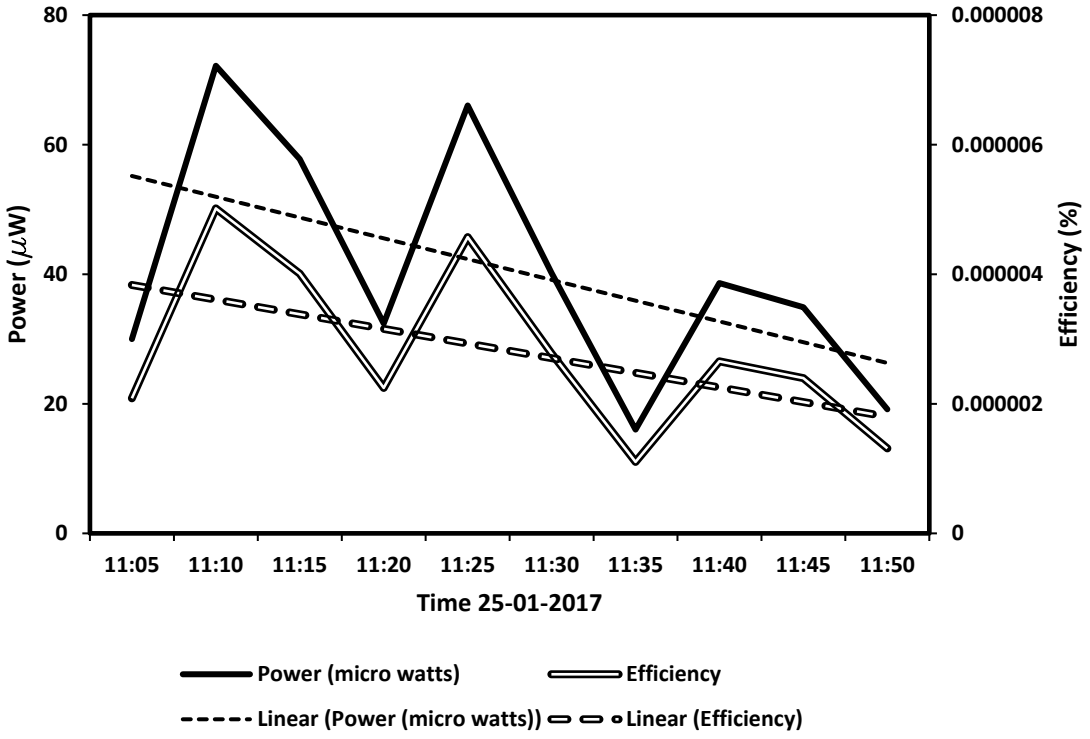

Figure 5.15. Variation of power produced and efficiency of Model III aided with reflectors

5.5.7 Uncertainty Analysis

The uncertainty analysis was carried by two methods as presented in the section above. Uncertainty by the first method is determined by finding the mean of the maximum and minimum possible errors by considering the accuracy of the instrument. Uncertainty by the second method involves the consideration of combined standard deviation. The second method is accurate for determining uncertainty for parameters associated with two or more determined experimental variables. The uncertainty in the measured temperature is $\pm$ 0.5% of the full-scale reading. Unlike temperature readings, the uncertainty associated with power measurement and efficiency determination is dependent on two or more determined variables of the experimental work. The uncertainty in the calculation of power is $\pm$ 0.45787μW and $\pm$ 2.81%. Furthermore, uncertainty associated with the determination of efficiency is $\pm$ 1.691E-06% with an accuracy of $\pm$ 2.985%.

5.6 Conclusions of Experimental Analysis

The conclusions of the experimental work are as follows:

- For an SCPP model III without reflectors, the average ambient temperature during experimental hours was found to be 21.18^{0}C, while the average temperature of the floor, collector cover (glass), and air in the collector are 39.93^{0}C, 29.08^{0}C, and 26.51^{0}C, respectively.
- For an SCPP aided with reflectors, increase in floor temperature and air in the collector was found to be 10.67% and 18.56%, respectively.

- The average power output and efficiency of the SCPP model III are 16.308 μW and 1.69E-06 %, respectively. With the aid of reflectors, increase in power output and efficiency was found to be 149.78% and 66.86%, respectively.
- Detail uncertainty analysis was performed by two methods, one considering the accuracy associated with instrumentation. While the other method determines the uncertainty by considering the combined standard deviation. All the uncertainties are within the acceptable range.

CHAPTER 6

RESULTS AND DISCUSSION

In this chapter, results of the aforementioned mathematical models are presented and discussed in detail. The discussion of the results proceeds as follows. It starts with the demonstration of results from the energy and exergy analysis of solar chimney power plant presented in Chapter 3. Then, the results associated with the energy and exergy analysis of solar chimney power plant aided with reflectors modeled in chapter 4 are presented. Afterwards, a comparative study of the solar chimney power plant aided with reflectors and conventional SCPP are discussed. Dhahran, Saudi Arabia was selected as an illustrative example to evaluate the proposed models.

All the formulated energy and exergy equations in chapters 3 and 4 are solved simultaneously using engineering equation solver (EES) software. For solar irradiation data of 2016, power output, energy, and exergy efficiency, a variation of density, a variation of mass flow rate, a variation of temperature for the floor, deck, chimney and air, and the variation of velocities at location 1, 2, and 3 for each month of the year are reported. And, a comparative study of SCPP model aided with reflectors is presented.

6.1 Solar Chimney Power Plant

In this section, the results of the solar chimney power plant are presented. Various parameters such as power output, energy, and exergy efficiency, a variation of temperature for the floor, deck, chimney and air, and the variation of velocities at location 1, 2, and 3 for each month of the year are reported.

6.1.1 Solar Irradiance Pattern

Figure 6.1 depicts the average solar irradiance pattern for Dhahran, Saudi Arabia for a given year. Peak summer is experienced during the months of June to August corresponding to an average solar insolation of 550 W/m^2 and the extreme winter is experienced during the months of December to February, during which the average solar insolation is the lowest at 330 W/m^2.

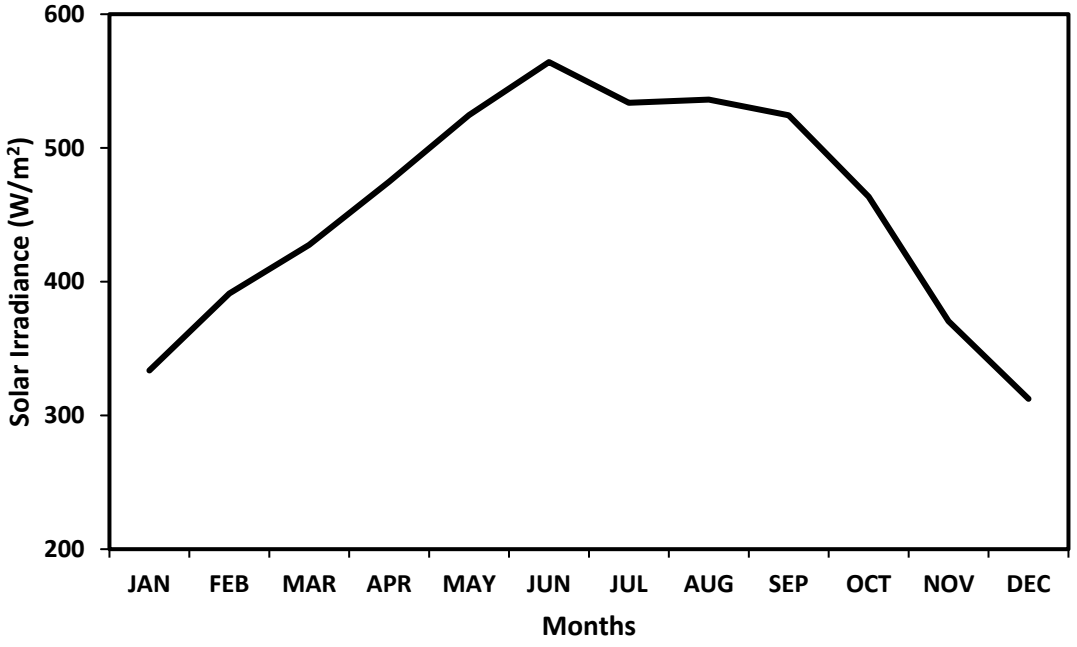

Figure 6.1. Yearly variation of the solar irradiance at Dhahran, Saudi Arabia

6.1.2 Pressure Variation across SCPP

Figure 6.2 depicts the pressure variation across the different points of the SCPP for each month of the year. The pressure difference across points 1, 2, and 3 is adequate to drive a low-pressure turbine. The pressure at the outlet of the chimney at a height of H_3 is equal to the atmospheric pressure, which prevents a negative draft. Although the pressure variation over the year at each point is small, it is significant enough to affect the mass flow rate of air through the SCPP which is evident from Figure 6.3.

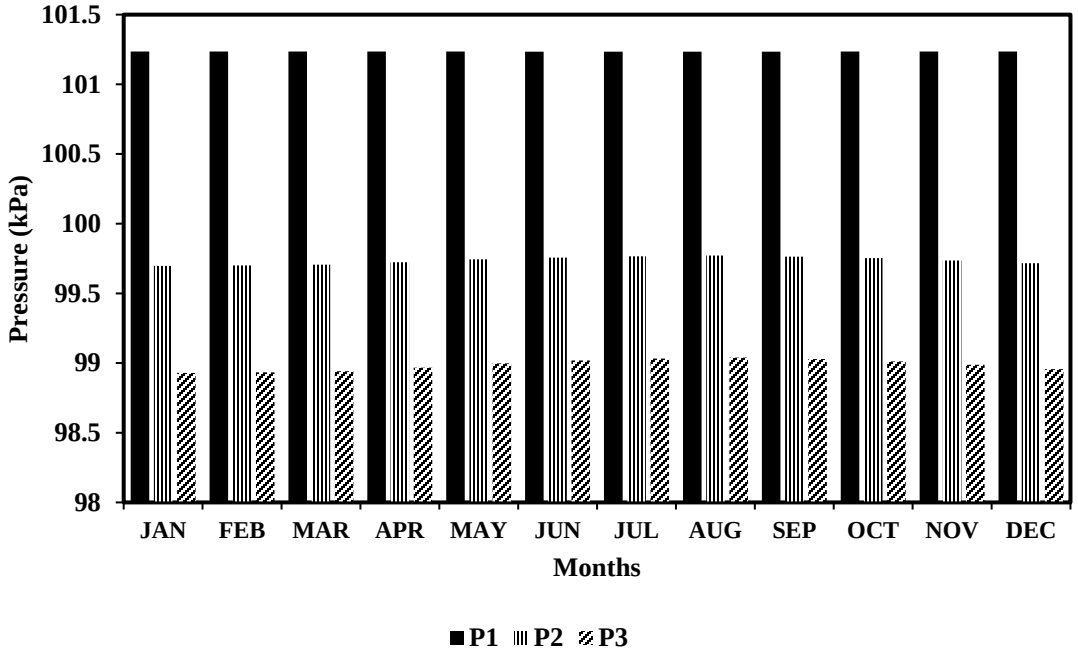

Figure 6.2. Yearly variation of the pressure at locations 1, 2, and 3

6.1.3 Velocity and Mass Flow Rate Variation along SCPP

The mass flow rate was found to vary with the solar energy which is evident from Figure 6.3. The highest mass flow rate and velocities are observed for the months of July and August, which has the highest incident solar radiation. Also, the highest power output is observed for the summer months as shown in Figure 6.4. Over a given year, the velocities

and the mass flow rate follow the same trend because they are directly related to one another. The average velocity at the inlet of the turbine (w_1) is 0.533 m/s.

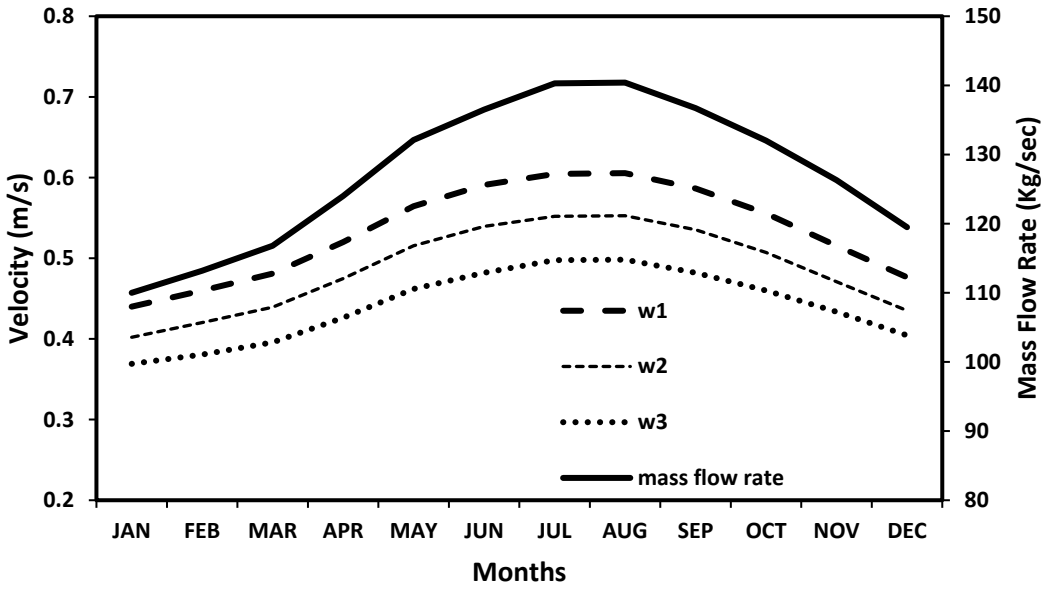

Figure 6.3. Yearly variation of the mass flow rate and the velocities

6.1.4 Variation of Power Output and Mass Flow Rate

Figure 6.4 depicts the variation of power output and mass flow rates over the year, which indicates that the power output is directly proportional to the mass flow rate. The mass flow rate is dependent on the geometry of the plant, air velocity, and the density of the air. The assumed SCPP model has, on average, an air mass flow rate of around 127 kg/s.

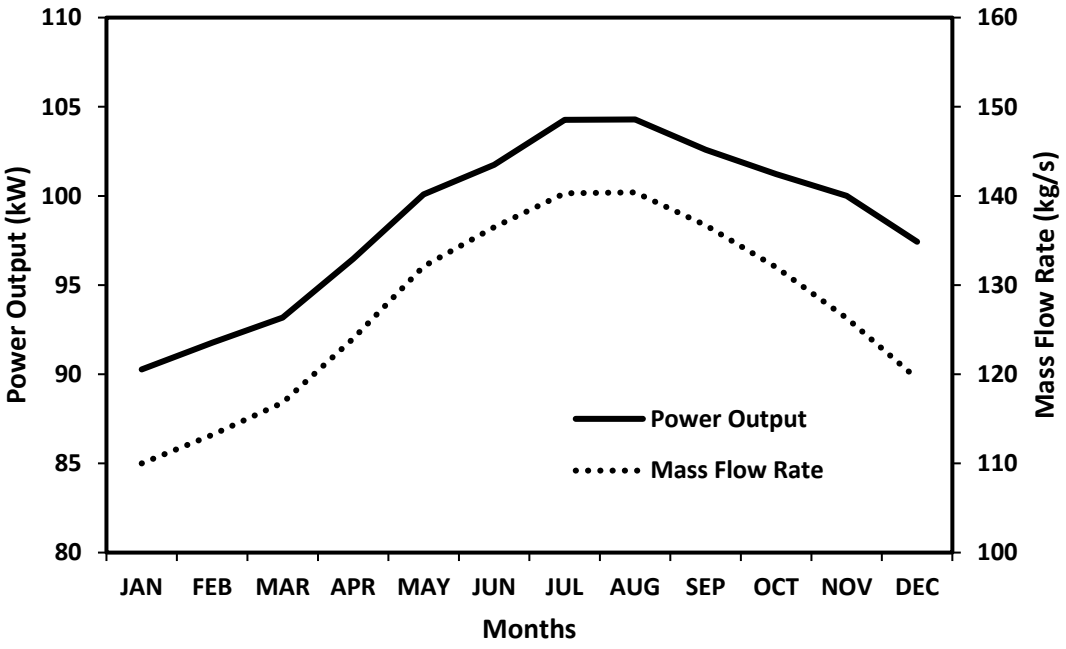

Figure 6.4. Yearly variation of the power output and the mass flow rate

6.1.5 Variation of Temperatures

Figure 6.5 depicts the yearly variation of the average temperature of the ambient air and components of the SCPP. The floor upon which the incident solar radiation falls on has the highest temperature. The average ambient temperature for Dhahran is 301 K, while the average temperature of the floor, deck, air in the collector and the chimney are 358 K, 320 K, 316 K, and 315 K, respectively. The higher floor temperature causes a variation of the density of air, which in turn moves the air towards the center where there is a low density and the chimney is located, thereby helping drive the turbine. The highest temperature is in the months of July and August, which are also the months with the highest power generation. Although the power output is low during the winter months due to the lower temperatures, the efficiency of the plant is at a maximum.

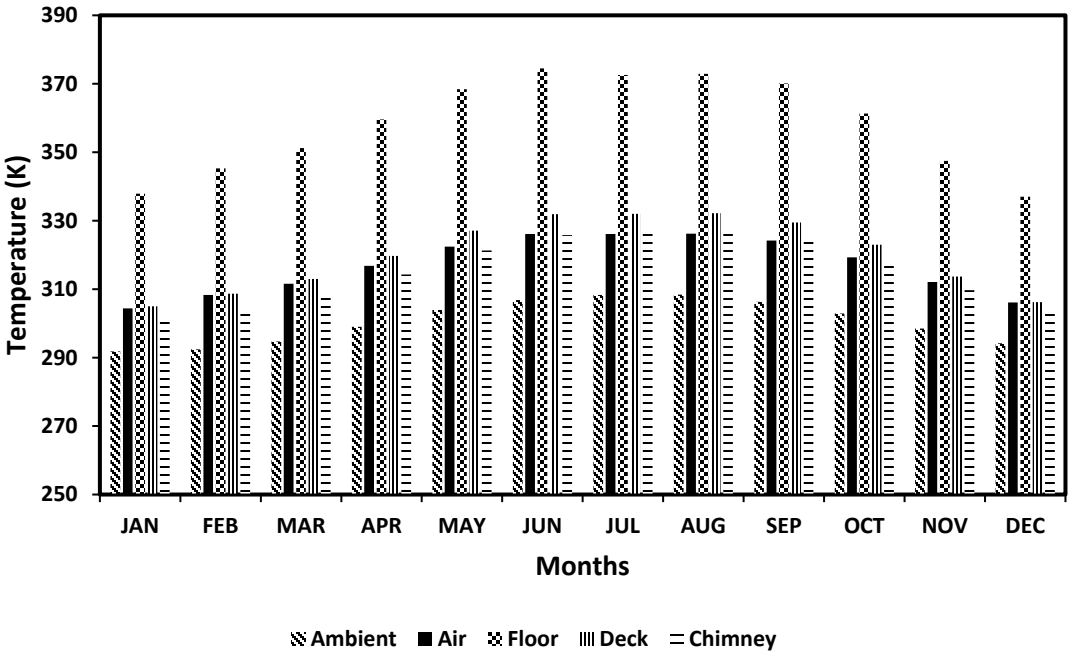

Figure 6.5. Yearly variation of the average ambient temperature, and the average temperature of the air, floor, deck, and the chimney

6.1.6 Exergy Destruction

Figure 6.6 depicts the exergy destruction or irreversibility for all the components of the SCPP, and the exergy destroyed is the highest for the floor. Although the floor is at a higher temperature, the air cannot absorb all the available energy due to the low heat capacity of air. Hence, energy is lost in the form of radiation and as heat to the other components as described in the analysis above. As the turbine is the only mechanical conversion device, its exergy destruction is a minimum. The isentropic efficiency of the turbine was assumed to be 0.7 for the analysis, which leads to lower entropy generation and yielding a lower exergy destruction. However, it is evident from the fact that along the constant volume process, exergy associated with work produced by the turbine is equal to the same work output of the turbine. Unaccounted losses of 1.21% due to the heat absorption by the components of the SCPP system are observed.

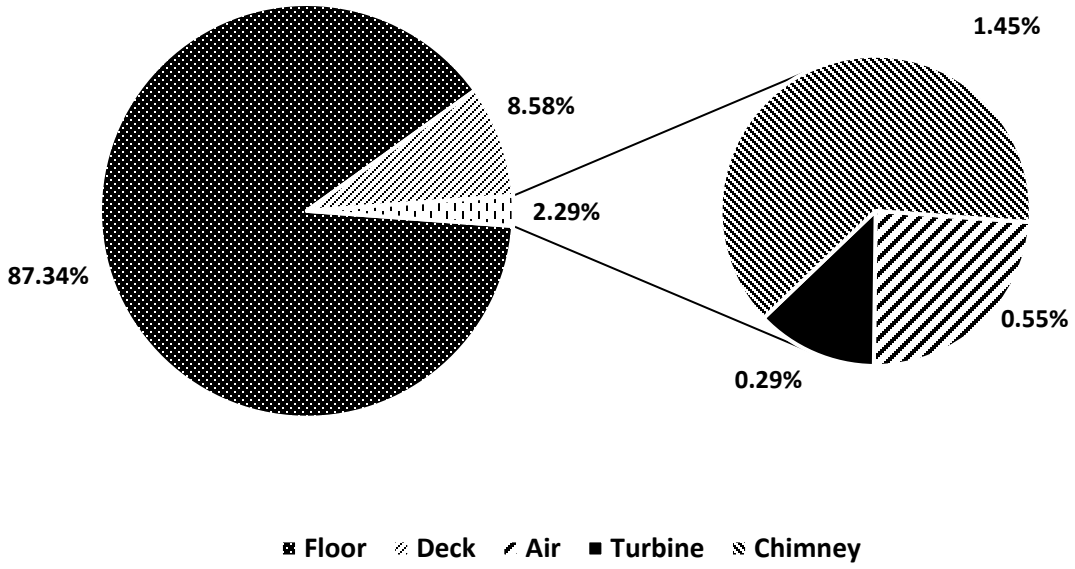

Figure 6.6. Distribution of exergy destruction across the floor, deck, air, turbine, and chimney

6.1.7 Variation of Power Output, Energetic and Exergetic Efficiencies

Figure 6.7 depicts the power output, as well as the energetic efficiency and exergetic efficiency of the SCPP system. A direct relationship between the energy output and the efficiency cannot be established as they are dependent on many inter-dependent parameters, such as the solar insolation, air velocity, and atmospheric temperature. Furthermore, the geometry of the SCPP plays a vital role, which was clearly shown by the results of Petela [28]. As indicated by Equation (3.63), X_s is 0.9 of E_s. Hence, the rational efficiency, which is the ratio between energetic and exergetic efficiency, remains constant throughout our analysis at 0.9. The assumed SCPP model under climatic conditions of Dhahran, Saudi Arabia can produce, on average, around 99 kW during the daytime. The average energetic and exergetic efficiencies are 0.523% and 0.581%, respectively.

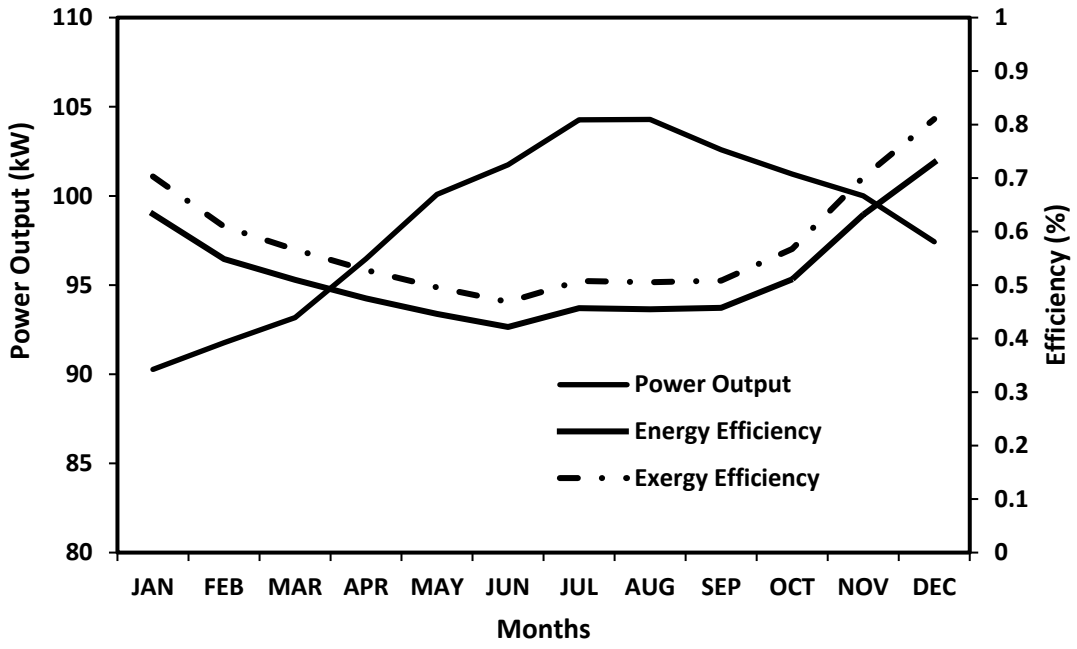

Figure 6.7. Yearly variation of the power produced, the energetic and exergetic efficiencies for Dhahran, Saudi Arabia

The results depicted in Figure 6.3, Figure 6.4, and Figure 6.7 indicate that the SCPP has the highest efficiency during the period of January and December, even though the power output is lower. Higher efficiency is due to the lower velocity, which increases the duration of contact between the air and floor allowing the air to absorb more heat from the floor, when compared with summer months. Thus, even though the power output is lower during the winter months due to the lower solar irradiation, the plant is more efficient.

6.2 Solar Chimney Power Plant Aided with Reflectors

In this section, the results of solar chimney power plant aided with reflectors are presented. Various parameters such as power output, energy efficiency, a variation of temperature of the floor and air, a variation of mass flow rate and inlet velocity of the turbine, and the density variation of air in the collector for each month of the year are reported and a comparative study with an SCPP model without reflectors is presented.

6.2.1 Irradiance Incident on Floor with the Aid of Reflectors

Figure 6.8 depicts the solar radiation incident on the floor of SCPP for Dhahran, Saudi Arabia for a given year. Peak summer is experienced during the months of June to August corresponding to average solar insolation of 600 W/m^2 and extreme winter is experienced during the months of December to February, during which the solar insolation is the lowest at 300 W/m^2. The solar radiation incident on the floor is 5% less than the solar insolation, due to the transmissivity of the deck being 95%. With the aid of reflectors, an increase of 90% of solar radiation incident on the floor is observed and 10% of it is lost due to absorption and transmission losses of the mirror. The average solar radiation incident on the floor with and without reflectors are 821 W/m^2 and 432 W/m^2, respectively.

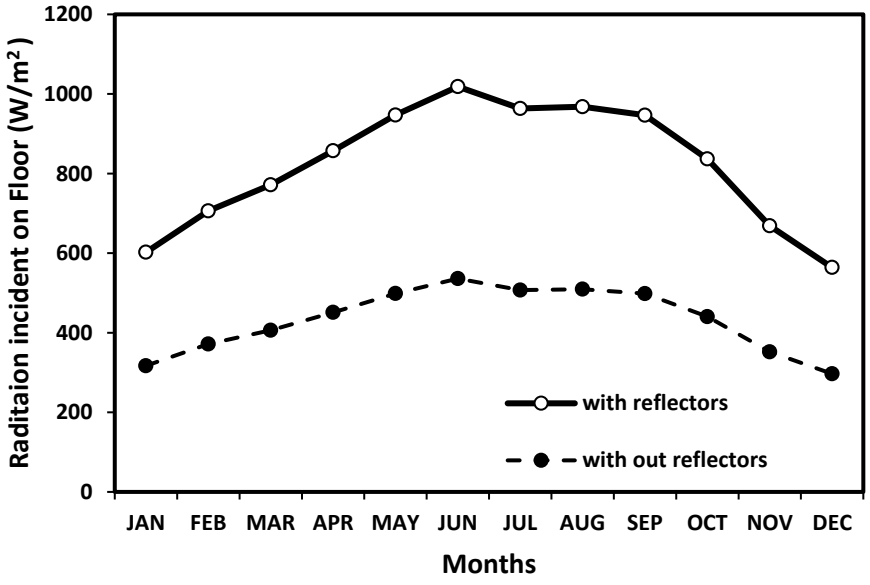

Figure 6.8. Yearly variation of solar radiation incident on floor of SCPP for Dhahran, Saudi Arabia

6.2.2 Variation of Mass Flow Rate with the Aid of Reflectors

Figure 6.9 depicts the variation of mass flow rates over the year for an SCPP with and without reflectors. The increase in incident radiation on the floor by 90% with the aid of reflectors, corresponds to the increase in mass flow rate by over 134%. The average mass flow rates with and without reflectors are 298 kg/s and 127 kg/s, respectively.

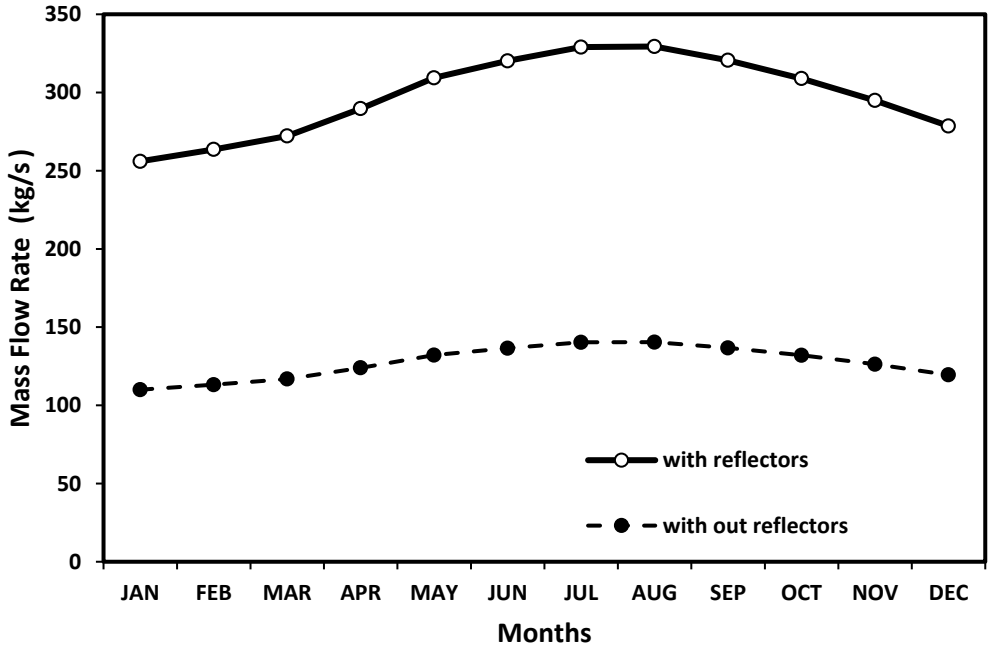

Figure 6.9. Yearly variation of Mass Flow Rate

6.2.3 Variation of Turbine Inlet Velocity

Figure 6.10 depicts the yearly variation of the velocity of air at location 1. The pattern of velocity variation is same as that of mass flow rate variation which is evident from Figure 6.9 because the mass flow rate is directly proportional to velocity. With the aid of reflectors, velocity is increased by 135%. The average inlet velocity with and without reflectors is 1.25 m/s and 0.53 m/s, respectively.

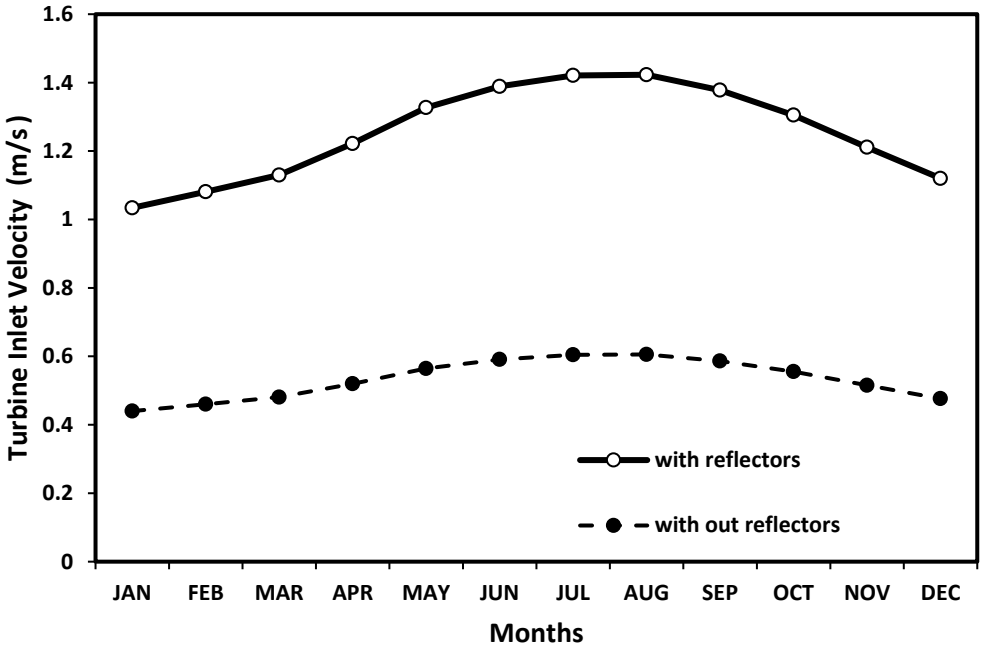

Figure 6.10. Yearly variation of turbine inlet velocity of air

6.2.4 Variation of Temperature of Floor

Figure 6.11 depicts the yearly variation of the temperature of the floor of an SCPP with and without the reflectors. With the increase in incident radiation on the floor by the aid of reflectors, an increase of 9.89% is observed for the temperature of the floor. The average temperature of the floor with and without reflectors is 393.71K and 358.19K, respectively.

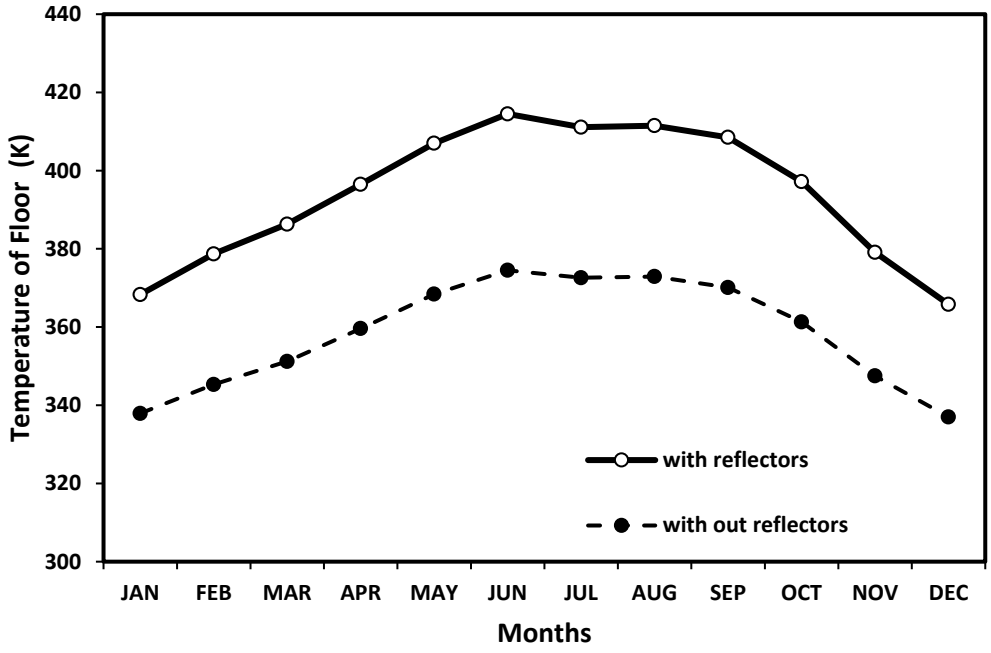

Figure 6.11. Yearly variation of temperature of floor

6.2.5 Variation of Temperature of Air in the Collector

Figure 6.12 depicts the yearly variation of the temperature of air in the collector of an SCPP with and without the reflectors. With the increase in incident radiation on the floor by the aid of reflectors, the temperature of air in the collector increases by 0.29% only. This little increase in temperature of the air is due to increase in heat transfer coefficient evident from Figure 6.14, corresponding to increase in temperature of the floor which is evident from Figure 6.11. But temperature of floor increases by 9.89%, whereas the temperature of air increases by only 0.29%, this is due to the fact that rate of heat transfer from the floor and deck to air increases due to increase in temperature of floor and deck, which dominates the change in velocity which is evident from Figure 6.10 rather than the heat absorption by air owing to low heat capacity of air. Hence a little gain in the temperature of the air is

observed. The average temperature of air in the collector with and without reflectors is 317.89K and 316.12K, respectively. This increase in temperature will affect the decrease in density of air in the collector, which is evident from Figure 6.13.

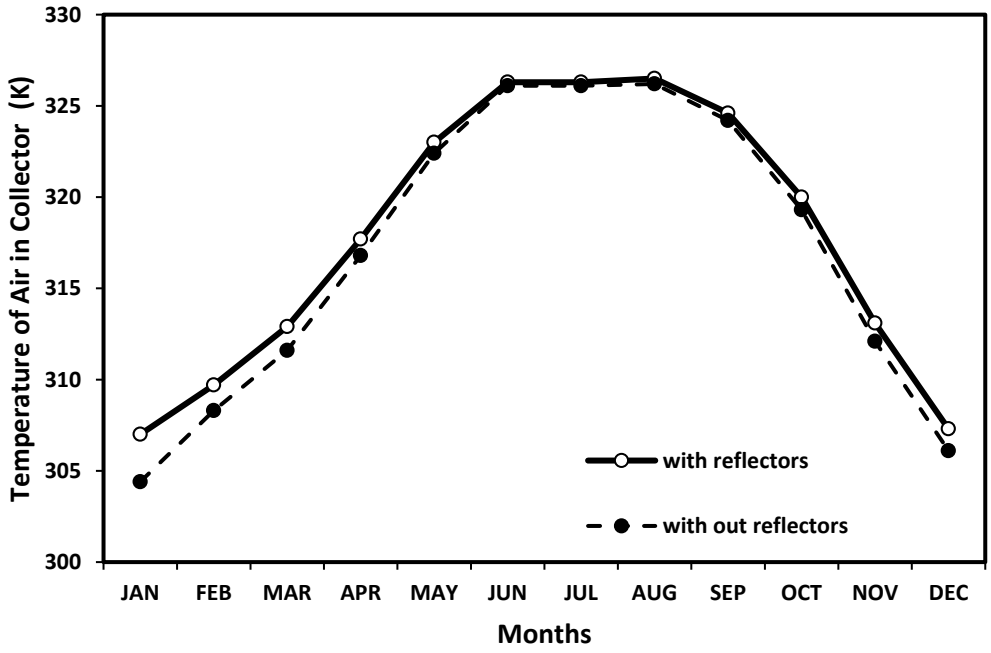

Figure 6.12. Yearly variation of temperature of air in the collector

6.2.6 Variation of Density of Air in the Collector

Figure 6.13 depicts the density variation of air in the collector of an SCPP over a year. With the increase in incident radiation on the floor by the aid of reflectors, the density of air in the collector decreases by 0.54%. The average density of air, with and without reflectors is 1.052kg/m^3 and 1.058kg/m^3, respectively. With the aid of reflectors increase in temperature of the floor which is evident from Figure 6.11 is observed, corresponding too little increase in temperature of the air, which decreases the density of air by a low amount. This little variation in density and a higher rate of heat transfer from floor to air, due to the high temperature of floor corresponds to a higher increase in velocity which is

evident from Figure 6.10.

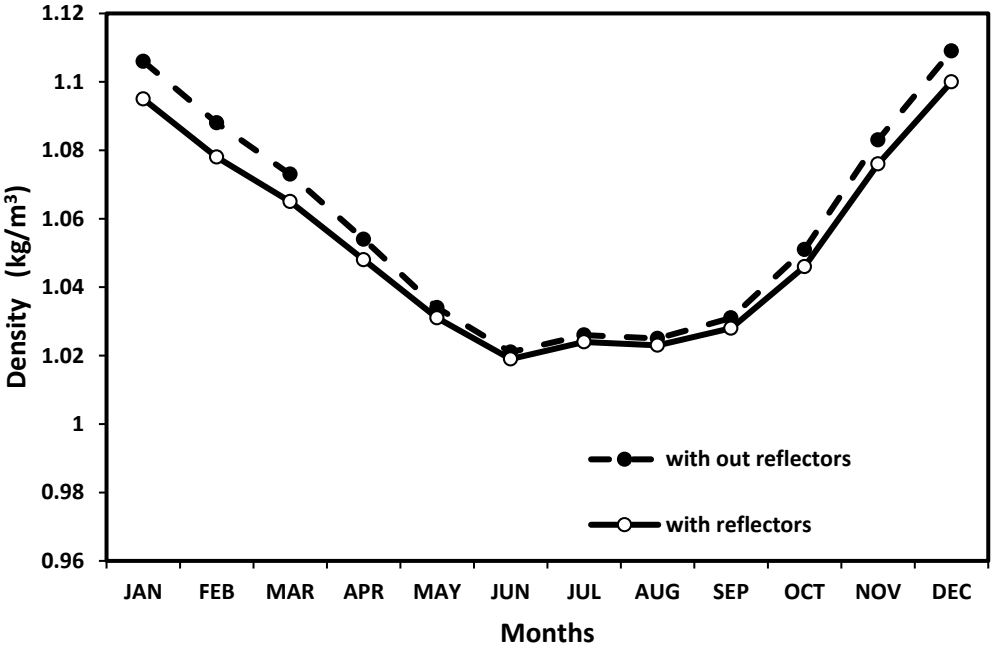

Figure 6.13. Yearly variation of density of air in the collector

6.2.7 Variation of Heat Transfer Coefficient

Figure 6.14 depicts the yearly variation of heat transfer coefficient between the floor and air in the collector, for an SCPP with and without reflectors. With the increase in incident radiation on the floor by the aid of reflectors, the temperature of the floor is increased which is evident from Figure 6.11 and, subsequently heat transfer rate increases. As heat transfer coefficient is a function of the Nusselt number, which in turn is dependent on Grashoff's number, and Grashoff's number is directly proportional to the temperature difference between the fluid and surface. Hence, with the aid of reflectors, increase in heat transfer coefficient is observed. With the aid of reflectors, heat transfer coefficient increases by 13.59%. The average heat transfer coefficient, with and without reflectors is 2.48 W/m^2K and 2.19 W/m^2K, respectively.

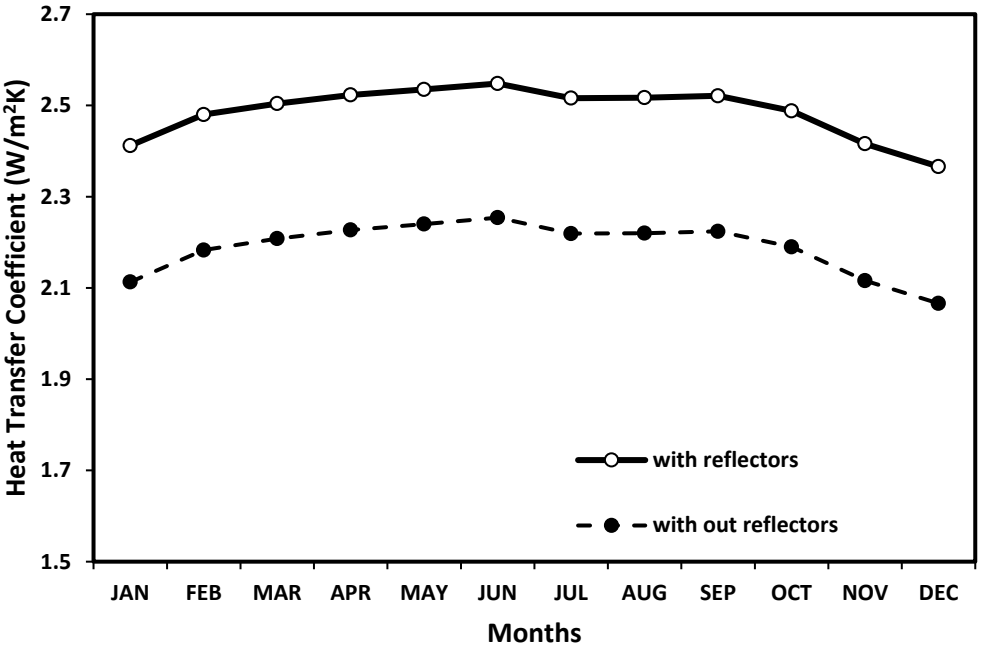

Figure 6.14. Yearly variation of heat transfer coefficient between the floor and air

6.2.8 Exergy Destruction of an SCPP Aided with Reflectors

Figure 6.15 depicts the exergy destruction or irreversibility for all the components of the SCPP aided with reflectors, and the exergy destroyed is the highest for the floor. Although the floor is at a higher temperature, the air cannot absorb all the available energy due to the low heat capacity of air. Hence, energy is lost in the form of radiation and heat to the other components as described in the analysis above. As the turbine is the only mechanical conversion device, its exergy destruction is a minimum. The isentropic efficiency of the turbine was assumed to be 0.7 for our analysis, which leads to lower entropy generation yielding a lower exergy destruction. However, it is evident from the fact that along the constant volume process, exergy associated with work produced by the turbine is equal to the same work output of the turbine. Unaccounted losses of 4%, due to the heat absorption by the components of the SCPP system are observed.

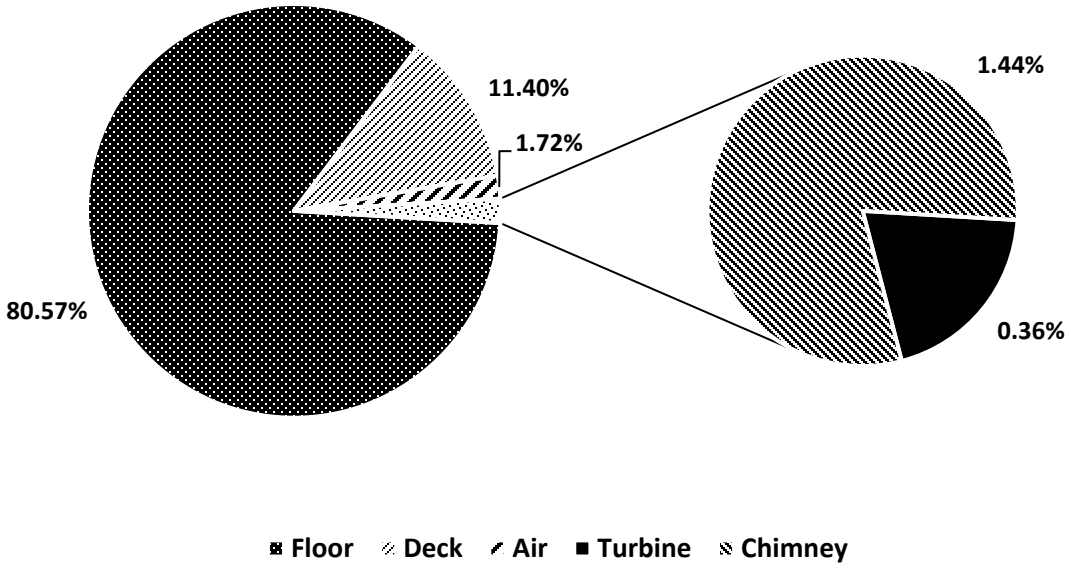

Figure 6.15. Distribution of exergy destruction across the floor, deck, air, turbine, and chimney

Table 6-1. Exergy Destruction Associated with the Components of SCPP

Exergy Destruction	Conventional SCPP	SCPP aided with Reflectors
Floor	87.34%	80.57%
Deck	8.58%	11.40%
Air	0.55%	1.72%
Turbine	0.29%	0.36%
Chimney	1.45%	1.44%
Unaccounted losses	1.21%	3.798%

Table 6-1 presents the exergy destruction associated with each component of an SCPP with and without reflectors. The exergetic efficiency of an SCPP with and without reflectors is, 0.712% and 0.581% respectively. The unaccounted losses of 3.798% and 1.21% for an

SCPP with and without reflectors, is due to the heat absorption of the components of an SCPP, which was not considered in the analysis. Results of SCPP aided with the reflectors show higher unaccounted losses when compared with the conventional SCPP, this is due to high incident energy, which leads to gain in temperature of components as shown in Figure 6.11, accounting to more absorption of heat energy by the components of an SCPP. The maximum amount of exergy destruction is associated with the floor, as the floor is the only component upon which the input energy is incident and it gets most of the radiant energy. As air is perfectly transparent to radiation, air does not gain any energy by radiation, the only source of energy transfer for air is by convective heat transfer with the floor, and, air has low heat absorbing capacity. Hence, air cannot absorb all the heat from the floor, and exergy destruction associated with the floor becomes maximum. Exergy destruction associated with the floor of an SCPP aided with reflectors is less due to the high mass flow rate which can be inferred from Figure 6.9.

Exergy destruction for deck and air, is higher for an SCPP aided with reflectors this is due to the fact that with the increase in radiant energy by the aid of reflectors increases the mean temperature of deck and air having low heat absorbing capacity, cannot absorb heat from the deck leading to the loss of available work. As far as, increase in exergy destruction for air flowing through the collector of an SCPP aided with reflector is concerned, this is due to lower gain in temperature of air attained which is evident from Figure 6.12 and higher mass flow rate produced which is depicted in Figure 6.9.

As far as, the turbine is concerned it is the only mechanical conversion device whose isentropic efficiency is equal to 0.7 in our analysis, yielding to lower entropy generation. And, conversion of kinetic energy to rotational energy is done along the constant volume

process. Along the constant volume process, exergy associated with work produced by the turbine is equal to the same work output of the turbine. Hence among all the components of an SCPP, exergy destruction associated with the turbine is minimum, these losses are accounted for frictional and thermal losses.

6.2.9 Variation of Power Output

Figure 6.16 depicts the yearly variation of the power output of an SCPP aided with and without reflectors. Power output pattern is similar to that of mass flow rate and turbine inlet velocity which is evident from Figure 6.9 and Figure 6.10, respectively. The power output is almost directly proportional to the mass flow rate, which in turn is dependent on the geometry of the plant, air velocity and density of air in the collector. With the aid of reflectors, power output is increased by 133%. The yearly average power output with and without reflectors is 230kW and 99kW, respectively.

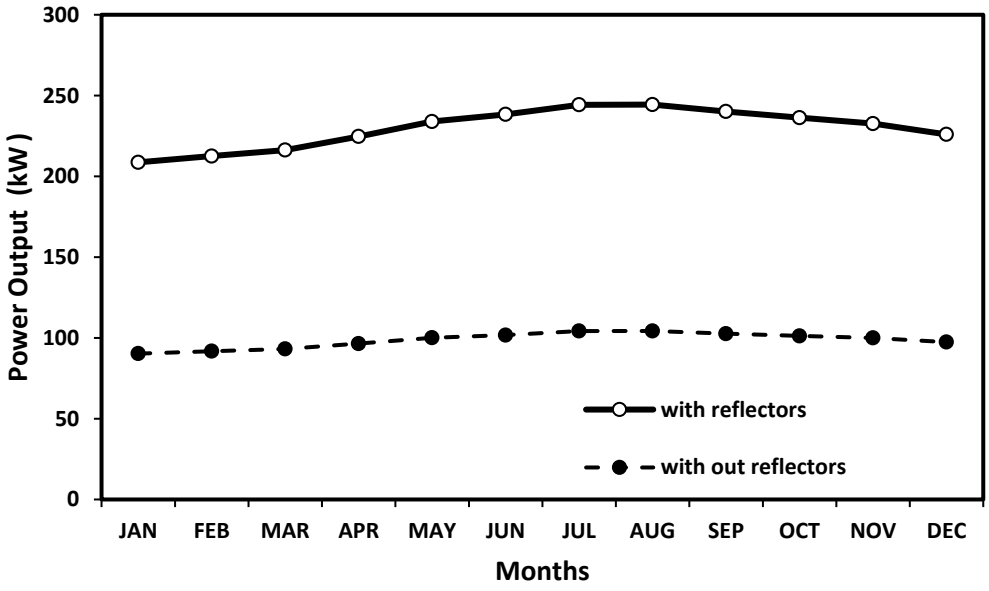

Figure 6.16. Yearly variation of power output

6.2.10 Variation of Energetic Efficiency

Figure 6.17 depicts the yearly variation of the energetic efficiency of an SCPP aided with and without reflectors. A direct relationship between power output and efficiency could not be established as they are dependent on many inter-dependent parameters, such as the solar insolation, air velocity, and atmospheric temperature. But, efficiency follows the same trend as the density variation which is evident from Figure 6.13. With the aid of reflectors, the efficiency of an SCPP is enhanced by 22.6%. The yearly average efficiency of an SCPP with and without reflectors is 0.641% and 0.523%, respectively.

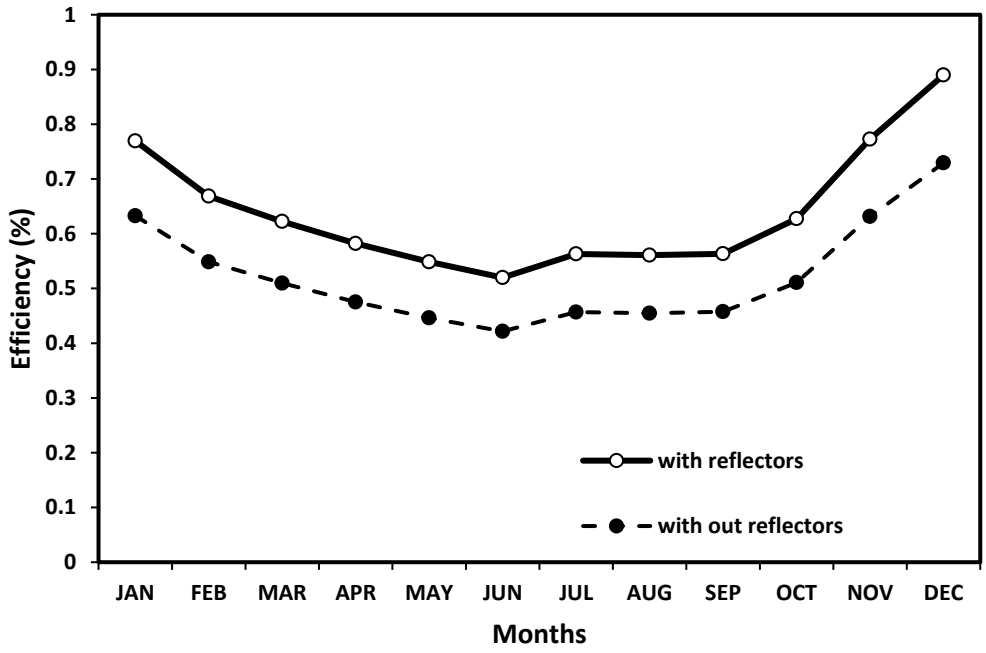

Figure 6.17. Yearly variation of the energetic efficiency

6.2.11 Variation of Exergetic Efficiency

Figure 6.18 depicts the yearly variation of the exergetic efficiency of an SCPP aided with and without reflectors. A direct relationship between energetic efficiency and exergetic

efficiency is established from Equation (4.27). So, exergetic efficiency follows the same trend as the energetic efficiency which is evident from Figure 6.17. With the aid of reflectors, exergetic efficiency of an SCPP is enhanced by 22.6%. The yearly average exergetic efficiency of an SCPP with and without reflectors is 0.712% and 0.581%, respectively.

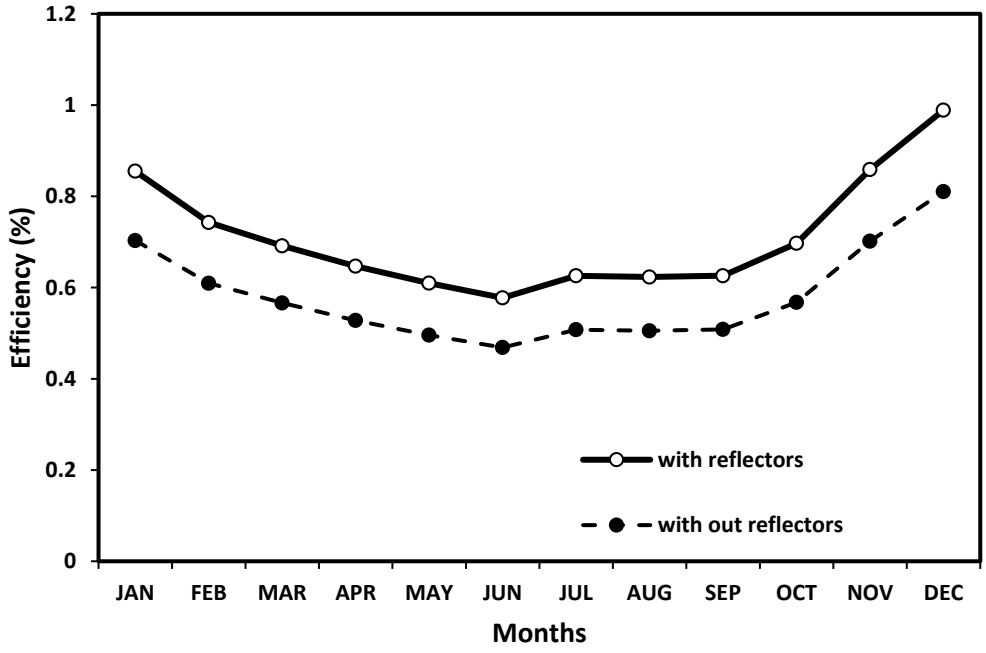

Figure 6.18. Yearly variation of exergetic efficiency

6.2.12 Variation of Power Produced, Energetic and Exergetic Efficiency for an SCPP with the aid of Reflectors

Figure 6.19 depicts the power output, as well as the energetic efficiency and exergetic efficiency of the SCPP system aided with reflectors. A direct relationship between the power output and the efficiency cannot be established as they are dependent on many inter-dependent parameters, such as the solar insolation, air velocity, and atmospheric temperature. Furthermore, the geometry of the SCPP plays a vital role, which was clearly

shown by the results of Petela [28]. As indicated by Equations (4.27) & (4.28), X_s is 0.9 of E_s. Hence, the rational efficiency, which is the ratio between energetic and exergetic efficiency, remains constant throughout our analysis at 0.9.

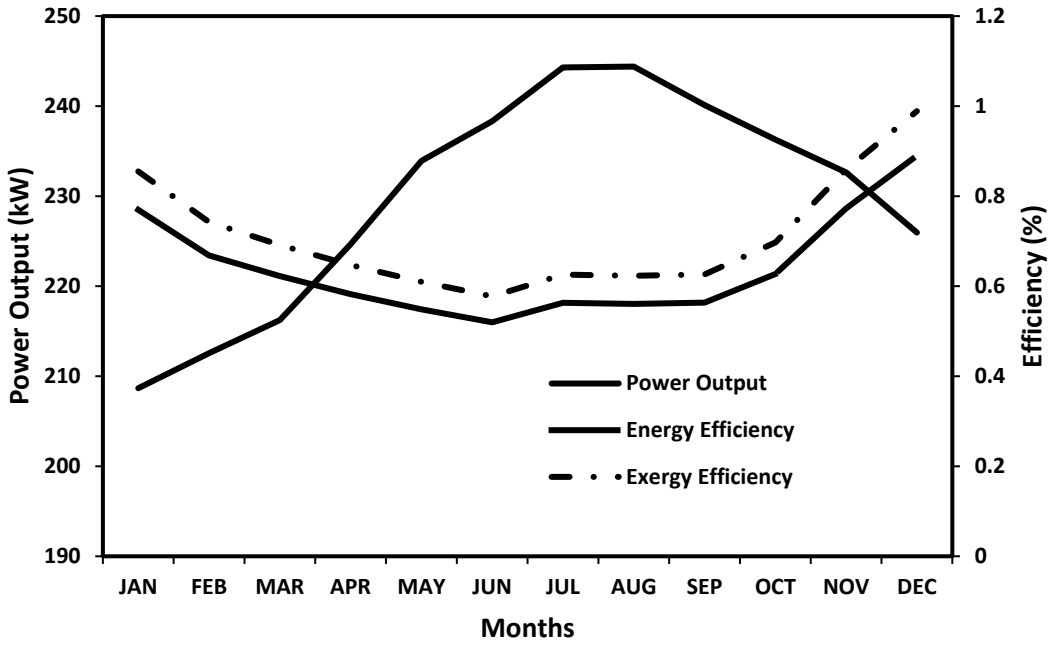

Figure 6.19. Yearly variation of the power produced, and efficiencies for an SCPP aided with reflectors at Dhahran, Saudi Arabia

The proposed SCPP model aided with reflectors can produce, on average, around 230 kW during the daytime and has, on average, an air mass flow rate of around 298 kg/s. The average energetic and exergetic efficiencies are 0.641% and 0.712%, respectively.

CHAPTER 7

CONCLUSIONS AND RECOMMENDATIONS

In this chapter, the conclusions of this study and the results that were elaborated in the previous chapter have been presented and discussed. Furthermore, the future work and recommendations are also presented.

7.1 Conclusions

A model was developed to analyze the SCPP thermodynamically, by determining the energetic and exergetic performance. All the equations of the developed model were solved simultaneously by using Engineering Equation Solver (EES) software considering sufficient and necessary conditions. The current study employs the detailed method for determining the effective diameter of the 3D flow and the heat transfer coefficient. Results of the developed model are validated with the analytical case study, experimental and numerical models available in the literature.

The conclusions of the validation are as follows:

— The values obtained for heat transfer coefficient in the literature were randomly varying due to the use of the dimensionally inconsistent formula to determine the effective diameter of a 3D flow. Also, a formula based on forced convection is used to determine the Nusselt number, while the flow between the floor and deck is due to free convection. This inconsistency was corrected in the model developed in the present study.

— The increase in the temperature of air flowing through the collector as indicated by the results of analytical validation is expected to correspond to a higher power output and efficiency. However, as the density of air decreases with increasing temperature, there is a decrease in the mass flow rate. Hence, a lower power output and efficiency are observed in this study, when compared with the results available in the literature.

— The developed model was validated with the 3D numerical model available in the literature. The geometry of the 3D model is same as considered in the present study. The model was validated for two cases with varying solar insolation of 800 Wm^{-2} and 850Wm^{-2} respectively. The average relative error for two cases between the results of the present study and 3D numerical model is less than 5.6%, almost all results were in consensus with one another. There exist a wide relative error for the velocity of air at location1 (w_1), due to a lower order of velocity which is less than 1m/s. The deviation in temperature of the floor (T_{fE}) and temperature of the deck (T_{dE}) is due to incorrect Nusselt number correlation used in the models available in the literature, for determining the heat transfer coefficient ($h_{f\text{-}a}$) and inconsistent formula for determining the effective diameter (D_E). The error for chimney surface temperature (T_{ch}) is 7%, this is due to inappropriate modeling for losses of chimney surface, which is corrected in the present study.

— When the results of simplified models as developed in our case, are in consensus with the numerical models, simplified models get an edge of an economic advantage as it requires little computation time and saves man-hours.

— The analytical model developed predicts the real values of temperature and efficiency with the variance of 5-6%

The conclusions of the SCPP model developed are as follows:

— Dhahran, Saudi Arabia was selected as an illustrative example to evaluate the proposed model. For solar irradiation data of 2016, power output, energy, and exergy efficiency, a variation of temperature for the floor, deck, chimney and air, and the variation of velocities at location 1, 2, and 3 for each month of the year are reported.

— Over a given year, the velocities and the mass flow rate follow the same trend because they are directly related to one another. Furthermore, variation of energy output and mass flow rate indicates that they are, almost directly proportional to one another. The mass flow rate is dependent on the geometry of the plant, air velocity, and the density of the air.

—The higher floor temperature causes a variation of the density of air, which in turn moves the air towards the center where there is a low density and the chimney is located, thereby helping drive the turbine. The highest temperature is in the months of July and August, which are also the months with the highest power generation. Although the power output is low during the winter months due to the lower temperatures, the efficiency of the plant is at a maximum.

— The SCPP has the highest efficiency during the period of January and December, even though the energy output is lower. Higher efficiency is due to the lower velocity, which increases the duration of contact between the air and floor allowing the air to absorb more heat from the floor, when compared with summer months.

Thus, even though the power output is lower during the winter months due to the lower solar irradiation, the plant is more efficient.

— The proposed SCPP model can produce, on average, around 99 kW during the daytime and has, on average, an air mass flow rate of around 127 kg/s. The average energetic and exergetic efficiencies are 0.523% and 0.581%, respectively.

— The maximum exergy destruction is observed for the floor. Thus, the floor has the highest exergy improvement potential.

In the present study, with the quest of high power output, a mathematical model is developed for a novel method of enhancement. In this model, SCPP is aided with reflectors to increase the radiation incident on the floor of SCPP. All the reflectors are arranged in the similar pattern as heliostats of solar tower reflecting towards the deck.

The conclusions for an SCPP model aided with reflectors are as follows:

— The objective of this study was to streamline the interpretative mathematical model of the SCPP aided with reflectors and to present the comparative study with the conventional SCPP.

— With the aid of reflectors, an increase in 90% of solar radiation incident on the floor is observed and 10% of it is lost due to absorption and transmission losses of the mirror. For the proposed model, the average solar radiation incident on the floor with and without reflectors is 821 W/m^2 and 432 W/m^2, respectively.

— For the proposed model of an SCPP aided with reflectors, mass flow rate is increased by 134%, turbine inlet velocity is increased by 135%, the temperature of the floor is increased by 9.89%, power output is increased by 133%, and, the efficiency is escalated by 22%.

— The proposed SCPP model aided with reflectors can produce, on average, around 230 kW during the daytime and has, on average, an air mass flow rate of around 298 kg/s. The average energetic efficiency and exergetic efficiency is 0.641% and 0.712%, respectively.

Hence, SCPP aided with reflectors is one of the promising enhancement technology to improve the potential of SCPP. A lot of research is still in need to determine intricate mechanisms associated with the SCPP and reflector field. Below are the few recommendations.

7.2 Recommendations

The recommendations for future research are given below:

— Optimization of reflector field, to accommodate continuous real-time tracking.

— Means of making SCPP operational for 24 hours by employing storage medium along the floor of an SCPP.

— The scope of introducing the floating chimney for a plant aided with reflectors.

— Design of turbine, which requires low starting torque and runs at below atmospheric pressure.

Nomenclature

C_D	Chimney wall thickness coefficient
C_P	Specific heat at constant pressure
D	Diameter (m)
D_E	Effective diameter of collector
E	Energy rate
Gr	Grashoff number
g	Acceleration due to gravity
H	Height (m)
h	Convective heat transfer coefficient
Nu	Nusselt number
P	Pressure
Pr	Prandtl number
R	Gas constant
Ra	Rayleigh number
Re	Reynolds number
T	Turbine
T_x	Temperature of the component ‘x’
V	Volume of collector between deck and floor
X	Exergy rate
ΔX	Exergy destruction rate

Subscripts Representation

x-y	From component x to y
Mn	Mode of energy content (enthalpy, kinetic or potential) at State points (0,1,2,3) E.g., a1 (enthalpy at location 1)

List of Greek Symbols

α	Absorptivity
β	Volumetric Coefficient of expansion
ε	Emissivity
η	Efficiency
θ	Inclination angle
κ	Thermal conductivity of the fluid
υ	Kinematic viscosity
τ	Transmissivity
φ	Shape factor

Subscripts Representation

a	Air
a	Enthalpy
amb	Ambient
ch	Chimney
d	Deck
f	Floor
gr	Ground

p	Potential Energy
power	Power produced by a Turbine
sky	Sky
S	Sun
w	Kinetic Energy or Velocity
0,1,2,3	State Points

References

[1] Musunuri, R. K., Sanchez, D., and Rodriguez, R., 2007, *Solar Thermal Energy*, Gavle, Sweden.

[2] Bogdanienko, J., 1989, *Renewable Energy Sources*, PWN, Warsaw.

[3] Twidell, J., and Weir, T., 2015, *Renewable Energy Resources*, Routledge, London and New York.

[4] "SOLARGIS" [Online]. Available: https://solargis.info/. [Accessed: 16-Apr-2017].

[5] Said, S. A. M., El-Amin, I. M., and Al-Shehri, A. M., 2004, "Renewable Energy Potentials in Saudi Arabia," *Beirut Regional Collaboration Workshop on Energy Efficiency and Renewable Energy Technology*, pp. 76–82.

[6] Haaf, W., Friedrich, K., Mayr, G., and Schlaich, J., 1983, "Solar Chimneys Part I: Principle and Construction of the Pilot Plant in Manzanares," Int. J. Sol. Energy, **2**(1), pp. 3–20.

[7] Schlaich Jorg, 1995, *The Solar Chimney-Electricity from the Sun*, Axel Menges, Stuttgart.

[8] HAAF, W., 1984, "Solar Chimneys," Int. J. Sol. Energy, **2**(2), pp. 141–161.

[9] Mullett, L. B., 1987, "The Solar Chimney—overall Efficiency, Design and Performance," Int. J. Ambient Energy, **8**(1), pp. 35–40.

[10] Pasumarthi, N., and Sherif, S. A., 1998, "Experimental and Theoretical Performance of a Demonstration Solar Chimney Model — Part I : Mathematical Model Development," Int. J. Energy Res., **22**(3), pp. 277–288.

[11] Pasumarthi, N., and Sherif, S. A., 1998, "Experimental and Theoretical Performance of a Demonstration Solar Chimney Model — Part II : Experimental and Theoretical Results," Int. J. Energy Res., **22**(5), pp. 443–461.

[12] Gannon, A. J., and Backstrom, T. W. Von, 2000, "Solar Chimney Cycle Analysis With System Loss and Solar Collector Performance," J. Sol. Energy Eng., **122**, pp. 133–137.

[13] von Backström, T. W., and Gannon, A. J., 2000, "Compressible Flow Through Solar Power Plant Chimneys," J. Sol. Energy Eng., **122**(3), p. 138.

[14] Backstrom, T. W., and Fluri, T. P., 2006, "Maximum Fluid Power Condition in Solar Chimney Power Plants - An Analytical Approach," Sol. Energy, **80**(11), pp. 1417–1423.

[15] Pastohr, H., Kornadt, O., and Gürlebeck, K., 2004, "Numerical and Analytical

Calculations of the Temperature and Flow Field in the Upwind Power Plant," Int. J. Energy Res., **28**(6), pp. 495–510.

[16] Hedderwick, R. A., 2000, "Performance Evaluation of a Solar Chimney Power Plant. M. Sc. Thesis," University of Stellenbosch, South Africa.

[17] Pretorius, J. P., 2007, "Optimization and Control of a Large-Scale Solar Chimney Power Plant, PhD Thesis," University of Stellenbosch, South Africa.

[18] Pretorius, Johannes P; Kroger, D., 2006, "Solar Chimney Power Plant Performance," J. Sol. Energy Eng., **128**(3), pp. 302–311.

[19] Pretorius, Johannes P; Kroger, D., 2006, "Sensitivity Analysis of the Operating and Technical Specifications of a Solar Chimney Power Plant," J. Sol. Energy Eng., **129**(2), pp. 171–178.

[20] Hamdan, M. O., 2011, "Analysis of a Solar Chimney Power Plant in the Arabian Gulf Region," Renew. Energy, **36**(10), pp. 2593–2598.

[21] Zhou, X., Yang, J., Xiao, B., Hou, G., and Xing, F., 2009, "Analysis of Chimney Height for Solar Chimney Power Plant," Appl. Therm. Eng., **29**(1), pp. 178–185.

[22] Dehghani, S., and Mohammadi, A. H., 2014, "Optimum Dimension of Geometric Parameters of Solar Chimney Power Plants – A Multi-Objective Optimization Approach," Sol. Energy, **105**, pp. 603–612.

[23] Guo, P., Li, J., Wang, Y., and Wang, Y., 2016, "Evaluation of the Optimal Turbine Pressure Drop Ratio for a Solar Chimney Power Plant," Energy Convers. Manag., **108**, pp. 14–22.

[24] Kasaeian, A., Ghalamchi, M., and Ghalamchi, M., 2014, "Simulation and Optimization of Geometric Parameters of a Solar Chimney in Tehran," Energy Convers. Manag., **83**, pp. 28–34.

[25] Xu, G., Ming, T., Pan, Y., Meng, F., and Zhou, C., 2011, "Numerical Analysis on the Performance of Solar Chimney Power Plant System," Energy Convers. Manag., **52**(2), pp. 876–883.

[26] Gholamalizadeh, E., and Kim, M. H., 2016, "CFD (Computational Fluid Dynamics) Analysis of a Solar-Chimney Power Plant with Inclined Collector Roof," Energy, **107**, pp. 661–667.

[27] Mehrpooya, M., Shahsavan, M., and Sharifzadeh, M., 2016, "Modeling , Energy and Exergy Analysis of Solar Chimney Power Plant-Tehran Climate Data Case Study," Energy, **115**, pp. 257–273.

[28] Petela, R., 2009, "Thermodynamic Study of a Simplified Model of the Solar Chimney Power Plant," Sol. Energy, **83**(1), pp. 94–107.

[29] Nizetic, S., Ninic, N., and Klarin, B., 2008, "Analysis and Feasibility of

Implementing Solar Chimney Power Plants in the Mediterranean Region," Energy, **33**(11), pp. 1680–1690.

[30] Zhou, X., Yang, J., Xiao, B., and Hou, G., 2007, "Experimental Study of Temperature Field in a Solar Chimney Power Setup," Appl. Therm. Eng., **27**(11–12), pp. 2044–2050.

[31] Maia, C. B., Silva, J. O. C., Cabezas-gómez, L., Hanriot, S. M., and Ferreira, A. G., 2013, "Energy and Exergy Analysis of the Air Flow inside a Solar Chimney," Renew. Sustain. Energy Rev., **27**, pp. 350–361.

[32] Mekhail, T., Rekaby, A., Fathy, M., Bassily, M., and Harte, R., 2017, "Experimental and Theoretical Performance of Mini Solar Chimney Power Plant," J. Clean Energy Technol., **5**(4), pp. 294–298.

[33] Kreetz, H., 1997, "Theoretische Untersuchungen Und Auslegung Eines Tempora ¨ren Wasserspeichers Fu¨r Das Aufwindkraftwerk, Diploma Thesis," Technical University Berlin, Germany.

[34] Bernardes, M. A., 2004, "Technical, Economical and Ecological Analysis of Solar Chimney Power Plants. Diss. Ph. D. Thesis," Stuttgart University, Germany.

[35] Dos S. Bernardes, M. A., Voss, A., and Weinrebe, G., 2003, "Thermal and Technical Analyses of Solar Chimneys," Sol. Energy, **75**(6), pp. 511–524.

[36] Pasumarthi, N., and Sherif, S. A., 1997, "Performance of a Demonstration Solar Chimney Model for Power Generation," *Proceedings of the 35th Heat Transfer and Fluid Mechanics*, Sacremento, CA, USA, pp. 230–240.

[37] Pretorius, J. P., and Kroger, D. G., 2006, "Critical Evaluation of Solar Chimney Power Plant Performance," Sol. Energy, **80**, pp. 535–544.

[38] Bilgen, E., and Rheault, J., 2005, "Solar Chimney Power Plants for High Latitudes," Sol. Energy, **79**(5), pp. 449–458.

[39] Papageorgiou, C. D., 2007, "Floating Solar Chimney versus Concrete Solar Chimney Power Plants," Int. Conf. Clean Electr. Power, ICCEP '07, pp. 760–765.

[40] Papageorgiou, C., 2003, "Floating Solar Chimney, US7735483 B2."

[41] Papageorgiou, C., 2007, "Floating Solar Chimney Technology: A Solar Proposal for China," Proc. {ISES} World Congr. 2007 (Vol. I – Vol. V), pp. 172–176.

[42] Zhou, X., Yang, J., Wang, J., and Xiao, B., 2009, "Novel Concept for Producing Energy Integrating a Solar Collector with a Man Made Mountain Hollow," Energy Convers. Manag., **50**(3), pp. 847–854.

[43] Alrobaei, H., 2007, "Hybrid Geothermal / Solar Energy Technology For Power Generation," Engineering [Online]. Available: ttp://www.environmental-expert.com/resultEachArticle.aspx?cid=24847&codi

=14612&lr=1&word=hybrid+geothermal. [Accessed: 31-Oct-2017].

[44] Zuo, L., Zheng, Y., Li, Z., and Sha, Y., 2011, "Solar Chimneys Integrated with Sea Water Desalination," Desalination, **276**(1–3), pp. 207–213.

[45] Zuo, L., Yuan, Y., Li, Z., and Zheng, Y., 2012, "Experimental Research on Solar Chimneys Integrated with Seawater Desalination under Practical Weather Condition," Desalination, **298**, pp. 22–33.

[46] Islamuddin, A., Al-Kayiem, H. H., and Gilani, S. I., 2013, "Simulation of a Collector Using Waste Heat Energy in a Solar Chimney Power Plant System," *WIT Transactions on Ecology and The Environment*, pp. 933–944.

[47] Islamuddin, A., Al-Kayiem, H. H., and Gilani, S. I., 2013, "Simulation of Solar Chimney Power Plant with an External Heat Source," *IOP Conference Series: Earth and Environmental Science*, pp. 1–4.

[48] Nizetic, S., 2011, "Technical Utilisation of Convective Vortices for Carbon-Free Electricity Production: A Review," Energy, **36**(2), pp. 1236–1242.

[49] Ninic, N., and Nizetic, S., 2009, "Elementary Theory of Stationary Vortex Columns for Solar Chimney Power Plants," Sol. Energy, **83**(4), pp. 462–476.

[50] Beerbaum, S., and Weinrebe, G., 2000, "Solar Thermal Power Generation in India-a Techno-Economic Analysis," Renew. Energy, **21**(2), pp. 153–174.

[51] Zhou, X., Yang, J., Wang, F., and Xiao, B., 2009, "Economic Analysis of Power Generation from Floating Solar Chimney Power Plant," Renew. Sustain. Energy Rev., **13**(4), pp. 736–749.

[52] Fluri, T. P., Pretorius, J. P., Dyk, C. Van, Backstro, T. W. Von, and Zijl, G. P. A. G. Van, 2009, "Cost Analysis of Solar Chimney Power Plants," Sol. Energy, **83**, pp. 246–256.

[53] Pretorius, J. P., 2008, "Thermoeconomic Optimization of a Solar Chimney Power Plant," J. Sol. Energy Eng., **130**(2), pp. 1–9.

[54] Gholamalizadeh, E., and Mansouri, S. H., 2013, "A Comprehensive Approach to Design and Improve a Solar Chimney Power Plant : A Special Case – Kerman Project," Appl. Energy, **102**, pp. 975–982.

[55] Li, W., Wei, P., and Zhou, X., 2014, "A Cost-Benefit Analysis of Power Generation from Commercial Reinforced Concrete Solar Chimney Power Plant," Energy Convers. Manag., **79**, pp. 104–113.

[56] Gholamalizadeh, E., and Kim, M.-H., 2014, "Thermo-Economic Triple-Objective Optimization of a Solar Chimney Power Plant Using Genetic Algorithms," Energy, **70**, pp. 204–211.

[57] Petela, R., 2009, "Gravity Influence on the Exergy Balance," Int. J. Exergy, **6**(3),

pp. 343–356.

[58] Petela, R., 2009, “Thermodynamic Analysis of Chimney,” Int. J. Exergy, **6**(6), pp. 868–880.

[59] Petela, R., 2008, “Influence of Gravity on the Exergy of Substance,” Int. J. Exergy, **5**(1), pp. 1–17.

[60] W.C. swinbank, 1963, “Long-Wave Radiation from Clear Skies,” J. R. Meteorol. Soc., **89**(381), pp. 339–348.

[61] Hollands, K. G. T., Unny, T. E., Raithby, G. D., and Konicek, L., 1976, “Free Convective Heat Transfer across Inclined Air Layers,” ASME,Journal Heat Transf., **98**(May), pp. 189–193.

[62] Mc Adams, W., 1954, “Heat Transmission,” PMAN, New York.

[63] Duffie, J. A., and Beckman, W. A., 2013, *Solar Engineering of Thermal Processes: Fourth Edition*, Wiley.

[64] Petela, R., 1964, “Exergy of Heat Radiation,” J. Heat Transfer, **86**(2), pp. 187–192.

[65] Petela, R., 2008, “An Approach to the Exergy Analysis of Photosynthesis,” Sol. Energy, **82**(4), pp. 311–328.

[66] Petela, R., 2003, “Exergy of Undiluted Thermal Radiation,” Sol. Energy, **74**(6), pp. 469–488.

[67] Szargut, J. ; Morris, D.R. ; Steward, F. R., 1988, *Exergy Analysis of Thermal, Chemical, and Metallurgical Processes*, Hemisphere Publishing, New York.

[68] Guo, P., Wang, Y., Meng, Q., and Li, J., 2016, “Experimental Study on an Indoor Scale Solar Chimney Setup in an Artificial Environment Simulation Laboratory,” Appl. Therm. Eng., **107**, pp. 818–826.

[69] Hussain, F. M., and Al-sulaiman, F. A., “An Improved Model for Energy and Exergy Analyses of a Solar Chimney Power Plant: A Case Study for Dhahran, Saudi Arabia,” Appl. Energy, (Under Review).

[70] Hottel, H. C., 1954, “Radiant-Heat Transmission,” *Heat Transmission by W.H.McAdams*, McGraw-Hill, New York, p. 532.

Vitae

Name	:	Faisal Moiz Hussain
Nationality	:	Indian
Date of Birth	:	3/14/1992
Email	:	faisalmoiz92@gmail.com
Address	:	Imlipura Street, Warangal, Telangana, India.
Academic Background	:	Bachelor of Technology, May 2013, Mechanical Engineering, Kakatiya University, India.